Environmental controls of sediment mercury accumulation in a large, glacially-fed lake

by

Nelson Zabel

A thesis
presented to the University of Waterloo
in fulfillment of the
thesis requirement for the degree of
Master of Science
in
Biology (Water)

Waterloo, Ontario, Canada, 2017

AUTHOR'S DECLARATION

I hereby declare that I am the sole author of this thesis. This is a true copy of the thesis, including any required final revisions, as accepted by my examiners.

I understand that my thesis may be made electronically available to the public.

Abstract

Mercury is an environmental contaminant of concern, especially in northern regions where human exposure to mercury through fish consumption can be high. Mercury accumulation in northern lakes has increased over the past 100 years, largely due to increased anthropogenic emissions of mercury to the atmosphere and subsequent deposition of mercury on remote lakes and catchments. In this study, I investigated approximately 1,200 years of sediment history in Kluane Lake, a large, dynamic, glacially-fed lake in the southwestern Yukon. This lake is an important traditional food source to Kluane First Nation, and citizens have become concerned about environmental contaminants, and with recent changes in glacial meltwater feeding Kluane Lake. Previous research has described two hydrological periods in Kluane Lake during the past 1,200 years: the Duke River period (ca CE 750 to CE 1650) and the Ä'äy Chù period (ca CE 1650 to CE 2015). Using a multi-proxy paleolimnological approach, I characterized the spatiotemporal variation in sediment mercury dynamics in Kluane Lake with sediment cores collected from several regions (Southern, Middle, Talbot Arm regions) in the lake. During the Duke River period, sediment accumulation and composition appeared to be relatively stable throughout the lake. Glacial sediments transported via the Duke River diluted mercury delivered to the lake from catchment soils and bedrock. The transition to the Ä'äy Chù period, marked by a reversal of inflows and outflows, was characterized by increased variability in sediment accumulation and composition, with numerous earthquakes preserved in core stratigraphies. In the Middle region of the lake, mercury accumulation rates and concentrations did not differ between the two hydrologic periods, while in the Talbot Arm, mercury accumulation rates and concentration were significantly higher during the Ä'äy Chù period. Mercury delivered to Kluane Lake during the Ä'äy Chù period appeared to be derived from terrestrial particles, including organic matter, and the sediments transported by the Ä'äy Chù. The recent piracy of the Kaskawulsh Glacier meltwaters by the Kaskawulsh River in spring 2016 has marked a new

hydrological period in Kluane Lake: continued monitoring is necessary to determine the effects on mercury cycling and bioavailability, and the implications for communities that rely on the lake.

Acknowledgements

I acknowledge that the University of Waterloo is located on the Haldimand Tract, part of the traditional territory of the Neutral, Anishinaabek, and Haudenosaunee peoples. This tract was promised to the Six Nations, which includes six miles on each side of the Grand River.

First and foremost, I would like to thank my supervisors, Dr. Heidi Swanson and Dr. Roland Hall, who took a chance on me and my wild ideas, and supported me throughout my research, from the first day in the field, covered in grey clay, until today as I submit my thesis. Thank you for your unyielding patience, support, and mentorship, and for always having time to talk – I've learned so much from you both. I would like to thank Dr. Brian Branfireun for going far beyond what is expected of a committee member by acting as a third supervisor and mentor for me, providing important insight, guidance, and support both in the field and in the lab. Thank you for your support while working at the Biotron Experimental Climate Change Research Centre. Finally, I'd like to thank Dr. Mark Servos for providing feedback on my research and providing mentorship throughout my Master's degree, especially during the Collaborative Water Program. Your endless enthusiasm and tireless effort made for a phenomenal learning experience.

Next, I would like to thank Kluane First Nation (KFN) and the KFN chief and council, including Math'ieya Alatini, Geraldine Pope, Grace Southwick, Kate van Ballegooyen, and Mary Jane Johnson, who drove the major research program that I was very fortunate to be a part of. Thank you for welcoming our research team and myself to your lands and teaching us about your traditions. I'd also like to thank the KFN youth and councilors who worked alongside us in the field, collecting and processing samples, and in the laboratory: Lenita Alatini, Skyler van Lieshout, Nadaya Johnson, Monica Johnson, and Jared Dulac – it was fantastic to get to know you all and to work alongside you during this project.

Special thanks go out to Norma Kassi, Jody Butler Walker, Katelyn Friendship, and the rest of the team of Arctic Institute of Community-Based Research. Your shared passion for community-based research has been inspiring and working with you all has been invaluable. I'd like to thank Tookie Mercredi for his expert filming throughout the project and support during our work. Thank you to Brenda Carson as well, for your support throughout the summer and your endless positivity.

I'd like to thank the Dän Keyi Renewable Resources Council (DKRRC) for their financial support of this research project. Special thanks to Pauly Wroot for accommodating us, providing support, and making us feel welcome. I'd also like to thank the Kluane Lake Athletic Association for allowing us to participate in the Fishing Derby.

Much of this research would not have been possible without the help and support of Lance Goodwin and Sian Williams – thank you both for going out of your way to help and accommodate us, no matter the weather or season. My experience at Kluane Lake would not have been the same without you both, and Bronwyn too! To the students I was fortunate to spend a summer with at Kluane Lake Research Station (KLRS): thank you for your warmth and friendship – I won't forget the late-night grilled cheese or bonfires on the beach. Thanks to the Arctic Institute of North America (AINA) for their financial support of this research and for operating KLRS.

Thank you to Carmen Wong at Kluane National Park and Reserve for donating samples, and for your support during this research. I'd also like to extend thanks to Oliver Barker and Aaron Foos at Yukon Environment for donating additional samples to our research program.

A huge thank you to the students of the Swanson Lab – it's been amazing to work, learn, and grow alongside you all as a family of grad students. Thank you for your support and help and comradery throughout my Master's degree, and thank you for willingness to listen to me talk about dirt. Special thanks to Dr. Leanne Baker for always having time to answer my statistics, research, or philosophical

questions, and for your guidance. Thank you to Sarah Lord for your work on the Kluane National Park sample analysis and interpretation. To my other lab family, the Hall Lab, thank you for your support and comradery, and letting me use the oven on short notice. Special thanks to Dr. Johan Wiklund for his expert dating work and advice regarding metals in sediments.

I'd like to thank Dr. David Hik for support with field logistics and vehicles. To Ellorie McKnight: thank you for all your help in the field, helping me to get to know the lay of the land, and your friendship. Our experiences together helped me fall in love with the Kluane Region.

Last but not least, I'd like to say thank you to everyone who helped out in the field or in the laboratory, with sample collection and processing, analysis (and re-analysis), and interpretation. Thank you to Jamie Turner, Robbert van Leeuwen, and our Austrian friends for help during winter sediment core collection. A special thank you to Randy Johnson for taking the youth and I fishing, and for teaching us how to set gill nets! Thank you to Ashley Alberto, Alex Crichton, Ainslie Crookshank, Sam Burke, Mason Elwood, Maddy Mead, Josh Neale, and Sam White for your help in the field cleaning fish, collecting and processing samples, during Harvest Camp, and keeping our spirits up throughout the field season. Thanks to Shyann Hang, Erin MacDonald, Eva Mehler, Amy Nguyen, and Heather Short for volunteering to help in the laboratory doing sample preparation and analysis.

I would like to thank my family and friends for supporting me throughout my Master's research. Thank you for your love, encouragement, and kindness, and for taking care of me when I needed it (even when I didn't think I did).

Thank you to Rachel DeJong, Sarah Ghorpade, and Justin Hoffmann for their feedback on early versions of my thesis. Thank you to Heidi and Roland for reading through every single version I produced and always providing constructive feedback through each iteration.

Funding and/or in-kind support for this research project were provided by Kluane First Nation (KFN), the Dän Keyi Renewable Resource Council (DKRRC), the Arctic Institute for Community-Based Research (AICBR), the National Sciences and Engineering Research Council of Canada (NSERC), the Northern Contaminants Program (NCP), the Yukon Fish & Wildlife Enhancement Trust Fund (YFWET), the W. Garfield Weston Foundation & the Wildlife Conservation Society (WCS) Canada, the Northern Scientific Training Program (NSTP), and the Arctic Institute of North American (AINA) Grant-in-Aid program. I am grateful for your support – thank you!

Dedication

I dedicate my thesis to my Opi, Arthur Zabel, who always encouraged me to aim higher and push farther. Thank you for supporting me and loving me throughout my life, and for encouraging me to pursue higher learning. I love you and I miss you daily.

Table of Contents

List of Figures

List of Tables

Chapter 1
Introduction

Northern North America is sparsely populated, with limited industrial development and few local sources of contamination. However, many areas of the North have been contaminated with pollutants that have arrived via long-range atmospheric transport from temperate regions (e.g., AMAP 2011). Among these pollutants is mercury, a natural metallic element that has become mobilized by anthropogenic activities globally, resulting in increased amounts of mercury being circulated in the atmosphere (Schuster *et al.* 2002; AMAP 2011). Accumulation of mercury in lakes throughout Arctic and subarctic regions has increased during the past 100 years, due largely to anthropogenic emissions of mercury to the atmosphere from industrial activities in temperate and tropical regions (e.g., Fitzgerald *et al.* 1998; Lockhart *et al.* 2005; Kirk *et al.* 2011). Once in the atmosphere, mercury can be transported long distances from local point sources to remote lakes and watersheds. Mercury is then deposited across the landscape and ultimately into aquatic ecosystems while undergoing biogeochemical changes (see Mason *et al.* 1994; Selin 2009). In remote regions, mercury research has focused primarily on the pathways of mercury delivery to lakes and the movement of mercury through food webs. The organic form of mercury, methylmercury, is of particular interest because it can bioaccumulate and biomagnify through aquatic food webs and may reach levels that pose risks to human health (see Mergler *et al.* 2007; Dórea 2008).

Concentrations of mercury in biota in subarctic and Arctic lakes have increased during the past 50 years, reflecting increased anthropogenic mercury loading (see Lockhart *et al.* 2005; e.g., Carrie *et al.* 2010). Elevated mercury concentrations have been found in long-lived, predatory fishes (see Lockhart *et al.* 2005) that serve as subsistence food sources for northerners (see Braune *et al.* 1999; Kuhnlein & Chan 2000; Van Oostdam *et al.* 2005). Many remote communities, especially First Nations communities, rely on lakes as subsistence food sources (e.g., Wein & Freeman 1995) and increases in

mercury loading to lakes place these communities at greater risk to mercury exposure (e.g., Hermanson & Brozowski 2005; see Kuhnlein & Chan 2000; Van Oostdam *et al.* 2003). There is growing concern in northern communities and with regulators regarding increasing mercury levels in subsistence food species in the North (e.g., KFN 2014; Receveur *et al.* 1998), and an increased need to strength the ability to predict mercury in important fish species under future climate change scenarios (see Reist *et al.* 2006; Ficke *et al.* 2007).

The biogeochemical cycle of mercury in freshwater ecosystems is complex (see Braaten *et al.* 2014; Lehnerr 2014; Chételat *et al.* 2015). Predicting mercury in fish requires information on trophic ecology, food web structure, water chemistry (e.g., Ravichandran 2004), mercury loading (from both the atmosphere and the catchment), and sediment chemistry (e.g., Greenfield *et al.* 2001; Carrie *et al.* 2010). The environmental factors which control the biological and environmental mechanisms that transform mercury into the highly toxic and bioaccumulative form, methylmercury, are not well understood. However, the amount of methylmercury available to bioaccumulate in food webs depends on the amount of mercury loading to the ecosystem, and the processes that regulate mercury methylation and demethylation (see Braaten et al. 2014; Chételat *et al.* 2015; Paranjape & Hall 2017). In general, loading of mercury to remote lake ecosystems has increased by 2 – 4 times since the Industrial Revolution (Drevnick *et al.* 2012; Muir *et al.* 2009; Drevnick *et al.* 2016), although temporal patterns of mercury accumulation in lakes vary within and among northern regions (e.g., Stern *et al.* 2009; Kirk *et al.* 2011). Variation in mercury loading to northern lakes can be attributed to numerous factors, including catchment area to lake area ratio (e.g., Lucotte *et al.* 1995; Muir *et al.* 2009; Drevnick *et al.* 2016), catchment soil composition (e.g., Johansson *et al.* 1991; Fitzgerald *et al.* 2005; Luo *et al.* 2015; see Grigal 2002; Gabriel & Williamson 2004), abundance of wetlands and peatlands within the catchment (e.g., St. Louis *et al.* 1994; Rydberg *et al.* 2010; see Rudd 1995), and atmospheric deposition rates (e.g., Engstrom *et al.* 1994; Wiener *et al.* 2006).

Sediment-mercury interactions are important in determining the rate of mercury accumulation and the bioavailability of mercury to organisms (Driscoll *et al.* 1995; Ullrich *et al.* 2001). These interactions are complex, and are influenced by a variety of environmental factors. Sediment organic matter, including algal-derived, dissolved, and particulate fractions, adsorbs mercury and can influence the rate of mercury delivery to lake-bottoms. Organic matter has been shown to have a high affinity for mercury, forming complexes with both inorganic and organic forms of mercury (Driscoll *et al.* 1995; El Bilali *et al.* 2002; Arias *et al.* 2004; Liu *et al.* 2012). While the organo-mercury complexes are strong, high concentrations of labile carbon in sediments have been linked to increased microbial reduction of mercury, which releases the mercury from the sediment-organic complexes and makes it bioavailable (Brazeau *et al.* 2013a).

Interactions between inorganic and organic fractions of sediment affect mobility and availability of mercury in sediment. Clay particles have a high capacity to adsorb mercury, which limits mercury bioavailability (Desauziers *et al.* 1997; Ullrich *et al.* 2001; Arias *et al.* 2004; Zhu & Zhong 2015). This adsorption capacity increases with increasing DOC in lake waters, due to strong affinity between DOC and mercury (Arias *et al.* 2004; Zhu & Zhong 2015). Mercury also readily forms colloids with metal oxides, hydroxides, and, particularly, sulphides (Desauziers *et al.* 1997; El Bilali *et al.* 2002; Wolfenden *et al.* 2005; Liu *et al.* 2012). Several ions in lake water can interfere with mercury complex formation, reducing mercury adsorption and forming mercury-ion complexes (Reimers & Krenkel 1974; Liu *et al.* 2012; Brazeau *et al.* 2013a). Generally, it is believed that organic and inorganic colloids are the dominant factors controlling the mobility, speciation, and availability of mercury in lake sediments (Liu *et al.* 2012). Differences in the abundance of organic and inorganic mercury ligands, sediment grain size and mineralogy, and water chemistry all can affect mercury accumulation rates in sediments.

The scarcity of long-term environmental monitoring in northern regions has made it difficult to determine the spatial extent and temporal variability of anthropogenic mercury pollution in northern lakes. Lake sediments can provide a way of determining the extent of anthropogenic mercury pollution in locations with little to no environmental monitoring (Adrian *et al.* 2009), and can be used to reconstruct past mercury delivery to sediments and the environmental controls on that delivery (Lockhart *et al.* 2000; Biester *et al.* 2007; Goodsite *et al.* 2013), including primary production, catchment erosion, and sedimentation rates, as these sediment records represent the net effects of all processes that influence mercury accumulation (Smol & Douglas 2007; Schindler 2009). Paleolimnological studies have been used to reconstruct mercury accumulation in lake sediments across North America, ranging from temperate to High Arctic lake systems (e.g., Muir *et al.* 2009, Drevnick *et al.* 2016).

1.1 Paleolimnological Studies of Mercury in northern North America

Many paleolimnological mercury studies have used mercury enrichment metrics in order to quantify recent changes in sediment mercury concentration and accumulation rates relative to pre-anthropogenic time periods (Landers *et al.* 1995; Lockhart *et al.* 1995; Lockhart *et al.* 1998; Fitzgerald *et al.* 2005; Muir *et al.* 2009; Kirk *et al.* 2011; Köck *et al.* 2012; Brazeau *et al.* 2013b). There are several mercury enrichment metrics commonly used in paleolimnological mercury studies: enrichment factors (EF), flux ratios (FR), and anthropogenic fluxes (ΔF), which include sediment focus-corrected (ΔF_F), sedimentation rate-corrected (ΔF_{adj}), and both sediment focus- and sedimentation rate-corrected ($\Delta F_{adj,F}$) forms (see Muir *et al.* 2009, Kirk *et al.* 2011). All of these metrics use either mercury concentrations or accumulation rates from a pre-industrial period (typically pre-1850) and a post-industrial or recent period (typically post-1950). Enrichment factors (EF) determine the ratio of recent to pre-industrial sediment mercury concentrations. Flux ratios (FR)

are similar, except the ratio of recent to pre-industrial mercury accumulation rates (or fluxes) is determined. Anthropogenic fluxes (ΔF) or excess fluxes are the difference between pre-industrial and recent mercury accumulation rates: corrected forms account for differences in sedimentation rate between periods (ΔF_{adj}) or for sediment focusing effects at a sediment core site (ΔF_F), or both ($\Delta F_{adj,F}$; see *Muir et al.* 2009). These metrics allow for comparisons between lake systems, which differ in pre-industrial mercury dynamics, and provide indices of anthropogenic mercury pollution relative to lake-specific baseline or background conditions.

Mercury enrichment metric values vary across northern North America, reflecting regional variations in anthropogenic mercury loading to lakes and catchments. Flux ratios have been found to decline from east to west, and are higher in subarctic Ontario than in the Yukon (Lockhart *et al.* 1995; Lockhart *et al.* 1998). Flux ratios and $\Delta F_{adj,F}$ are also negatively correlated with latitude (Muir *et al.* 2009). Lockhart *et al.* (1995) concluded that lakes with mercury flux ratios less than 2 were more influenced by geological or catchment sources of mercury, whereas lakes with flux ratios greater than two were more influenced by long-range atmospheric transport and direct deposition of mercury. These metrics indicate that anthropogenic mercury pollution is widespread across the North, regardless of direct or indirect sources of anthropogenic mercury to lakes.

While evidence for anthropogenic mercury pollution in Arctic and subarctic lakes is widespread, spatial differences and trends in mercury pollution have been identified (Landers *et al.* 1995; Lockhart *et al.* 1995; Lockhart *et al.* 1998; Muir *et al.* 2009; Drevnick *et al.* 2016). Similar to mercury flux ratios, longitudinal decreases in the atmospheric deposition of mercury to lakes moving from east to west have been noted (Lockhart *et al.* 1995; Lockhart *et al.* 1998). Latitudinal trends in mercury accumulation have also been observed in northern North American lakes, with decreasing rates of mercury accumulation moving northward (Landers *et al.* 1995; Muir *et al.* 2009; Drevnick *et al.* 2016). Drevnick *et al.* (2016) also identified a strong positive relationship between level of catchment

disturbance and recent increases in mercury accumulation rates in lake sediments. This finding highlights the compounding influence of localized anthropogenic disturbance and long-range atmospheric transport on mercury accumulation rates in lake sediments, especially in highly-disturbed catchments. Point sources and anthropogenic disturbances are not common in the North, but where they occur, they have also contributed to localized increases in mercury accumulation (Hermanson 1993, 1998; Hermanson & Brozowski 2005; Michelutti *et al.* 2007; Laperrière *et al.* 2009). However, not all point sources have discernably affected mercury accumulation (Permaki & Stone 2007; MacDonald *et al.* 2016). Mercury delivery to lake sediments depends on proximity to anthropogenic sources, lake surface area, sediment accumulation rates, and a variety of catchment characteristics. Catchment contributions of mercury vary among lakes, and will be greater when the ratio of catchment area to lake area is high and when catchment disturbances (e.g., flooding, mining, road construction, permafrost thaw) enhance erosional inputs to nearby lakes.

Both allochthonous and autochthonous process affect mercury delivery to lakes sediments. Catchment and geological weathering and erosion are the primary mechanism by which naturally occurring mercury is delivered to lake sediments, although anthropogenically-derived mercury that has been deposited on lake catchments from the atmosphere is also delivered to lakes via catchment erosion. Numerous studies have noted the importance of catchment contributions of mercury to northern lakes, and in some landscapes, including delta, mountain, glacial, and thermokarst environments, high inputs of eroded sediments can dilute atmospheric mercury enrichment (Allen-Gil *et al.* 1997; Permaki & Stone 2007; Deison *et al.* 2012; Köck *et al.* 2012; MacDonald *et al.* 2016). However, terrestrial organic matter can serve as a transport vector, and increased organic matter export from the catchment can increase mercury delivery to lakes (e.g., Korosi *et al.* 2015). Additionally, the erosion of certain bedrock types and transport of eroded materials to lakes can be a source of mercury to lake

sediments (Rytuba 2003; Outridge *et al.* 2017), although this source is dependent on the bedrock geology of a lake catchment.

While allochthonous inputs of mercury to lakes from catchments can exert strong influence on mercury accumulation rates, increases in primary productivity in lakes can also increase mercury delivery to sediments within subarctic and Arctic lakes. Mercury delivery to sediments that is driven by primary production has been termed 'algal scavenging'. Algal scavenging is a process by which algal organic matter, described as soluble organic matter (SOM) that includes algal-derived lipids and pigments, binds and concentrates mercury. Mercury is delivered to the sediment as the organic matter settles to the lake bottom (Sanei & Goodarzi 2006). Climate-driven increases in algal productivity result in increased mercury scavenging by algal cells or algal detritus, leading to increases in mercury delivery rate to sediments (Outridge *et al.* 2005). Evidence for algal scavenging has been found in many subarctic and Arctic lakes across the North (e.g., Outridge *et al.* 2005; Sanei & Goodarzi 2006; Outridge *et al.* 2007; Stern *et al.* 2009; Carrie *et al.* 2010; Cooke *et al.* 2012; Sanei *et al.* 2012; Brazeau *et al.* 2013b). However, Kirk *et al.* (2011) found that, in several High Arctic lakes, there was no relationship between mercury concentration and algal carbon. There was also no relationship between mercury concentration and diatom abundance or community composition. Of the lakes where significant relationships between algal productivity and mercury concentration were found, they were attributed to the diagenesis of algal organic matter following deposition observed in collected cores (Kirk *et al.* 2011). Algal scavenging appears to be driven by anthropogenic climate changes, as this phenomenon has not been observed in pre-industrial sediments from numerous lakes (Cooke *et al.* 2012; Outridge *et al.* 2017). The algal scavenging hypothesis has emerged as an important yet controversial mechanism (see Outridge *et al.* 2011) to explain recent increases in sediment mercury concentration across the north, and has received much attention in the past 12 years.

Differing findings among studies regarding controls of mercury delivery to lake sediments reflect an incomplete understanding of the numerous factors that can contribute to mercury delivery to lake sediments, and the spatial diversity in the importance of each factor to northern lakes. For example, few studies have acknowledged catchment contributions of mercury and increases in algal production together, despite the understanding that both processes influence sediment mercury dynamics. Further, studies that claim no evidence of anthropogenic mercury loading have rarely acknowledged changes in sedimentation rate, erosion, or primary productivity. The relationship between mercury and lake sediments is complex and this complexity should be further explored in order to better understand environmental mercury dynamics in northern lakes, especially in light of continued global climate change.

1.2 Glacial Lakes and Climate Change

Many of the factors that regulate mercury loading to lakes and mercury delivery to lake sediments are expected to be altered by global climate change (see Rydberg *et al.* 2010, Stern *et al.* 2012). Climate change is expected to alter the biogeochemical cycling of mercury by causing increases in global mercury fluxes (see Selin 2009). In northern regions, it is likely that increases in the export of organic matter, sediments, and nutrients from watersheds to lakes will result in increased mercury delivery to lakes, due to higher decomposition rates in terrestrial soils subsequently releasing mercury bound with organic matter, and increased thaw of permafrost (see Stern *et al.* 2012). Increased glacial melt is also expected to increase mercury loading to lakes, particularly at subpolar latitudes, by releasing atmospherically-transported mercury that has accumulated on the glacier's surface (see Stern *et al.* 2012). Increases in algal productivity in northern lakes have also been linked with increases in mercury accumulation rates in sediments, due to the strong affinity between algal organic matter and

mercury in the water column (e.g., Outridge *et al.* 2005, Sanei & Goodarzi 2006, Outridge *et al.* 2007, Stern *et al.* 2009, Carrie *et al.* 2010, Cooke *et al.* 2012, Sanei *et al.* 2012, Brazeau *et al.* 2013b).

Paleolimnological studies have generally focused on smaller lakes with simple basin morphometry. These systems are abundant in northern environments, tend to respond more quickly to environmental changes, such as climate or water temperature, and are therefore suitable for paleoenvironmental reconstructions of change during recent decades (Cohen 2003; Schindler & Smol 2006; Adrian *et al.* 2009). Smaller lakes, however, can be highly sensitive to changes that result in 'noise' in sediment records, masking long-term trends (Adrian *et al.* 2009). Relatively few studies have investigated large northern lakes (e.g., Stoermer *et al.* 1990; Stern *et al.* 2009; Chakraborty *et al.* 2010; Köck *et al.* 2012), which can more effectively integrate responses to environmental changes over time, reducing 'noise' (e.g., Chakraborty *et al.* 2010; Adrian *et al.* 2009). Large lakes can be more morphometrically and hydrologically complex, which may reduce the ability to make strong and/or broad inferences about lake-specific or regional responses to environmental changes. However, large lakes are of considerable interest to commercial and subsistence fishers, as they are often home to important subsistence fish species. Therefore, understanding the impacts of environmental changes, including climate change, on these lake systems and on mercury cycling in these lakes is of critical importance.

Glacially-fed lakes are particularly vulnerable to climate change impacts, as glacial retreats have been accompanied by marked changes in summer meltwater inflow, and with projected continued retreat, increases in water temperature and changes in suspended sediment loads are expected in glacial streams, which will alter mercury dynamics in receiving lakes (Schindler & Smol 2006; Moore *et al.* 2009). Contributions of glacial materials to lake sediments may sequester mercury from the water column due to the binding between fine grained sediments and mercury (Frenet-Robin & Ottmann 1978; El Bilali *et al.* 2002), and thus reduce mercury bioaccumulation in lake food webs (Zhu & Zhong 2015). Glacially-fed lakes are relatively abundant in western and northern North America, and

are important sources of subsistence foods for northern indigenous peoples, and recreational and/or commercial fisheries (e.g., Northrup *et al.* 2010; Environment Yukon 2010). Mercury dynamics in glacially-fed lakes are understudied, despite the vulnerability of these ecosystems to climate change-related impacts and the importance of many glacially-fed lakes to local communities. Thus, further study is required to understand these dynamic systems.

1.3 Kluane Lake

Kluane Lake, the largest lake in the Yukon, is located in the southwestern Yukon along the Alaska Highway and adjacent to Kluane National Park and Reserve. The lake is located within the Shakwak Trench and bordered by the St. Elias and Ruby mountain ranges (Rampton & Shearer 1978). Kluane Lake was fed mainly by glacial meltwaters from the Kaskawulsh Glacier via Ä'äy Chù, formerly the Slims River, until recently (Figure 1; Rampton & Shearer 1978; Shugar *et al.* 2017). This deep (maximum depth 80 m), cold lake receives meltwater from many small, sometimes seasonal creeks, which flow off the surrounding mountain ranges (Figure 1; Rampton & Shearer 1978; Dodds & Campbell 1992).

Kluane Lake is part of the traditional territories of both the Kluane First Nation (KFN) and the Champagne and Aishihik First Nations (CAFN), and provides an important source of traditional and subsistence food fishes for these Southern Tutchone nations, as the closest grocery store is over 300 km away from their communities. The lake is also an important destination for recreational fishing, and has a commercial fishing quota for Lake Trout (Environment Yukon 2010). Despite the ease of access and the presence of the Kluane Lake Research Station (Arctic Institute of North America) on the southern shore of the lake for over 50 years (Danby *et al.* 2014), the lake has received little scientific attention. Minimal information is available concerning environmental contaminants in Kluane Lake fish (however, see Lockhart *et al.* 2005), and the lake is not actively monitored by

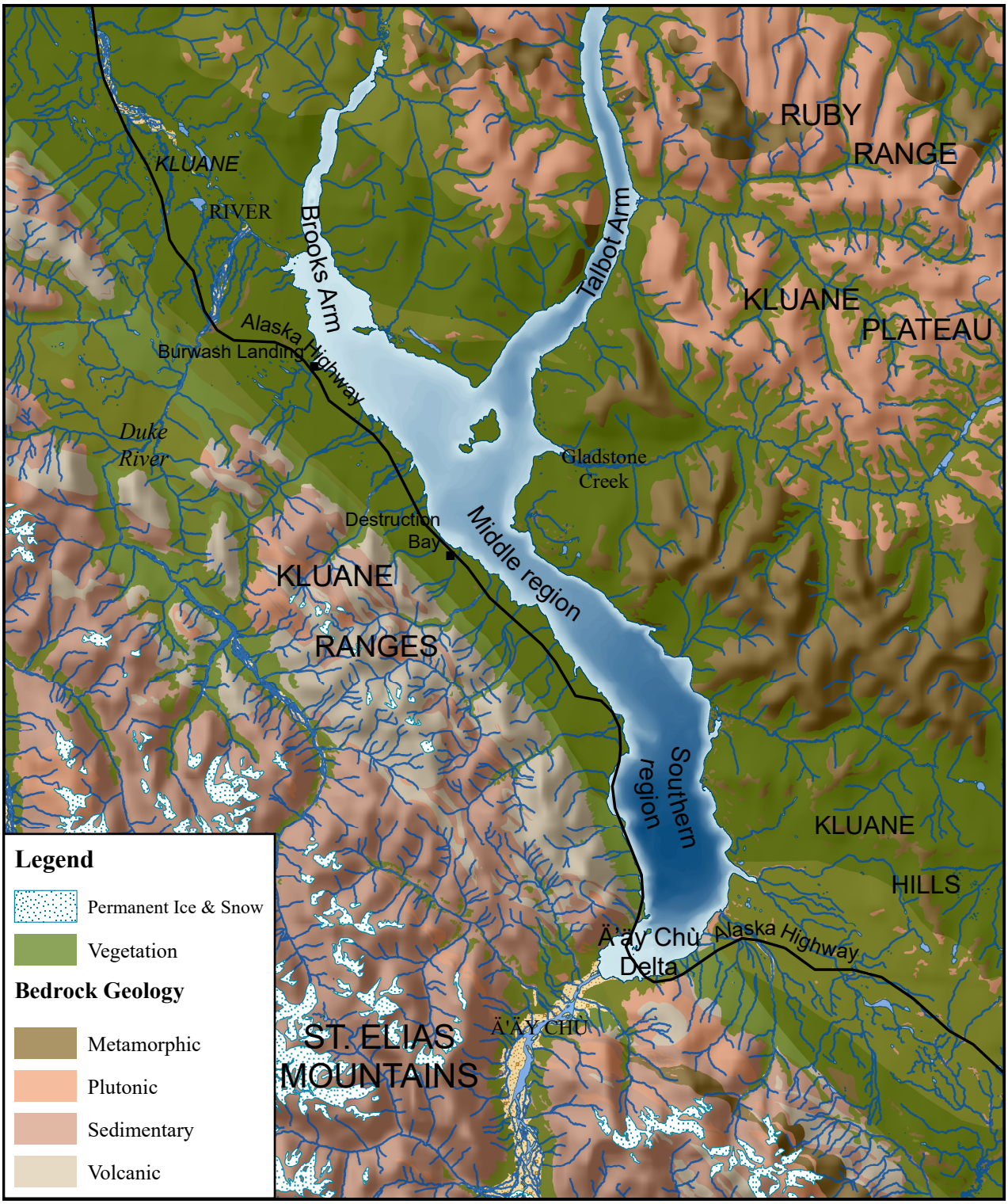

Figure 1. Map of the Kluane Lake Region.

Data Sources: Geomatics Yukon, E. McKnight (bathymetric DEM).

N

0 2.5 5 10 15 20 Kilometers

communities or government agencies. Relatively high concentrations of mercury and other organic contaminants have been found in fish from several other Yukon lakes, including Atlin Lake, Fox Lake, Lake Laberge, Kusawa Lake, Kloo Lake, and Sekulmun Lake (see Lockhart *et al.* 2005, Stern 2013). Previous paleolimnological studies of mercury in Yukon lakes (Lake Laberge, Kusawa Lake, Fox Lake, Little Atlin Lake) have found increases in sediment mercury concentration and accumulation during the past 100 years (Lockhart *et al.* 1995, 1998; Stern *et al.* 2009). Many other lakes in the Yukon remain under studied with respect to monitoring of environment contaminants. This leaves both the extent of anthropogenic impacts and possible risk of contaminant exposure to northerners unquantified in many parts of the territory, including Kluane Lake. Levels of environmental contaminants and the safety of traditional foods are growing concerns among Yukon First Nations (e.g., KFN 2014; Receveur *et al.* 1998).

There is growing concern over climate change and environmental contaminants, including mercury, within the citizenry of Kluane First Nation. Community members are concerned that increased melting of the Kaskawulsh Glacier, long-range transport of mercury, and climate change-related environmental impacts may be increasing mercury loading to Kluane Lake and also increasing mercury concentrations in fish found in the lake. In early 2016, an exponential decline in discharge was observed in Ä'äy Chù, caused by river piracy at the headwaters of the river (Shugar *et al.* 2017). This river was fed primarily by meltwaters from the Kaskawulsh Glacier, which also fed the adjacent Kaskawulsh River (Figure 1). Ice wall collapse at the toe of the glacier resulted in the complete diversion of meltwater from Ä'äy Chù to the Kaskawulsh River, a change that is likely permanent (Shugar *et al.* 2017). Only small creeks along the Ä'äy Chù valley now feed into Ä'äy Chù following this diversion. The loss of this meltwater has resulted in record (contemporary) low water levels (Shugar *et al.* 2017), and severely decreased water and sediment delivery to Kluane Lake. Even

before this dramatic hydrological event, community concerns about mercury and observed declines in lake water levels motivated an investigation into mercury dynamics in Kluane Lake.

Due to the large size of Kluane Lake, four major regions (*sensu* Gilbert & Desloges 2005) have been identified, based on the relative influence of inflows and outflows, and sediment and limnological characteristics (E. McKnight, unpublished data). The four major regions of Kluane Lake include the Southern region, the Middle region, the Talbot Arm, and the Brooks Arm (Figure 1). Until 2016, the cold and turbid Southern region (Figure 1), which includes the Ä'äy Chù delta, received large amounts of water and sediment from Ä'äy Chù. The Ä'äy Chù valley has a complex bedrock stratigraphy (Figure 1; Yukon Geological Survey 2017). This valley comprises sedimentary bedrock primarily, including marble, gypsum, greywacke, siltstone, and large formations of limestone, and igneous bedrock, including gabbro and granodiorite (Yukon Geological Survey 2017). Impacts resulting from the loss of most of these inflow waters on the limnological and ecological characteristics of the Southern region have yet to be documented. The Middle region (Figure 1) forms the main body of Kluane Lake, and receives water from the other regions, as well as meltwaters from ephemeral creeks and streams that drain from the surrounding Kluane and Brooks Ranges, which form the western and eastern borders of the lake, respectively. The Talbot Arm (Figure 1) is a narrow northeastern valley region with waters that are warmer, clearer, and more productive than the more southerly regions. Finally, the Brooks Arm (Figure 1) is the warmest and shallowest region, and is also relatively productive (E. McKnight, unpubl. data). The outflow of the lake, the Kluane River (Figure 1), drains from the Brooks Arm.

During the past 2 200 years, other major hydrologic changes, similar to the recent loss of Ä'äy Chù, have occurred several times to Kluane Lake, including changes in water supply and drainage outlets, resulting in marked increases and decreases in water level (Brahney *et al.* 2008a,b). Initially, ca. BCE 200, Kluane Lake was a closed basin and water levels were approximately 25 m lower than present,

and water drained southwards via the Ä'äy Chù valley into the Alsek River (Brahney *et al.* 2008a,b). Anoxia developed in the deep lake sediments by BCE 50, due to semi-permanent stratification or meromixis (Brahney *et al.* 2008a,b). The groundwater flowing into Kluane Lake was rich in solutes, including sulphate, and may have caused the meromictic, and even possibly euxinic (anoxic and sulphidic) conditions in sediments, due to differences in density between groundwater and surface water inflows (Brahney *et al.* 2008a,b). However, by CE 650, the Duke River (Figure 1) began to flow back into Kluane Lake in the Brooks Arm, ending the anoxic and meromictic period, raising lake levels approximately 10 to 15 m below current levels (Brahney *et al.* 2008a,b). This glacially-fed river drains the Kluane Ranges and St. Elias Mountains and originates from the Canada Peak glacier (Yukon Geological Survey 2017). The Duke River valley is comprised primarily of sedimentary bedrock, including greywacke & conglomerate, limestone, marble, gypsum, sandstone, and siltstone, and igneous bedrock, including andesite, granodiorite, peridotite, and volcanic tuff (Figure 1; Yukon Geological Survey 2017).

During the Little Ice Age (ca. CE 1200s to CE 1800s, Luckman 2000), the Kaskawulsh Glacier advanced beginning ca. CE 1500, and reached its maximum extent ca. CE 1750 (Lindsey *et al.* 1981; Clague *et al.* 2006; Reyes *et al.* 2006; Brahney *et al.* 2008a,b). The advance of the glacier blocked the southern outflow and routed glacial meltwaters into the lake which caused the lake to deepen rapidly, reaching more than 10 m above current lake levels (Brahney *et al.* 2008b). The glacial advance was also coincident with the loss of the Duke River inflow by CE 1650 (Brahney *et al.* 2008a,b). The high water levels in Kluane Lake eroded through the Duke River sediment fan at the north end of Kluane Lake and formed the Kluane River ca. CE 1690 (Figure 1), which drained the lake to present levels (Lindsey *et al.* 1981; Clague *et al.* 2006; Brahney *et al.* 2008a,b; Brahney *et al.* 2010). The dynamic history of Kluane Lake likely resulted in spatial and temporal variations in both sediment and mercury dynamics. In order to predict possible changes to mercury dynamics in Kluane Lake as a

result of the recent loss of Ä'äy Chù inputs, an understanding of the impact of previous hydrological changes on mercury dynamics is necessary.

Sources of mercury to Kluane Lake are watershed contributions, including bedrock erosion and in-washing from catchment soils, dissolved mercury in catchment runoff, and direct deposition of atmospherically-transported mercury to the lake surface. Anthropogenic point source contributions of mercury to the lake are likely minimal, as the communities along the lake (Figure 1) are small and local placer mines operate infrequently (Van Loon & Bond 2014). The major changes in lake hydrology during the late Holocene (see Brahney *et al.* 2008a,b, Brahney *et al.* 2010) have undoubtedly affected sediment accumulation, which in turn has likely affected sediment-mercury dynamics.

Mercury dynamics in lake sediments are complex due to a multitude of interacting processes that can affect the form and bioavailability of mercury in aquatic sediments, and these processes vary spatially in large lakes like Kluane Lake. I hypothesized that hydrological processes, watershed inputs, and primary production are the main controls of mercury deposition in Kluane Lake sediments. The relative importance of hydrology, watershed inputs, and primary production in delivering mercury to lake sediments likely differs throughout the history of Kluane Lake, since it is known that past changes in hydrology have affected lake regions differently (Brahney *et al.* 2008a,b; Brahney *et al.* 2010). Primary production in Kluane Lake has not been formally studied. However, a north-south trend has been observed with greater primary production in the Brooks and Talbot Arms (E. McKnight, unpubl. data). Given positive relationships between primary productivity and mercury in a similar lake in the southwestern Yukon (Kusawa Lake, Stern *et al.* 2009), it is possible that climate change-driven increases in algal productivity have occurred in Kluane Lake, especially in the northern regions, and these increases in productivity may have increased mercury delivery to sediments in the lake in recent times.

The dynamic hydrological history of Kluane Lake has shaped sediment dynamics during the past 2 000 years, and has likely resulted in spatiotemporal differences in the relative importance of environmental controls on mercury deposition to Kluane Lake sediments. This research seeks to characterize the spatiotemporal variation in sediment mercury accumulation among regions of Kluane Lake and investigate the importance of different environmental controls on mercury accumulation in lake sediments. Further, this research will lend insight into mercury dynamics in glacially-fed lakes, using Kluane Lake as a model system.

1.4 Study Objectives & Approach

The objectives of this study are to: (1) relate past hydrological changes to mercury accumulation, and drivers of mercury accumulation, in sediments of Kluane Lake, and (2) compare mercury accumulation in Kluane Lake to other published lake sediment work in the Yukon.

To address these objectives, I collected lake sediment cores from two regions in Kluane Lake that capture variability in distance to current and past inflows and outflows. Using these cores, I determined dry mass accumulation rates, sediment mercury concentrations, and sediment characteristics that could affect mercury accumulation rates. Several proxies were used to investigate controls on mercury delivery to, and accumulation in, lake sediments. Visible reflectance spectroscopy (VRS)-inferred chlorophyll-*a* was used as a proxy for autochthonous primary production, carbonate content was used as a proxy for glacial inputs to the lake, due to the carbonate-rich bedrock in both the Ä'äy Chù and Duke River catchments, and magnetic susceptibility was used as a proxy for terrestrial inputs, including eroded soils and bedrock materials (see Oldfield *et al.* 1983, Sandgren & Snowball 2001). Sediment core stratigraphies were interpreted in the context of previously reconstructed hydrological changes and known history of atmospheric mercury. Mercury accumulation rates and drivers of accumulation were compared among hydrological periods and core

locations, and indices of anthropogenic mercury pollution were compared among cores and to other lakes in Yukon.

Results from this research will lend insight into spatial and temporal variation in controls on mercury accumulation in Kluane Lake, highlight landscape trends in mercury accumulation in the southern Yukon, shed light onto sediment mercury dynamics in glacially-fed lakes, and provide a basis for future predictions of mercury dynamics in Kluane Lake and other glacial lakes in the North.

Chapter 2
Methodology

2.1 Lake Sediment Core Collection

Two sediment cores were collected at one site within each of two regions of Kluane Lake: the Middle region and Talbot Arm (Figure 2). Cores were collected on April 4 - 5, 2015, using a hammer gravity corer (Glew *et al.* 2001) operated through lake ice. After collection, cores were transported to the Kluane Lake Research Station, and sectioned into either 0.5-cm or 1-cm sections (site-dependent) using a vertical "push rod type" extruder (Glew 1988; Glew *et al.* 2001). Sections were stored in the dark at 4°C during shipping and until analysis.

2.2 Loss-on-Ignition Analysis

Loss-on-ignition (LOI) analysis is a sequential heating method used for determining water, organic, carbonate, and mineral content of lake sediments (Heiri *et al.* 2001). LOI analysis was conducted on all cores, following a procedure published by Smith (2003), which includes longer ignition and combustion times (from 2 hours to 2.5 hours) and hotter final combustion temperature (to 1000°C) than the standard method (Heiri *et al.* 2001). These modifications accommodated for the clay- and silt-rich sediments found in Ä'äy Chù (Harris 1990), which contain structurally-bonded water molecules (Smith 2003). Bound water can represent up to 13% of the weight of the total sample and is not removed using the Heiri *et al.* (2001) standard LOI procedure (Smith 2003).

For each sample, approximately 0.68 g (± 0.17, SD; n = 403) of wet sediments were weighed, dried at 90°C for 24 hours, stored in a desiccator for 24 hours, and weighed again to determine water content (% wet weight). The dried sediments were then ignited at 550°C for 2.5 hours, stored in a desiccator for 24 hours, and weighed again to determine organic content (% dry weight). Finally, the sediments were combusted at 1000°C for 2.5 hours, stored in a desiccator for 24 hours, and weighed to determine carbonate content (% dry weight). Mineral

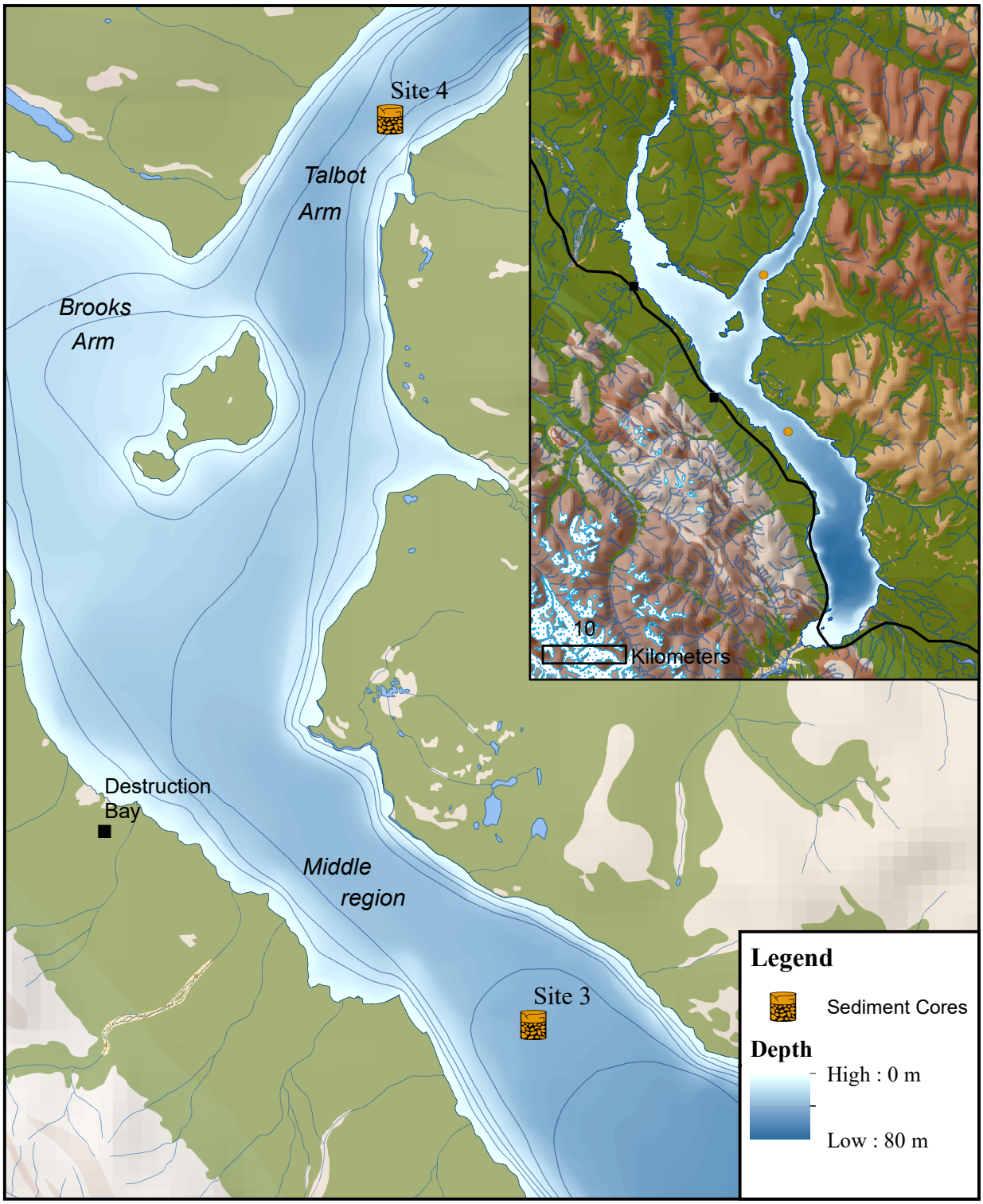

Figure 2. Sediment core collection sites.

N

Data Sources: Geomatics Yukon, E. McKnight (bathymetric DEM).

0 1 2 4 6 Kilometers

content (% dry weight) was determined using the residue after the final combustion. LOI data, core section weight, and corer tube diameter were used to calculate sediment density (g cm^{-3}) in each section.

For the two sites, one core was selected for further analysis: core 3B from the Middle region and core 4A from the Talbot Arm. Loss-on-ignition data were used to determine similarity in stratigraphic variations between core pairs (see Appendix A), and for core selection for later analysis. LOI data, along with additional analyses, were also used in identifying past events that altered sediment composition, including hydrological changes and earthquakes.

2.3 Magnetic Susceptibility

Magnetic susceptibility measures the degree to which a material can be magnetized when exposed to a magnetic field (Oldfield *et al.* 1983; Thompson & Oldfield 1986). This susceptibility is a ratio of the temporary magnetization induced in a sample by a magnetic field to the field itself, and is thus unitless (Verosub & Roberts 1995). The majority of magnetic materials in lake sediments originate from catchment materials that eroded from bedrock, subsoils, and topsoils (Oldfield *et al.* 1983; Sandgren & Snowball 2001). Minor sources of magnetic materials include dust transported by wind storms, air-borne materials emitted during volcanic eruptions, and some particles produced by anthropogenic activity, such as fossil fuel combustion (Oldfield *et al.* 1983; Sandgren & Snowball 2001). Magnetic susceptibility is therefore commonly used as a paleolimnological proxy for catchment erosion (Oldfield *et al.* 1983; Verosub & Roberts 1995; Sandgren & Snowball 2001).

Magnetic susceptibility was measured for every 0.5-cm or 1-cm (core-specific) section of each selected core using a Bartington MS2E high-resolution surface scanning sensor system at the WATER Laboratory, University of Waterloo. Wet sediments, contained in Whirlpak® bags, were compressed into a minimum 1-cm deep ‘block’ and measured for 2 seconds. Storage bags were thin

and did not interfere with sensor function, therefore no correction was needed. A calibration standard was measured after every 10 samples to detect and correct for sensor drift. Peaks in magnetic susceptibility were used to identify known historical events in sediment stratigraphies, including earthquakes, the formation of the Kluane River, and the White River tephra layer (Bertrand *et al.* 2008; Brahney *et al.* 2008b; Bunbury & Gajewski 2009).

2.4 Inferred Chlorophyll-*a*

Past variations in in-lake primary production were tracked as VRS-inferred chlorophyll-*a* concentrations in cores 3B and 4A. In core 3B, the top 13 sections (surface to 6 cm depth) were analyzed, followed by alternating samples (every 2 cm) to the bottom of the core. In core 4A, the top 10 sections (surface to 4.5 cm depth) were analyzed, followed by every other section to 10 cm depth, followed by every fourth section to the bottom of the core. Measurements were made at the Paleoecological Environmental Assessment and Research Lab (PEARL) at Queen's University, Kingston, ON. The method provides an estimate of total primary production as it estimates the concentration of chlorophyll-*a* and its derivatives, which accounts for any pigment diagenesis (Michellutti *et al.* 2010). Briefly, freeze-dried sediments were homogenized and sieved through a 125-μm mesh to remove the influence of particle size and water content on reflectance (Michellutti *et al.* 2010). Sieved samples were analyzed using a FOSS NIRS (Near Infrared Spectrophotometer) Model 6500 series Rapid Content Analyzer operating over the range of 400 to 2500 nm. See Wolfe *et al.* (2006) for calibration information for chlorophyll-*a* family pigment quantification.

2.5 Sediment Mercury Concentrations

Total mercury concentrations in sediment were measured on cores 3B and 4A. In core 3B, every 0.5-cm section was measured from the surface to 10-cm depth, followed by alternate sections (every 1 cm) down to 25-cm depth, followed by alternate sections (every 2 cm) to the core bottom. In core 4A,

every section was measured from surface to 5-cm depth, followed by alternate sections (every 1 cm) down to 25-cm depth, followed by alternate sections (every fourth section) to the core bottom.

Total mercury concentration in sediments was determined using a Milestone DMA-80 (direct mercury analyzer) in accordance with EPA method 7473 and ISO 17025 QA/QC at the Biotron Experimental Climate Change Research Centre, Western University, London, ON. The calibration detection limit was 1 ng g^{-1}. Briefly, approximately 25 mg of freeze-dried, homogenized sediments were weighed into tin boats and analyzed by the DMA. After every 10^{th} sample, a duplicate sample was analyzed (mean % difference ± SD: 3.82% ± 4.04%, n = 37). A certified reference material (MESS-3: 0.091± 0.009 μg g^{-1} dw; National Research Council of Canada) was analyzed every 10 samples (mean recovery ± SD: 117.93% ± 3.79%, n = 32). Blanks were analyzed at the start of each run and after every 10 samples (mean ± SD: 0.070 ng Hg ± 0.045 ng, n = 35).

2.6 Sediment Dating

To develop age-depth relations in recently deposited sediments (i.e., last 150 years), subsamples of freeze-dried sediments were analyzed for a minimum of two days for radioisotope activities of ^{210}Pb, ^{226}Ra (as ^{214}Bi and ^{214}Pb together), and ^{137}Cs, using an Ortec co-axial HPGe Digital Gamma Ray Spectrometer interfaced with Maestro 32 software, at the University of Waterloo Environmental Change Research (WATER) laboratory. Weighed sediments were packed into 8-mL polypropylene tubes to a standard height of 35 mm, and a TFA Silicone Septum (Supelco™) was placed over top. The tubes were sealed with 1 cm^3 quick-cure epoxy resin (Devcon® product No. 14310), and allowed to equilibrate for a minimum of 14 days prior to analysis. Core chronologies were developed using the Constant Rate of Supply (CRS) model (Appleby 2001). Peaks observed in ^{137}Cs, corresponding to the 1963 maximum nuclear fallout in the Northern Hemisphere, were used to confirm sediment chronologies (Jaakkola *et al.* 1983).

To determine sediment ages beyond the range of $^{210}Pb/^{137}Cs$ dating techniques, two wood fragments, found in cores 3B (52 cm depth) and 4A (38 cm), were processed for ^{14}C dating. The wood fragments were pre-treated at the University of Waterloo Environmental Isotope Laboratory (UW-EIL) using the acid-alkali-acid method to remove inorganic carbonates, adhered humates, and any atmospheric carbon that may have been incorporated since deposition (Gupta & Polach 1985). Treated samples were then combusted and the carbon dioxide released was trapped in 6-mm OD Pyrex glass break-seal tubes. Break-seal tubes were analyzed using DirectAMS radiocarbon techniques at Accium Biosciences Accelerator Mass Spectrometry Laboratory, Seattle, WA. A subsample of carbon dioxide was evolved for stable carbon isotope analysis to correct ^{14}C ages (Stenström *et al.* 2011).

The White River tephra, a widespread layer of volcanic ash that covered the southwestern Yukon at approximately CE 803 ± 60 years, was also used to define age-depth relationships (Clague *et al.* 1995; Bunbury & Gajewski 2009). This layer was identified in core 3A by qualitative sediment descriptions characterized during core sectioning and by a distinct maximum in magnetic susceptibility in the core stratigraphy following previous research (Brahney et al. 2008b; Bunbury & Gajewski 2009).

2.7 Age-Depth Modelling

Preliminary analyses of dry density, magnetic susceptibility, and LOI data indicated the preservation of several historical earthquake events as homogenite-like layers (Clague 1981 Fig. 9; Bertrand *et al.* 2008; Lamontagne *et al.* 2008) in Kluane Lake sediments. The known CE 1899 Yakutat Bay earthquakes and two regional earthquakes in CE 1956 were identified in cores 3B and 4A, and were used as chronological markers during age-depth model development. The formation of the Kluane River (CE 1680 – 1700; Clague *et al.* 2006) was also identified in both sediment cores and used as an additional marker. An error value was assigned for the Kluane River formation based on the range

provided by Clague *et al.* (2006), and earthquakes were assigned error values that reflect the core section interval (0.5 or 1 cm) in which the earthquake was identified.

The White River tephra, ^{14}C ages and error, CRS-modelled $^{210}Pb/^{137}Cs$ ages and error, and historical hydrological and earthquake events were used, as applicable, to develop age-depth models for both cores using a Bayesian model implemented within the software package "Bacon" (Blaauw & Christen 2011). This software package, executed within the R statistical environment, combines multiple methods of sediment dating and prior knowledge about accumulation rates in a lake to reconstruct sediment accumulation rates (Blaauw & Christen 2011; R Core Team 2016). Radiocarbon ages were converted to calendar ages distributions using the IntCal13 calibration curve during age-depth model development (Reimer *et al.* 2013). Briefly, sediment cores are divided into *n*-sections (*n* is user-defined) and the accumulation rate is estimated for each section using the probability density function for each age. The number of sections used in age-depth model development was selected to minimize errors in ages and was core-specific. For core 3B, 32 sections (2-cm each) were used, and for core 4A, 19 sections (3-cm each) were used. The resulting age-depth models combined the estimated accumulation rates and their variability through millions of Markov Chain Monte Carlo (MCMC) iterations. Sediment ages were determined using the weighted mean age for each sediment interval (either 1-cm or 0.5-cm intervals). More information regarding the Bacon age-depth model procedure can be found in Blaauw & Christen (2011, 2013) and Appendix A.

Weighted mean ages, dry density (g cm^{-3}), and vertical accumulation rate (cm yr^{-1}) were used to calculate dry mass accumulation rates for each sediment core section

2.8 Numerical and Statistical Analyses

All statistical analyses were conducted using the software R version 3.2.5. R packages used included 'Bacon' v2.2, 'rioja' v0.9-9, and 'Hmisc' v4.0-3 (Blaauw & Christen 2011; Juggins 2015; Harrell 2017).

To characterize the effect of past hydrological changes on mercury dynamics in Kluane Lake, periods of hydrological influence were determined *a priori* following Brahney *et al.* (2008a,b). Two periods were determined within the past 1 200 years: the Duke River period (ca. CE 750 to CE 1650) and the Ä'äy Chù period (ca. CE 1650 to CE 2015). Periods were bounded to reflect the time in which these rivers were the major source of water and sediment to Kluane Lake.

Mercury accumulation rates were calculated as the product of dry mass accumulation rates of sediment and sediment mercury concentrations. Mean mercury accumulation rates, dry mass accumulation rates, and sediment mercury concentrations were compared between and within hydrological periods within and among cores using Student's t-tests. During the Ä'äy Chù period, data were subdivided between pre-industrial (CE 1700 to CE 1850) and recent (CE 1950 to CE 2015) time blocks and compared within and among sediment cores using Student's t-tests in order to determine the differences in these parameters prior to and during the height of anthropogenic mercury release.

To determine whether dry mass accumulation rate or sediment mercury concentration was more important in determining mercury accumulation within lake regions during each *a priori* hydrological period, mercury accumulation rates were regressed against each of mercury concentration and dry mass accumulation rate, in order to determine the strongest predictor of mercury accumulation rate. The predictor that had a stronger relation with mercury accumulation rates, based on R^2 and p-values from the linear regression, was then correlated with paleolimnological proxies from that core,

including organic content, carbonate content, magnetic susceptibility, and VRS-inferred chlorophyll-*a*. In the case where both predictors had strong relations with mercury accumulation rate, both predictors were correlated with proxies. Visual inspection of regression residual plots and the Shapiro-Wilk test ($\alpha = 0.05$) were both used to evaluate residual normality. A Levene's test was used to assess homogeneity of variances ($\alpha = 0.05$) for linear regression analysis.

Prior to regression analysis, statistical outliers were removed from stratigraphic data, in order to elucidate broad relationships in sediments without the influence of sediment disturbance events. Outliers were defined as being less than: $1st\ quartile - 2 \times IQR$, or greater than: $3rd\ quartile + 2 \times IQR$, where IQR is the interquartile range. Mercury accumulation rates, mercury concentration, and dry mass accumulation rates were evaluated for outliers.

To place the results of this study in the broader context of the southern Yukon, mercury accumulation rates, focus-corrected mercury accumulation rates, sediment mercury concentrations, and dry mass accumulation rates from Kluane Lake were compared to nine other southern Yukon lakes (data from Drevnick *et al.* 2016). Mercury enrichment metrics were used to evaluate anthropogenic mercury loading to these southern Yukon lakes and to compare among lakes. To do this, uncorrected anthropogenic accumulation rate (termed anthropogenic flux in the literature: ΔF), adjusted anthropogenic flux (ΔF_{adj}), focus-corrected anthropogenic flux (ΔF_F), and focus-corrected and adjusted anthropogenic flux ($\Delta F_{adj,F}$) for cores from Kluane Lake and other Yukon lakes were calculated and compared qualitatively, where possible, following mathematical methods presented in Muir *et al.* (2009). For these analyses, stratigraphic records were truncated at CE 1700. The pre-industrial period was defined as ranging from CE 1700 to CE 1850, and the recent period was defined as ranging from CE 1950 to the top of a sediment core.

To calculate the proportion of anthropogenically-enriched mercury relative to baseline accumulation rate (anthropogenic flux, ΔF), the difference between recent and pre-industrial fluxes is calculated (Muir *et al.* 2009):

$$\Delta F = F_{recent} - F_{pre\text{-}industrial} \quad (1)$$

This metric assumes that the environmental baseline flux has not changed from the pre-industrial period to the recent period, and that the difference in fluxes must be the proportion of mercury flux due to anthropogenic contributions (Muir *et al.* 2009). However, as it is unlikely that sedimentation rate remains constant, adjusted anthropogenic flux (ΔF_{adj}) are calculated to correct for differences in sedimentation rate between pre-industrial and recent periods (Perry *et al.* 2005; Muir *et al.* 2009):

$$\Delta F_{adj} = \Delta F - (F_{pre\text{-}industrial} \cdot \text{sedimentation ratio} - F_{pre\text{-}industrial}), \quad (2)$$

where the sedimentation ratio is the ratio of recent sedimentation rate to pre-industrial sedimentation rate. This allows for the correction of mercury flux if the recent sedimentation rate is different from the pre-industrial sedimentation rate.

Lake sediments do not remain immobile once deposited on the lake bottom, and movement of sediments within a lake, from shallower to deeper parts of the lake, called 'sediment focusing', can affect dry mass accumulation rates and therefore mercury accumulation rates (van Metre & Fuller 2009). In order to correct for sediment focusing, anthropogenic flux is divided by a sediment focus factor determined during ^{210}Pb dating (Muir *et al.* 2009):

$$\Delta F_F = \Delta F / FF, \quad (3)$$

where *FF* is the focusing factor (see Muir *et al.* 2009). This factor is calculated as the ratio of observed ^{210}Pb accumulation rate (termed 'flux' in the literature; dpm cm^{-2} yr^{-1}) in a sediment core to the predicted ^{210}Pb flux for the latitude of the core site (see Muir *et al.* 2009).

Since in-lake sediment focusing and differences in sedimentation rates between the pre-industrial and recent periods can both affect anthropogenic mercury fluxes, corrections for both can be combined to produce a focus-corrected adjusted anthropogenic flux value (Muir *et al.* 2009):

$$\Delta F_{adj,F} = \Delta F_{adj} / FF. \quad (4)$$

Chapter 3
Results & Interpretation

3.1 Core Age-Depth Models

3.1.1 Core 3B

Total ^{210}Pb activity decreased with depth, from 7.92 dpm g^{-1} at the surface to 1.64 dpm g^{-1} at 5 cm, before increasing to 2.32 dpm g^{-1} at 8.0-cm depth (Figure 3A). Measured total ^{210}Pb activity at 3.5-cm depth (1.98 dpm g^{-1} ± 0.18, 1 SD) was within 1 standard deviation of the mean estimated supported ^{210}Pb activity (2.10 dpm g^{-1} ± 0.24, 1 SD), indicating that background was reached. However, measured ^{210}Pb activity exceeded background values at 4-cm depth, before returning to background at 4.5-cm depth (Figure 3A). The peak activity of ^{137}Cs (1.68 dpm g^{-1} ± 0.06, 1 SD) was measured at 2.75-cm depth, corresponding with a CRS date of CE 1963 (± 7.3 yr, 1 SD). The CRS model produced a core-bottom age of CE 732.

The normalized radiocarbon age of the twig recovered from core 3B was determined to be 1 108 radiocarbon YBP ± 26 (1 SD). The White River tephra was identified in core 3A using magnetic susceptibility, at a mean depth of 57.5 cm (SD: 0.5 cm), corresponding to 1147 YBP or CE 807 (SD: 60.5 years; Clague *et al.* 1995). Loss-on-ignition data were used to align cores 3A and 3B and allow use of the White River tephra layer in age-depth modeling for core 3B (see Appendix A). The tephra layer was not identified in core 3B. The Yakutat Bay earthquake event, corresponding to CE 1899, was identified in core 3B at 5.5 cm depth (± 0.5 cm) using several proxies, including dry density, magnetic susceptibility, and LOI data (Figures 4A & 5).

Radiocarbon age and standard deviation, CRS-ages and standard deviations, and the depth of White River tephra were used to develop an age-depth model for core 3B using a Bayesian model implemented in R ('Bacon' model; Figure 4A). Results from the Bacon model produced a core-

bottom weighted mean age of approximately CE 807 (95% confidence interval: CE 694 – CE 899; Figure 4A). See Appendix A for further information.

3.1.2 Core 4A

Total ^{210}Pb activity in core 4A increased from the surface (13.50 dpm g^{-1}) to 0.5-cm depth (13.74 dpm g^{-1}) before declining with depth to 2.16 dpm g^{-1} at 7 cm depth, at which point background was reached (Figure 3B). The peak activity of ^{137}Cs (2.22 dpm g^{-1} ± 0.06, 1 SD) was measured at 3.25-cm depth, corresponding with a CRS date of CE 1963 (± 16.7 yr, 1 SD). The CRS model produced a core-bottom age of CE 1262.

The normalized radiocarbon age of the twig recovered from core 4A was determined to be 577 radiocarbon YBP ± 25 (1 SD). The Yakutat Bay earthquake event, corresponding to CE 1899, was identified at 10.5 cm depth (± 1 cm) using several proxies mentioned above. Radiocarbon age and standard deviation, and CRS-ages and standard deviations were used to develop an age-depth model for core 4A using 'Bacon' (Figure 4B). This model produced a core-bottom weighted mean age of approximately CE 1009 (95% confidence interval: CE 729 – CE 1220; Figure 4B). See Appendix A for further information.

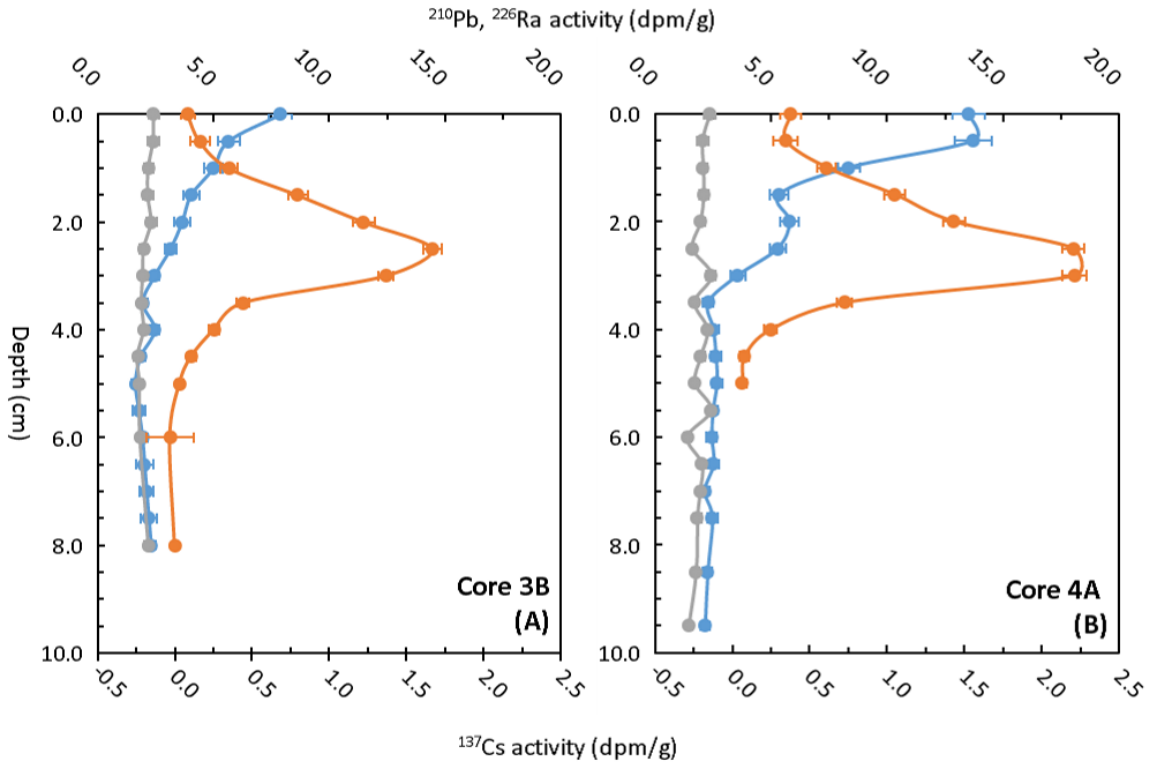

Figure 3. Radioisotope activities (dpm g^{-1}) and standard deviation (^{137}Cs in orange, ^{210}Pb in blue, ^{226}Ra in grey) measured in core 3B (A), and core 4A (B) from Kluane Lake. Peaks in ^{137}Cs activities in cores 3B (B) and 4A (C) correspond with CE 1963.

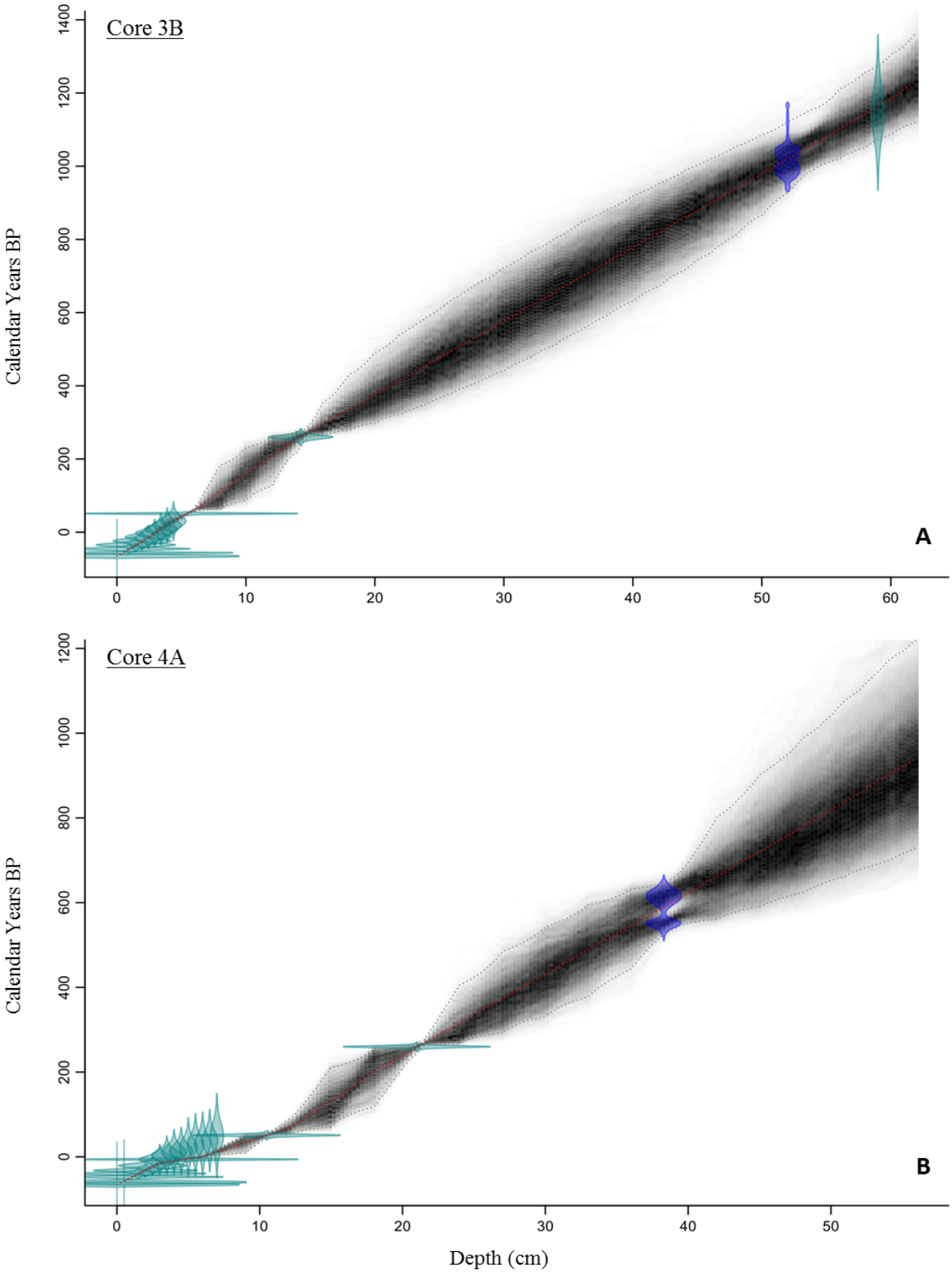
Core 3B
Calendar Years BP
0
200
400
600
800
1000
1200
1400
0
10
20
30
40
50
60
A
Core 4A
Calendar Years BP
0
200
400
600
800
1000
1200
0
10
20
30
40
50
B
Depth (cm)

Figure 4. Age-depth relations for core 3B (A) and core 4A (B) from Kluane Lake, developed using Bacon. Radiocarbon dates were calibrated using IntCal13 (Reimer *et al.* 2013) and plotted in blue. CRS model dates and marker layers (including the CE 1899 Yakutat Earthquake and formation of the Kluane River in CE 1690, and the White River tephra layer CE 803) are plotted in teal. The weighted mean age-depth model is plotted with a red dashed line, the 95% confidence intervals are plotted in a grey dotted line, and the MCMC iterations for each section age are plotted as a black cloud: darker black represents a higher frequency of occurrence. Ages are plotted as calendar years before present (YBP, before CE 1950). See Blaauw & Christen (2011, 2013) for more information on Bacon age-depth modelling.

3.2 Description of Sediment Stratigraphies

Age-depth relationships for the sediment cores indicated that cores 3B and 4A span two known and previously described periods of hydrological influence in Kluane Lake. Stratigraphic profiles in both cores show increased variability and changing trends in sediment core stratigraphies after ca. CE 1650, which corresponds with hydrological changes that occurred at this time (Brahney *et al.* 2008a,b). The two hydrological periods are herein defined as the Duke River Period (CE 750 to CE 1650) and the Ä'äy Chù Period (CE 1650 to CE 2015) (see Brahney *et al.* 2008a,b).

3.2.1 The Duke River Period (CE 750 to CE 1650)

During the Duke River period (shown in grey shading in Figures 5 & 6), distinct peaks in carbonate content, magnetic susceptibility, dry density, dry mass accumulation rate, mercury concentration, and mercury accumulation rate were observed in core 3B ca. CE 1535 (bottom red dashed line in Figure 5). Similar peaks were not observed in core 4A. These peaks may reflect effects of the Sheep Mountain landslide, a large slope-failure event in the Kluane Ranges, which occurred between ca. CE 49 (95% credible interval: BCE 58 – CE 179) and ca. CE 1426 (95% credible interval: CE 1324 – CE 1515; Clague 1981). Core site 3 is much closer than core site 4 to Sheep Mountain (Figures 1 & 2), which likely explains why this event was observed only in core 3B.

In general, few trends were evident in sediment stratigraphies during the Duke River period. Mercury accumulation rates were similar between cores 3B and 4A, but showed no obvious temporal trends (Figures 5 & 6). Sediment mercury concentrations ranged from 1.3 to 2.1 times higher in core 3B than in core 4A, while dry mass accumulation ranged from similar (1.0) to 2.2 times higher in core 4A than 3B during this period (Figures 5 & 6). No trends were obvious in either variable in the cores during this period. While somewhat higher in core 4A than in 3B, carbonate content decreased slowly in both cores during this period, indicating the slow decline of Duke River inflow and the carbonate-rich sediments it likely carried into Kluane Lake (Figures 5 & 6). VRS-inferred chlorophyll-*a* concentrations were generally higher in core 4A than in core 3B, but chlorophyll-*a* concentrations increased steadily in core 3B during this period and resembled those in core 4A after ca. CE 1580. The steady increase of chlorophyll-*a* concentration in core 3B may reflect increasing water clarity in the Middle region as sediment influx from the Duke River decreased to the end of this period. Temporal trends in other proxies were not evident in either core.

3.2.2 The Ä'äy Chù Period (CE 1650 to CE 2015)

Following the transition from the Duke River Period (CE 750 to CE 1650) to the Ä'äy Chù Period (unshaded in Figures 5 & 6; CE 1650 to CE 2015), increases in stratigraphic variability and the occurrence of distinct peaks were noted in cores 3B and 4A (Figures 5 & 6). Distinct peaks in multiple proxies, including carbonate content, mineral content, magnetic susceptibility, dry density, dry mass accumulation rate, mercury concentration, and mercury accumulation rate, were observed in both cores ca. CE 1690, CE 1900, and CE 1955 (Figures 5 & 6). The largest of the identified peaks occurred ca. CE 1690 (shown in blue on Figures 5 & 6) in magnetic susceptibility, dry density, dry mass accumulation rate, mercury concentration, and mercury accumulation rate in both cores, as well as carbonate content in core 4A only: these peaks conform with the formation of the Kluane River (CE 1680 – CE 1700; Clague *et al.* 2006). This event was previous identified by Brahney *et al.*

(2008b) using similar proxies. Water levels rose quickly ca. CE 1630 until the formation of the Kluane River, after which the lake drained rapidly (Brahney *et al.* 2008b). This water level increase and subsequent decrease is reflected in the structure of the observed peaks. The rising arm of the peaks reflects the rising water levels and the falling arm of the peaks reflects the draining of Kluane Lake.

The second set of peaks ca. CE 1900 (middle red dashed line in Figure 5; bottom dashed red line in Figure 6) were more distinct in core 3B than 4A, but included increases in carbonate content, magnetic susceptibility, dry density, dry mass accumulation rate, and mercury accumulation rate in core 3B (Figure 5), as well as an increase in mineral content in core 4A (Figure 6). A similar layer of dense, silty sediments was identified in a Kluane Lake sediment core around this time by Doig (1998). These peaks conform with the CE 1899 Yakutat Bay, Alaska, earthquakes (Lamontagne *et al.* 2008). This large earthquake event was likely more distinct in core 3B due to its proximity (approx. 20 km closer) to the epicenter compared with core 4A: the absolute increase in dry mass accumulation rate was similar between core 3B and 4A but the scale of the stratigraphic plot differs between cores, due to the magnitude of the effect that the ca. CE 1955 earthquake had on the stratigraphy of core 4A. The final series of peaks ca. CE 1955 (top red dashed line in Figures 5 & 6) were more distinct in core 4A than in core 3B, and included short-lived increases in magnetic susceptibility, dry density, dry mass accumulation rate, and mercury accumulation rate in both cores (Figure 5 & 6). These peaks conform with two regional earthquakes that occurred around Kluane Lake in CE 1956 with epicenters near the south end of Kluane Lake and adjacent to the Talbot Arm (Clague 1981 Fig. 9), in close proximity to core site 4 (Figure 2). The CE 1899 and CE 1956 earthquake events were used as marker layers during iterative development of the Bayesian sediment age-depth model.

Visual differences in stratigraphic profiles are evident between the Duke River and Ä'äy Chù periods in Kluane Lake. The Duke River period was characterized by lower relative stratigraphic variability, with similar mercury accumulation rates observed between the Middle region and the Talbot Arm. Generally, stratigraphic variability was higher in most proxies in both cores during the Ä'äy Chù period compared with the Duke River period, likely driven in part by the numerous earthquakes that occurred during the Ä'äy Chù period. Magnetic susceptibility and dry density declined in both cores during the Ä'äy Chù period (Figures 5 & 6), and a distinct decline in chlorophyll-a in both cores occurred during the early/mid 1900s (Figures 5 & 6). In core 3B, carbonate content and organic content appear similar between hydrological periods with no temporal trends observed between periods (Figure 5). In core 4A, mineral content appears to be similar between hydrological periods, although becomes more variable during the Ä'äy Chù period (Figure 6). Magnetic susceptibility and dry density both decline during the Ä'äy Chù period in core 4A, while organic content increases beginning around ca. CE 1900 (Figure 6). After CE 1900, mercury accumulation rates declined in both cores (Figures 5 & 6). Mean dry mass accumulation rate and mercury accumulation rate in both cores during the Ä'äy Chù period do not appear to differ from the Duke River period, although they do become more variable during the Ä'äy Chù period (Figures 5 & 6). While mercury concentration does not appear to differ between periods and shows no temporal trend throughout core 3B (Figure 5), mercury concentrations increase in core 4A during the Ä'äy Chù period, particularly following the formation of the Kluane River, beginning ca. CE 1750 (Figure 6). Mercury concentrations in core 4A are approximately 1.2 times greater during this period than during the Duke River period.

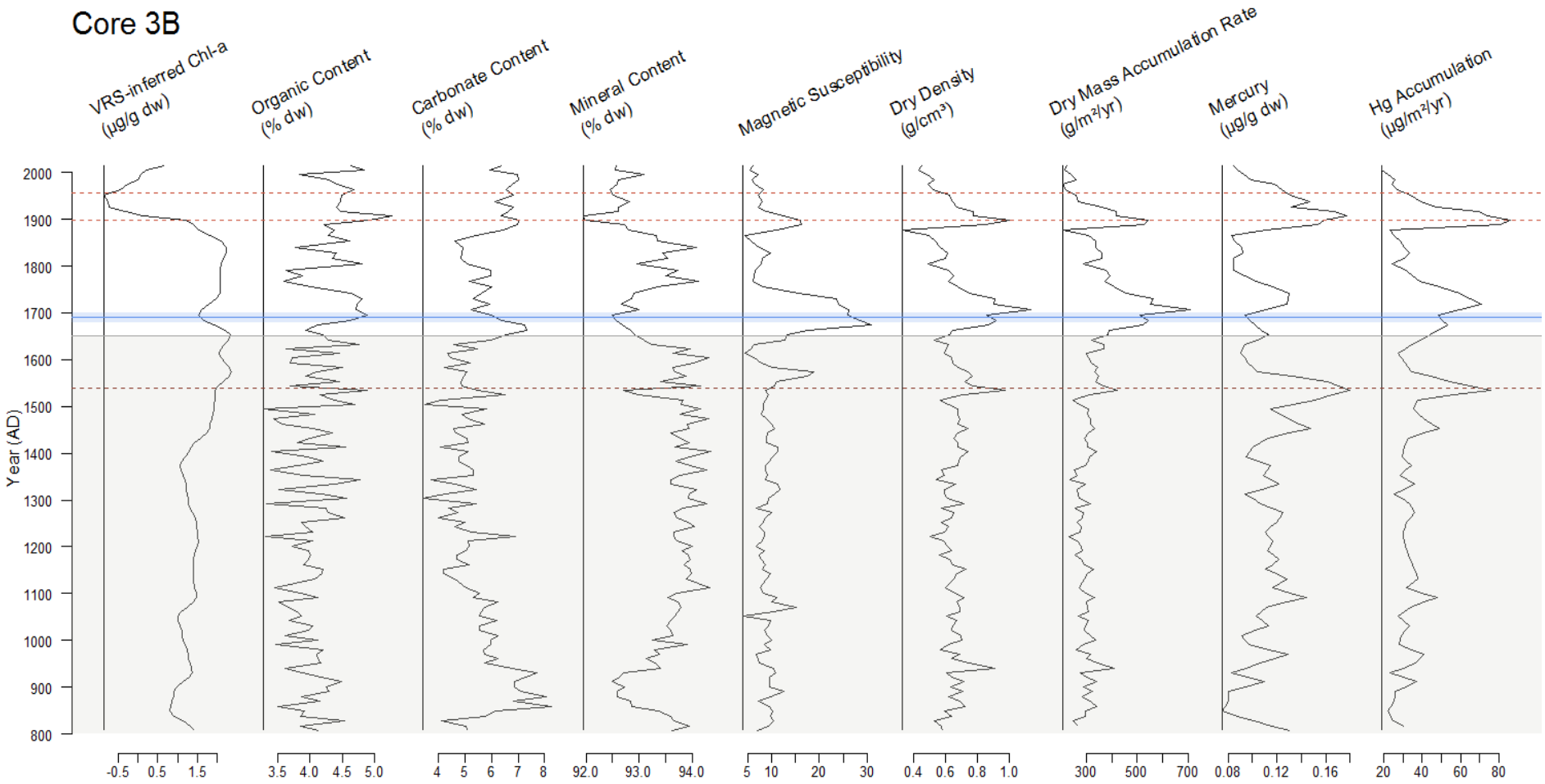
Core 3B
VRS-inferred Chl-a (µg/g dw)
Organic Content (% dw)
Carbonate Content (% dw)
Mineral Content (% dw)
Magnetic Susceptibility
Dry Density (g/cm³)
Dry Mass Accumulation Rate (g/m²/yr)
Mercury (µg/g dw)
Hg Accumulation (µg/m²/yr)
Year (AD)
2000
1900
1800
1700
1600
1500
1400
1300
1200
1100
1000
900
800
-0.5 0.5 1.5
3.5 4.0 4.5 5.0
4 5 6 7 8
92.0 93.0 94.0
5 10 20 30
0.4 0.6 0.8 1.0
300 500 700
0.08 0.12 0.16
20 40 60 80

Figure 5. Sediment stratigraphy for measured paleolimnological proxies in core 3B collected from the Middle region of Kluane Lake. The Duke River period is shown with grey shading, the Ä'äy Chù period is not shaded. The blue solid line represents the formation of the Kluane River (CE 1690) and the blue shading represents the year range for the river's formation (CE 1680 to 1700; Clague *et al.* 2006). The dark red dashed lines represent major sediment disturbance events: CE 1534, CE 1899, and CE 1956.

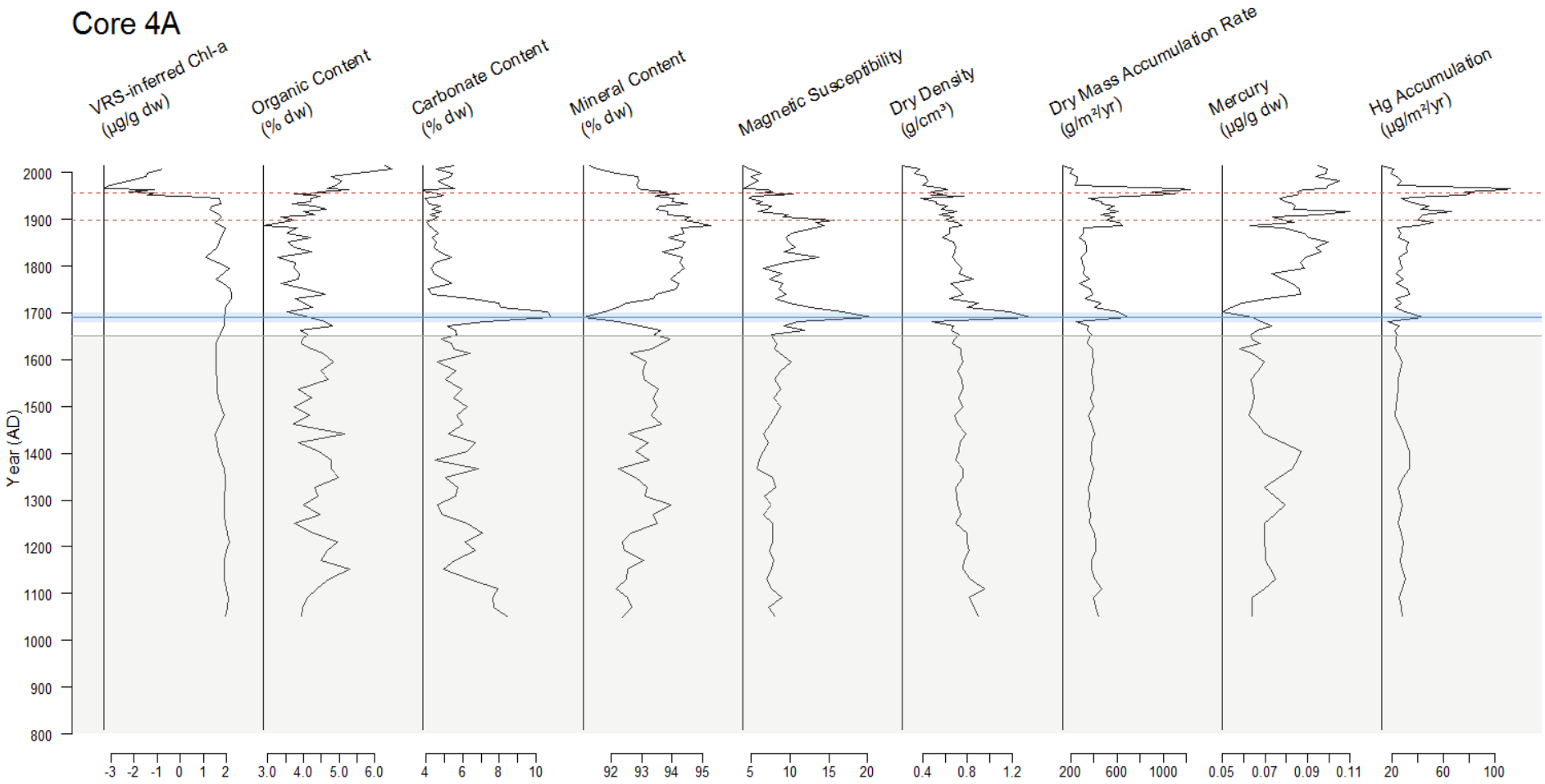
Core 4A
VRS-inferred Chl-a (µg/g dw)
Organic Content (% dw)
Carbonate Content (% dw)
Mineral Content (% dw)
Magnetic Susceptibility
Dry Density (g/cm³)
Dry Mass Accumulation Rate (g/m²/yr)
Mercury (µg/g dw)
Hg Accumulation (µg/m²/yr)
Year (AD)
2000
1900
1800
1700
1600
1500
1400
1300
1200
1100
1000
900
800
-3 -2 -1 0 1 2
3.0 4.0 5.0 6.0
4 6 8 10
92 93 94 95
5 10 15 20
0.4 0.8 1.2
200 600 1000
0.05 0.07 0.09 0.11
20 60 100

Figure 6. Sediment stratigraphy for measured paleolimnological proxies in core 4A collected from the Middle region of Kluane Lake. The Duke River period is shown with grey shading, the Ä'äy Chù period is not shaded. The blue solid line represents the formation of the Kluane River (CE 1690) and the blue shading represents the year range for the river's formation (CE 1680 to 1700; Clague *et al.* 2006). The dark red dashed lines represent major sediment disturbance events: CE 1899, and CE 1956.

3.3 Spatiotemporal Differences in Mercury Dynamics

Table 1. Mean (SD) mercury concentration, mercury accumulation rate, and dry mass accumulation rate in cores 3B and 4A in the Duke River period and the Ä'äy Chù period, including pre-industrial (pre-1850s) and recent (post-1950) mean values, and mean values for the entire Ä'äy Chù period.

Core	Duke River Period	Ä'äy Chù Period		
		Entire Period	Pre-Industrial	Recent
Mercury concentration (SD; μg g^{-1} dw)				
3B (Middle region)	0.113 (0.022)	0.113 (0.028)	0.101 (0.017)	0.105 (0.019)
4A (Talbot Arm)	0.069 (0.007)	0.083 (0.014)	0.075 (0.014)	0.094 (0.007)
Mercury accumulation rate (SD; μg m^{-2} yr^{-1})				
3B (Middle region)	36.92 (11.51)	34.32 (18.77)	30.48 (10.86)	24.34 (5.23)
4A (Talbot Arm)	26.63 (3.33)	37.70 (22.61)	27.37 (5.91)	53.21 (38.49)
Dry mass accumulation rate (SD; g m^{-2} yr^{-1})				
3B (Middle region)	324 (43)	301 (93)	317 (79)	231 (22)
4A (Talbot Arm)	388 (26)	476 (260)	374 (110)	627 (441)

3.3.1 The Duke River Period

During the Duke River period, mean mercury concentration and accumulation rate were significantly higher in core 3B than core 4A ($t_{59} = 8.4910$, $p < 0.0001$; $t_{58} = 3.8079$, $p = 0.0003$, respectively). However, mean dry mass accumulation rate was significantly higher in core 4A than 3B ($t_{113} = 7.9713$, $p < 0.0001$). The higher mercury accumulation rate in the Middle region (core 3B) was driven by higher mercury concentrations in sediments in this region (Table 1).

Following statistical outlier removal, mercury accumulation rates were better predicted by mercury concentration (3B: $R^2 = 0.532$, $p < 0.0001$; 4A: $R^2 = 0.490$, $p = 0.0018$; Figure 7 top) than by dry mass accumulation rate in both cores during the Duke River period. (3B: $R^2 = 0.404$, $p < 0.0001$; 4A:

R^2 = 0.400, p = 0.0065; Figure 7 bottom). Because both mercury concentration and dry mass accumulation were significant predictors of mercury accumulation rate, both were correlated with paleolimnological proxies to better understand ultimate drivers of sediment mercury accumulation in the lake (Table 2).

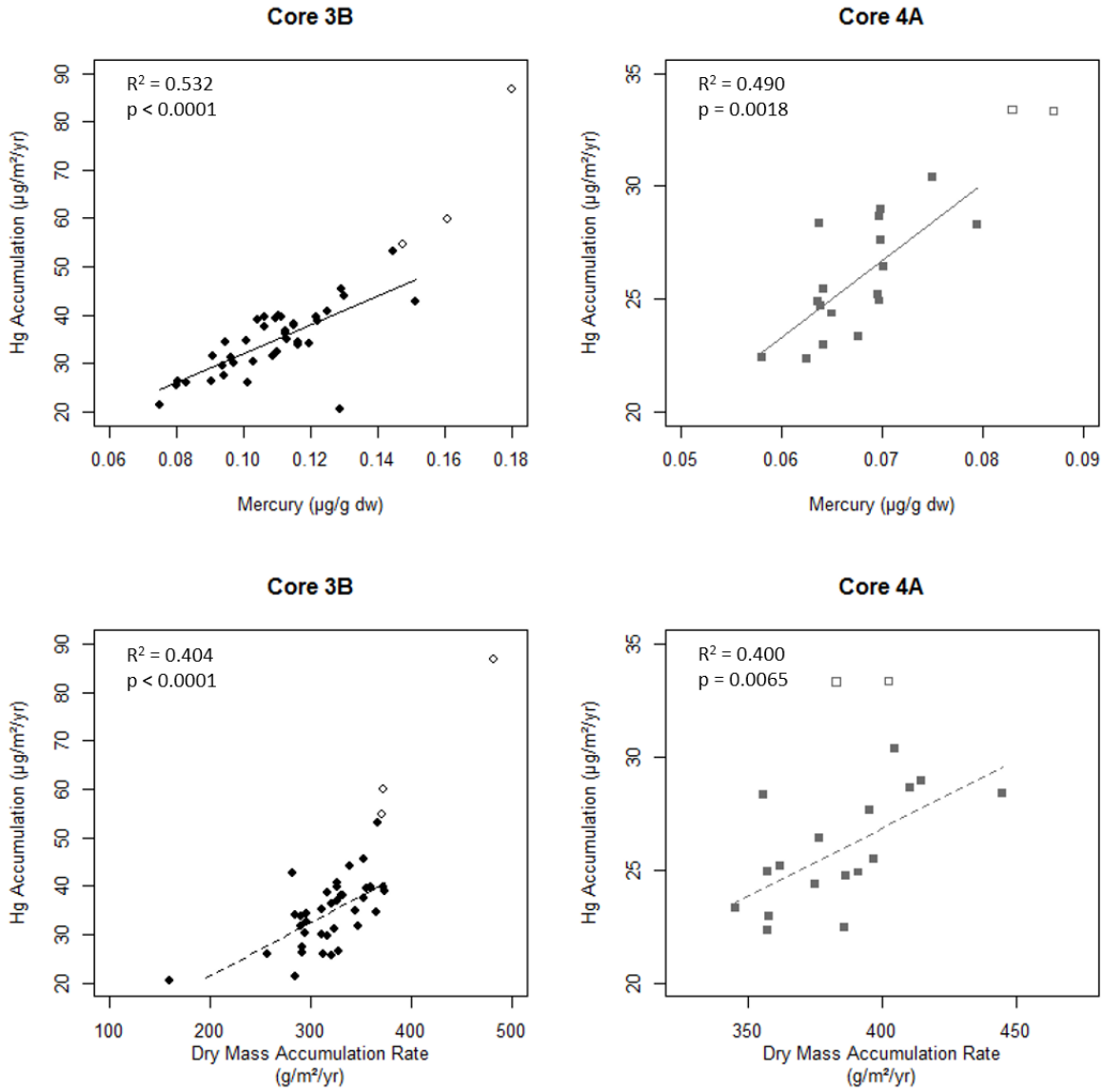

Figure 7. Linear regression relationships between mercury accumulation rates and mercury concentrations (top) and dry mass accumulation rates (bottom) in cores 3B (left) and 4A (right) during the Duke River period. Statistical outliers are plotted as hollow symbols but were not included in the regression analysis.

In core 3B, mercury concentration was positively correlated with mineral content, which suggests an inorganic or geologic source of mercury, and negatively correlated with carbonate content, indicating possible dilution of mercury by glacial sediment inputs (Table 2). Dry mass accumulation rate was positively correlated with magnetic susceptibility, which suggests watershed erosion was an important source of sediments to the Middle region (Table 2). In core 4A, mercury concentration was not significantly correlated with any other measured proxies (Table 2). Dry mass accumulation rate was positively correlated with carbonate content, which suggests that the glacial inflow was an important source of sediments to the Talbot Arm during the Duke River period, and negatively correlated with mineral content, which suggests geologic (and non-glacial) contributions to sediments were minimal (Table 2).

Table 2. Significant correlations between mercury concentration and paleolimnological variables, and dry mass accumulation rate and paleolimnological proxies in cores 3B and 4A, during the Duke River period in Kluane Lake.

Core	Proxy	Pearson R	p-value
Mercury concentration			
3B	Carbonate content	-0.430	0.0063
	Mineral content	0.400	0.0117
4A	*none*		
Dry mass accumulation rate			
3B	Magnetic susceptibility	0.329	0.0030
4A	Mineral content	-0.731	< 0.0001
	Carbonate content	0.644	0.0001

Overall, the results of the correlations indicate that allochthonous inputs of mercury drive accumulation rates in both regions during the Duke River period. However, different major sediment sources to each region drive the inter-core differences. The Talbot Arm during this period was closer

to the Duke River inflow and likely received more glacial sediments than the Middle region. As water levels were much lower during this period in Kluane Lake, site 3 (Middle region) would have received proportionally more terrestrial inputs than glacial inputs because it would have been much closer to the lake margins than the Duke River inflow (Figures 1 & 2).

3.3.2 Differences Between Hydrological Periods

Temporal differences between hydrological periods in mercury accumulation rates and drivers of mercury accumulation varied between sediment cores. In core 3B, there were no significant differences in mean mercury concentration, mean mercury accumulation rate, or mean dry mass accumulation rate between the Duke River and Ä'äy Chù periods ($t_{67} = 0.0665$, $p = 0.9472$; $t_{113} = 1.8416$, $p = 0.0682$; $t_{66} = 0.7092$, $p = 0.4807$, respectively; Table 1). However, values became more variable during the Ä'äy Chù period (Table 1), indicated by a higher standard deviation. Similar to core 3B, mean dry mass accumulation rate did not differ between periods in core 4A, but the variability increased during the Ä'äy Chù period (Table 1). Mean mercury concentration and accumulation rate in core 4A were significantly higher during the Ä'äy Chù period than during the Duke River period ($t_{61} = 4.1147$, $p = 0.0001$; $t_{61} = 2.1137$, $p = 0.0386$, respectively; Table 1), and the variability, as standard deviation, was also higher during this period than the Duke River period (Table 1). Increased seismic activity was noted during the Ä'äy Chù period in both sediments cores, and these events likely resulted in peak values for mercury concentration, dry mass accumulation rate, and mercury accumulation rate in both cores during the Ä'äy Chù period. The transition from the Duke River period to the Ä'äy Chù period was associated with a decrease in dry mass accumulation in the Talbot Arm (core 4A) (ignoring the sediment disturbance events identified; see Figure 6 CE 1750 to CE 1850). This decrease in dry mass sedimentation rate also reduced the sediment dilution effects of the Duke River in-flow, which may have resulted in the increased mercury concentration observed during the Ä'äy Chù period in core 4A.

3.3.3 The Ä'äy Chù Period

During the Ä'äy Chù period, mean mercury accumulation rates did not differ significantly between cores ($p = 0.5174$), but mean mercury concentration was significantly higher in core 3B than core 4A ($t_{69} = 6.0131$, $p < 0.0001$; Table 1), while mean dry mass accumulation rate was significantly higher in core 4A than core 3B ($t_{78} = 3.6946$, $p = 0.0004$; Table 1). Mean dry mass accumulation rate was 2.8 times more variable in core 4A than core 3B during this period (Table 1).

When broken down into pre-industrial (CE 1700 to CE 1850) and recent (CE 1950 to CE 2015) time blocks, mean dry mass accumulation and mercury accumulation rates did not differ significantly between cores during the pre-industrial portion of Ä'äy Chù period ($t_{34} = 1.7483$, $p = 0.0894$; $t_{28} = 1.0194$, $p = 0.3168$, respectively). However, mean mercury concentration was significantly higher in core 3B than 4A ($t_{28} = 4.5117$, $p = 0.0001$). During the recent portion of the Ä'äy Chù period, mean mercury concentration and accumulation rates did not differ significantly between cores ($p = 0.0861$, $p = 0.0686$, respectively). But, variability in mercury accumulation rate was 7.4 times higher in core 4A than in core 3B. Also, mean dry mass accumulation rates were significantly higher in core 4A than core 3B ($t_{17} = 2.3468$, $p = 0.0313$). Interestingly, the variability of dry mass accumulation rate during the recent portion of the Ä'äy Chù period was 20 times higher in core 4A than 3B. The earthquake identified in core 4A ca. CE 1956 likely contributed to the high variability in dry mass accumulation and mercury accumulation rate in core 4A during this period.

Within core 3B during the Ä'äy Chù period, mean mercury concentration and mercury accumulation rate did not differ significantly between pre-industrial and recent periods ($t_{16} = 0.5459$, $p = 0.5927$; $t_{16} = 1.3859$, $p = 0.1847$, respectively). However, mean dry mass accumulation rate was significantly higher during the pre-industrial period than the recent period ($t_{22} = 2.8096$, $p = 0.0102$), likely because of high dry mass accumulation rates following the formation of the Kluane River (ca. CE 1690), and the subsequent lowering of Kluane Lake, observed in core 3B.

In core 4A within the Ä'äy Chù period, mean mercury concentration, mean dry mass accumulation rate, and mean mercury accumulation rate were all significantly higher during the recent period than the pre-industrial period (Table 1; $t_{28} = 4.2102$, $p = 0.0002$; $t_{29} = 2.4111$, $p = 0.0255$; $t_{28} = 2.9038$, $p = 0.0071$, respectively). The increased mercury accumulation rates in core 4A during the recent part of the Ä'äy Chù period are being driven by parallel increases in both mercury concentration in sediments, possibly due to anthropogenic mercury pollution, and dry mass accumulation rates, driven by the CE 1956 earthquake near the Talbot Arm.

During the Ä'äy Chù period, mercury accumulation rates were better predicted by dry mass accumulation rate (3B: $R^2 = 0.844$, $p < 0.0001$; 4A: $R^2 = 0.817$, $p < 0.0001$; Figure 8 bottom) than by mercury concentration (3B: $R^2 = 0.761$, $p < 0.0001$; 4A: $R^2 = 0.017$, $p = 0.4123$; Figure 8 top) in both cores. Since both mercury concentration and dry mass accumulation were significant predictors of mercury accumulation rate in core 3B, both predictors were then correlated with paleolimnological proxies (Table 3). Although mercury concentration was not significantly related to mercury accumulation rates in core 4A in the Ä'äy Chù period, mercury concentration was also correlated with proxies (Table 3) in order to better understand the cause for increasing trends in mercury concentration in this core and to inform predictions.

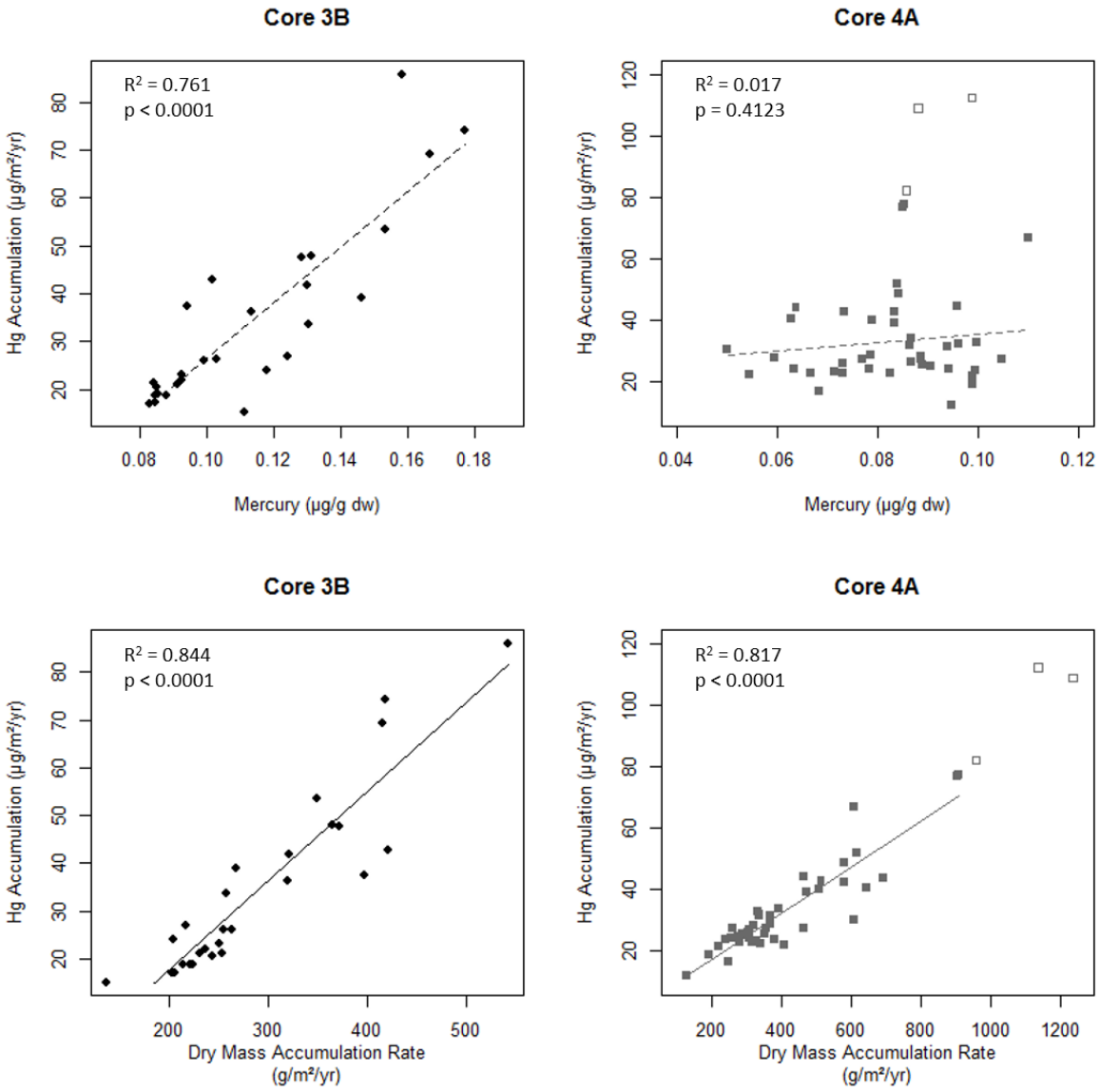

Figure 8. Linear regression relationships between mercury accumulation rates and mercury concentrations (top) and dry mass accumulation rates (bottom) in cores 3B (left) and 4A (right) during the Ä'äy Chù period. Statistical outliers are plotted as hollow symbols but were not included during regression analysis.

In core 3B, dry mass accumulation rate was positively correlated with magnetic susceptibility and organic content (Table 3), which suggests the importance of eroded terrestrial organic materials to lake sediments. Dry mass accumulation rate was negatively correlated with mineral content (Table 3),

suggesting that non-carbonate geologic contributions to sediment accumulation are minimal to this region during this period. During the Duke River period, there was no relationship between dry mass accumulation rate and mineral content in core 3B.

Mercury concentration in core 3B during the Ä'äy Chù period was positively correlated with organic content (Table 3), suggesting that organic matter is acting as a vector for mercury delivery to lake sediments. Mercury concentration was also positively correlated with carbonate content, which suggests that glacial materials may also be contributing mercury to Kluane Lake sediments in this region. These findings contrast with relationships observed during the Duke River period, which suggested glacial sediment dilution of mercury. Anthropogenic, atmospherically-transported mercury deposited on the surface of the Kaskawulsh Glacier is released as the glacial ice melts, and is carried to Kluane Lake via Ä'äy Chù during this period, whereas during the Duke River period, as Canada Peak glacial ice melted (and other smaller alpine glaciers within the catchment), naturally-accumulated mercury was released and transported to Kluane Lake via the Duke River. As the magnitude of atmospheric mercury flux has increased significantly with anthropogenic activities, the quantity of mercury delivered during the Duke River period via the Duke River would most likely be lower than that which was delivered via Ä'äy Chù during the Ä'äy Chù period. During the Ä'äy Chù period, it is possible that the meltwaters from the Kaskawulsh Glacier are acting as both as source of mercury and a diluting agent of mercury entering Kluane Lake.

In core 4A, dry mass accumulation rate was negatively correlated with organic content (Table 3), suggesting that organic materials are not greatly contributing to lake sediments. Similar to what was observed in core 3B, sediment mercury concentration in core 4A was positively correlated with organic content (Table 3), which suggests that organic matter may be a vector for mercury transport to lake sediments, and negatively correlated with carbonate content (Table 3), suggesting a possible dilution effect by carbonate-rich sediments including glacial sediments. Mercury concentrations in

core 4A were also negatively correlated with VRS-inferred chlorophyll-*a* (Table 3), which suggests that algal scavenging is not an important mechanism delivering mercury to lake sediments and supports an allochthonous origin for organic matter in lake sediments. Mercury concentration was also negatively correlated with magnetic susceptibility (Table 3). In this core, magnetic susceptibility was positively correlated with carbonate content (Pearson R = 0.585, p = 0.0001), and negatively correlated with organic content (Pearson R = -0.330, p = 0.0431) and mineral content (Pearson R = -0.331, p = 0.0422), suggesting that increased magnetic susceptibility is related to either glacial contributions or localized carbonate bedrock erosion. The negative relationship between magnetic susceptibility and mercury concentration suggests a possible sediment dilution effect of mercury by carbonate-rich sediments.

Table 3. Significant correlations between dry mass accumulation rate and paleolimnological variables in cores 3B and 4A, and mercury concentration and paleolimnological proxies in core 3B, during the Ä'äy Chù period in Kluane Lake.

Core	Proxy	Pearson R	p-value
Dry mass accumulation rate			
3B	Magnetic susceptibility	0.718	< 0.0001
	Mineral content	-0.459	0.0073
	Organic content	0.362	0.0383
4A	Organic content	-0.331	0.0284
Mercury concentration			
3B	Mineral content	-0.601	0.0009
	Carbonate content	0.499	0.0080
	Organic content	0.385	0.0472
4A	Carbonate content	-0.601	< 0.0001
	VRS-inferred chlorophyll-*a*	-0.504	0.0102
	Magnetic susceptibility	-0.442	0.0079
	Organic content	0.376	0.0153

Overall, the results suggest that there are differences in sediment sources to each region during the Ä'äy Chù period. In the Middle region, dry mass accumulation rates are being driven by terrestrial erosion, particularly organic sediments that originate from the catchment. In the Talbot Arm, organic content is not correlated with dry mass accumulation rates, which indicates that another sediment source is important. The lack of additional significant correlations with dry mass accumulation rate may be a result of small sample size following statistical outlier removal. Mercury in the sediments of the Middle region is likely primarily terrestrial in origin and transported into the lake by terrestrial organic matter. Further, glacial materials may also be contributing mercury to lake sediments in the Middle region. Mercury concentration in the suspended sediments of Ä'äy Chù are relatively high, however, mercury concentrations in the river water are very low, indicating that mercury is bound to the fine sediments carried by this glacial river (H. Swanson, unpubl. data). In the Talbot Arm, sediment mercury also likely originates from terrestrial sources and is delivered to the lake with organic matter acting as a transport vector. Glacial materials and/or localized carbonate bedrock erosion are likely diluting the mercury being delivered to this region, in contrast to the Middle region.

3.4 Mercury Accumulation in southern Yukon Lakes

Recent (post-1950 to ca. 1993) mercury accumulation rates and dry mass accumulation rates in the Middle region and Talbot Arm of Kluane Lake were within the ranges (6.20 – 71.40 μg Hg m^{-2} yr^{-1}; 76 – 2341 g m^{-2} yr^{-1}, respectively) of other southern Yukon Lakes (Table 4). Mean dry mass accumulation rate in the Southern region of Kluane Lake was 9.0 times higher than the next highest lake, Lake Laberge (Table 4). Mean mercury accumulation rate in this region was 5.2 times higher than the next highest lake, Little Atlin Lake (core 1; Table 4). Recent mercury concentration in the Southern region and the Talbot Arm of Kluane Lake fell within the range (0.026 – 0.095 μg g^{-1} dw) of other southern Yukon lakes. Mercury concentrations in the Middle region (0.105 ug g^{-1} dw) were similar to the highest southern Yukon lake, Fox Lake (0.095 μg g^{-1} dw; Table 4). Recent focus-

corrected mercury accumulation rates in all three regions of Kluane Lake fell within the range (6.50 – 264.97 μg m^{-2} yr^{-1}) of other southern Yukon Lakes (Table 4).

3.5 Mercury Enrichment Metrics in southern Yukon Lakes

To determine whether mercury concentration and/or accumulation rate increased since 1950 compared with pre-1850 in Kluane Lake, I chose to use $\Delta F_{adj,F}$ (solid light blue in Figure 9) as an index of anthropogenic mercury loading. However, to enable comparisons with the broader literature, I also calculated uncorrected (ΔF, the arithmetic difference between pre-industrial [pre-1850] and recent [post-1950] mercury accumulation rates), focus-corrected (ΔF_F), and sedimentation rate-adjusted (ΔF_{adj}) anthropogenic mercury accumulation rates (termed anthropogenic mercury fluxes in the literature) for Kluane Lake. These metrics were also calculated for other southern Yukon lakes, in order to make comparisons among lakes in a standardized manner (Figure 9).

Anthropogenic mercury fluxes in Kluane Lake differed among uncorrected and corrected forms (Figure 9). In the Middle region, anthropogenic flux values ranged from -3.01 to 5.61 μg Hg m^{-2} yr^{-1} and in the Talbot Arm, values ranged from -2.93 to 25.22 μg Hg m^{-2} yr^{-1} among corrected/adjusted and uncorrected forms. In Kluane Lake, $\Delta F_{adj,F}$ values suggest that anthropogenic mercury loading varies among regions and that there is no evidence of anthropogenic mercury loading to the Talbot Arm but there is to the Middle region (Figure 9).

Table 4. Comparison of recent mercury concentrations and accumulation rates among southern Yukon lakes. Values are calculated until only ca. CE 1993 to compare consistent time periods between studies.

Lake		Recent mean dry mass acc. rate ($g\ m^{-2}\ yr^{-1}$)	Recent mean [Hg] ($\mu g\ g^{-1}$)	Recent mean Hg acc. rate ($\mu g\ m^{-2}\ yr^{-1}$)	Recent focus-corrected Hg acc. rate ($\mu g\ m^{-2}\ yr^{-1}$)
Kluane Lake	Southern rg.*	8971	0.042	368.05	212.71
	Middle rg.	235	0.105	24.34	67.42
	Talbot Arm	716	0.094	53.21	67.52
Bennett Lake		1140	0.053	60.22	264.97
Fox Lake		119	0.095	11.28	11.28
Grayling Lake[1]		2341	0.028	65.55	*n/a* [1]
Hanson Lake		76	0.082	6.20	8.67
Kusawa Lake[2,3]		277[2]	0.036[2]	8.13[2]	6.50[2]
		371[3]	0.038[3]	9.59[3]	11.50[3]
Lake Laberge		999	0.026	25.81	36.13
Little Atlin Lake[4]	core 1	813	0.088	71.40	99.95
	core 2	441	0.084	36.91	33.22
Marsh Lake		374	0.058	21.62	21.62
Watson Lake[1]		239	0.087	20.73	62.20

All data for lakes other than Kluane Lake and Grayling Lake were retrieved from Drevnick *et al.* (2016) Supplemental Table 2.

* Sediment core collected by N. Zabel, H. Swanson, R. Hall in winter 2015. Data are presented here for comparison.

1. N. Zabel, unpublished data: sediments originally collected by J. Brahney (2004) and used with permission. No focusing factor was available for this lake.
2. Core collected by Lockhart *et al.* (1998).
3. Mean values for both cores collected by Stern *et al.* (2009) in the same location in Kusawa Lake.
4. Two cores were collected in different parts of Little Atlin Lake by Lockhart *et al.* (1998).

To compare anthropogenic mercury loading among southern Yukon lakes, I chose to focus on ΔF_F (Table 4; solid dark blue in Figure 9), as this metric corrects for sediment focusing in lakes and was able to be calculated for many previously studied southern Yukon lakes. Correction for differences in sedimentation rate within a lake between the recent and pre-industrial period was not possible for

many southern Yukon lakes, as a constant sedimentation rate was assumed for these lakes and this constant was used to calculate mercury accumulation rate. Since a constant sedimentation rate was used, the sedimentation ratio would equal 1, and provide no adjustment. However, since there are known differences in sedimentation rates between pre-industrial (CE 1700 to CE 1850) and recent (CE 1950 to CE 2015) periods of Kluane Lake and there are likely differences in sedimentation rates between pre-industrial periods of other lakes, this metric is considerably less informative than $\Delta F_{adj,F}$ used earlier. Focus-corrected anthropogenic mercury fluxes in Kluane Lake differed between regions: ΔF_F was negative in core 3B and relatively high in core 4A, compared with other southern Yukon lakes (Figure 9). In core 4A, several earthquake events have affected the sediments of this region by increasing dry mass accumulation rates and, therefore, mercury accumulation rates. In both cores, the formation of the Kluane River resulted in increase of dry mass accumulation rates as Kluane Lake drained, which increased mercury accumulation rates during the pre-industrial period. Correcting for differences in sedimentation rates between the pre-industrial and recent periods in Kluane Lake is important, as these past events have resulted in the large differences observed in ΔF_F between core 4A, core 3B, and other southern Yukon Lakes.

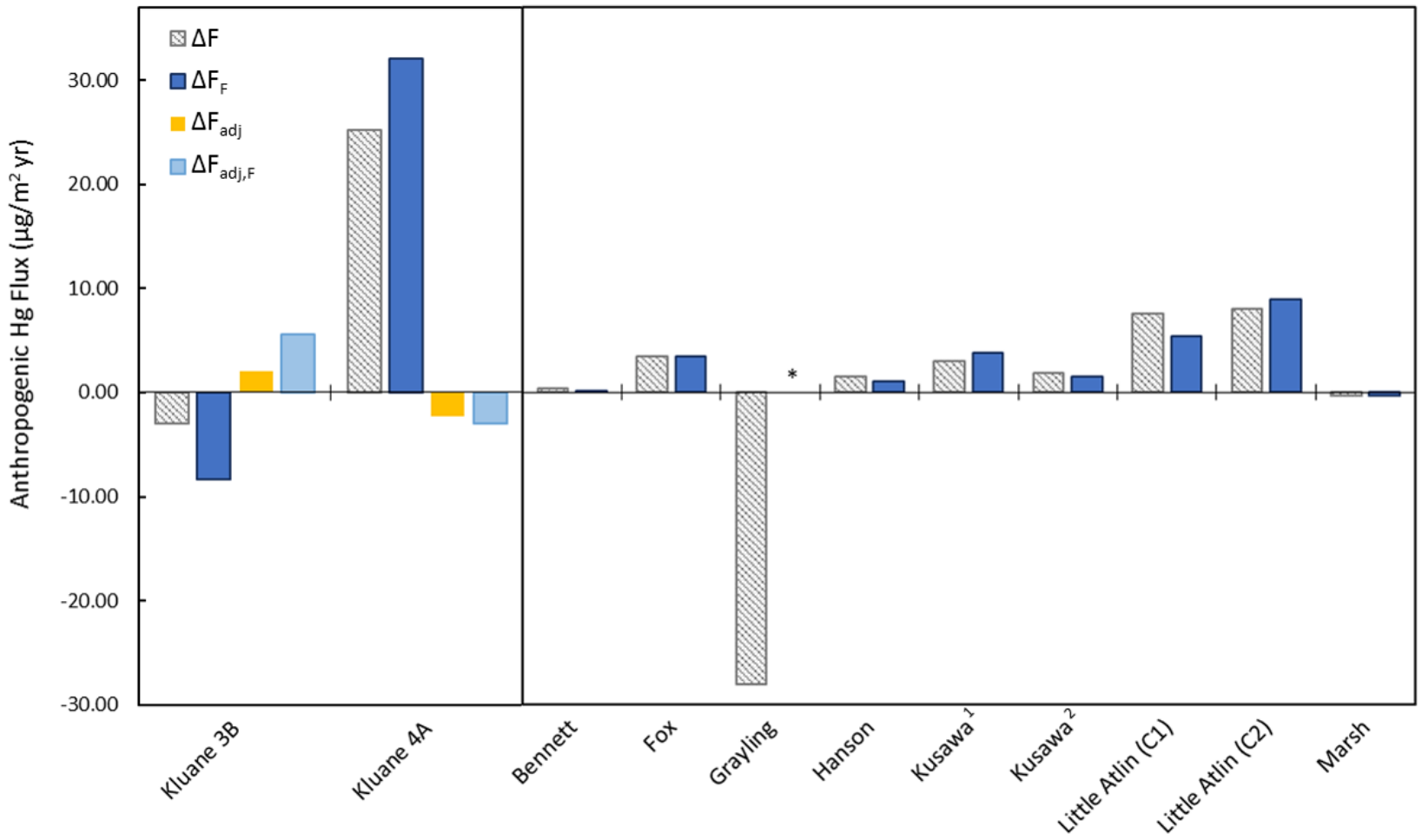
ΔF
ΔF_F
ΔF_adj
ΔF_adj,F
Anthropogenic Hg Flux (µg/m² yr)
30.00
20.00
10.00
0.00
-10.00
-20.00
-30.00
*
Kluane 3B
Kluane 4A
Bennett
Fox
Grayling
Hanson
Kusawa 1
Kusawa 2
Little Atlin (C1)
Little Atlin (C2)
Marsh

Figure 9. Anthropogenic mercury fluxes in both regions of Kluane Lake and other southern Yukon lakes. In Kluane Lake, four fluxes were calculated: uncorrected anthropogenic flux ΔF (grey striped), focus-corrected anthropogenic flux ΔF_F (solid dark blue), sedimentation rate-adjusted ΔF_{adj} (solid yellow), and focus-corrected, sedimentation rate-adjusted anthropogenic flux $\Delta F_{adj,F}$ (solid light blue). In other southern Yukon lakes, ΔF and ΔF_F were calculated (see text for further information). *Focus-correction was not possible for Grayling Lake as no focus factor was available. [1]Data for the core collected from Kusawa Lake from Lockhart *et al.* (1998). [2]Mean values for both cores collected from Kusawa Lake by Stern *et al.* (2009).

Chapter 4
Discussion

4.1 Trends in Mercury Accumulation in Southern Yukon Lakes

Lakes in the southern Yukon have large ranges in sediment mercury concentration, dry mass accumulation rates, and mercury accumulation rates, and at least some of this variation appears to reflect differences among lakes in inputs of glacial meltwater. Sediment mercury concentrations in the southern Yukon lakes included in the comparative portion of this study are below the interim Canadian Sediment Quality Guideline for total mercury (0.17 μg total Hg g^{-1}; CCME 1999); however, over half of these lakes were above the Canadian mean total mercury sediment concentration in lakes (0.074 μg total Hg g^{-1}; CCME 1999), including the Middle and Talbot Arm regions of Kluane Lake, Fox Lake, Hanson Lake, Little Atlin Lake, and Watson Lake. Many lakes that had relatively higher sediment mercury concentrations have sediments with relatively high organic content (Hart 1982; Rasmussen *et al.* 1998; Rawn *et al.* 2001; Kainz *et al.* 2003). This relationship between organic sediments and sediment mercury concentration is not surprising, as catchment-derived mercury is often transported to lakes bound with organic matter (eg. Korosi *et al.* 2015; Scherbastskoy *et al.* 1998; see Ravichandran 2004). Mercury concentrations in southern Yukon lake sediments, aside from Kluane Lake, declines moving east to west. The relative proportion of glaciers within lake catchments also increases moving east to west across the Yukon (Rawn *et al.* 2001). It is possible that high sediment loads associated with glacial meltwater inputs dilute sediment mercury in more westerly lakes southern Yukon lakes. In Kluane Lake, sediment mercury concentrations were highest in the Middle region, which also had the lowest dry mass accumulation rate. The lowest mercury concentrations were in sediments from the Southern region, which had the highest dry mass accumulation rate among regions studied in Kluane Lake. Low sediment mercury concentrations in

the Southern region appear to be a result of dilution by the glacially derived sediment load carried by the Ä'äy Chù and deposited in the Southern region.

Generally, southern Yukon lakes with higher dry mass accumulation rates had lower mercury concentrations than those with low dry mass accumulation rates, supporting the idea of sediment dilution of mercury concentrations in southwestern Yukon lakes. However, higher dry mass accumulation rates may result in higher mercury accumulation rates despite lower mercury concentrations. It is thus also important to understand the variation in dry mass accumulation among lakes. Whereas the highest dry mass accumulation rates were observed in lakes fed by glacial meltwater (the Southern and Talbot Arm regions of Kluane Lake, Bennett Lake) or large rivers (Lake Laberge), dry mass accumulation rates in Kusawa Lake were relatively low despite the highly glacierized catchment of the lake (Gilbert & Desloges 2005). This may be due to the morphology of Kusawa Lake, and the high spatial variation in sediment dynamics between regions of Kusawa Lake (Gilbert & Desloges 2005). Unexpectedly high dry mass accumulation rates were observed in Grayling Lake. This small, hydrologically closed kettle lake has no distinct inflows or outflows, and a small catchment (Brahney 2007). Grayling Lake is located in close proximity to Kluane Lake, and has undergone similar changes in water level as Kluane Lake over the past approximately 300 years, due to the groundwater and past surface water connectivity (Brahney *et al.* 2008b).

The analysis of cores from Kluane Lake revealed that in some regions and hydrologic periods, sediment mercury accumulation was more closely related to dry mass accumulation, whereas in other regions and hydrologic periods, sediment mercury accumulation was more closely related to mercury concentration. This variability in relative importance of drivers appeared to extend to other lakes in southern Yukon. Focus-corrected mercury accumulation rates were high in some southern Yukon Lakes with large glacial inputs and correspondingly high dry mass accumulation rates (the Southern region of Kluane Lake, Bennett Lake), but also high in some non-glacial lakes (Little Atlin Lake,

Watson Lake) with relatively high organic matter accumulation rates (and thus, mercury concentration; Rawn *et al.* 1999). Focus-corrected mercury accumulation rates in Kluane Lake were similar between the Middle and Talbot regions despite the hydrological and resulting sediment accumulation rate differences between these regions. In the Southern region, mercury accumulation rates were high due to high dry mass accumulation rates and sediment-focusing at the coring site.

Anthropogenic mercury loading to southern Yukon lakes, as quantified by focus-corrected anthropogenic accumulation rates (or fluxes, ΔF_F), is relatively low (< 10 μg Hg m^{-2} yr^{-1}) in all lakes except for Kluane Lake, compared with temperate midlatitude lakes (Muir *et al.* 2009). Generally, ΔF_F appears to decline moving east to west across the Yukon, similar to other studies (Lockhart *et al.* 1995; Lockhart *et al.* 1998). While overall anthropogenic accumulation rates are low, the recent increases observed in mercury loading to lake sediments may be due to increases in natural weathering and watershed contributions, and possibly due to increases in algal productivity and therefore algal scavenging of mercury in the water column. In Kluane Lake, a positive relationship between mercury concentration and organic content in both cores indicates that organic matter contributions to Kluane Lake are also contributing mercury to the lake. Increases in autochthonous organic matter have been shown previously to increase mercury delivery to sediments in Kusawa Lake (Stern *et al.* 2009). Relationships between organic matter, whether allochthonous or autochthonous, in other southern Yukon lakes has not been studied.

Focus-corrected ΔF is negative in the Middle region and high in the Talbot Arm of Kluane Lake: more than three times higher than other southern Yukon lakes. In both regions, differences in dry mass accumulation rate between the pre-industrial (CE 1700 to 1850) baseline period and the recent (post- CE 1950) period are driving the ΔF_F values observed. To address the effect of variable dry mass accumulation (aka sedimentation) rate, sedimentation-rate adjusted ΔF_F ($\Delta F_{adj,F}$) was

calculated: these values indicate that anthropogenic mercury loading to Kluane Lake is low (Middle region) or negligible (Talbot Arm).

The reconstruction of mercury dynamics is affected by the location a sediment core is taken, especially in a large lake. The importance of coring location was demonstrated in this study. There were differences in mercury enrichment metrics between regions in Kluane Lake. To date, spatial diversity in sediment stratigraphic records and associated effects on mercury reconstructions have been poorly acknowledged. Stern *et al.* (2009) used two sediment cores collected from the same sitre in Kusawa Lake, to reconstruct mercury dynamics for the entire lake. While good stratigraphic agreement was found in mercury and algal matter concentrations between cores, two cores from one collection site cannot accurately reconstruct mercury dynamics for all of Kusawa Lake, due to the physical structure of the lake and previously noted distinct lake regions (Gilbert & Desloges 2005). Kusawa Lake is similar to Kluane Lake: both are long and narrow lakes surrounded by mountains, and have spatial heterogeneity in sediment dynamics. Spatial differences in mercury accumulation dynamics would therefore be expected. In Kluane Lake, significant differences in mercury concentration, dry mass accumulation rates, and mercury accumulation rates were found between regions; relationships between environmental proxies and mercury accumulation dynamics also differed. It is not unlikely that similar spatial differences influence mercury accumulation in other large lakes in the southern Yukon and other mountainous lake systems.

Enrichment metrics such as those used in this study must be interpreted in the topographic and hydrological context of the lake, and should be accompanied by additional analysis into the history and controls of mercury accumulation within a given lake. I suggest that these metrics be employed with caution. In the cores from Kluane Lake, these metrics changed in response to disturbance events that caused sediment resuspension and/or large increases in dry mass accumulation rate, such as earthquakes. Many previous paleolimnological studies have assumed and used a constant

sedimentation rate (e.g., Lockhart *et al.* 1998, Stern *et al.* 2009) to determine mercury accumulation rates in sediment cores, and have attributed increases in mercury accumulation rates (often using a form of ΔF) to anthropogenically induced increases in mercury concentrations (e.g., Lockhart *et al.* 1998). However, a linear sedimentation rate is a poorly founded assumption, especially for lakes located in mountainous or seismically active terrain, where earthquakes, landslides, floods, or other sediment disturbance events can cause large changes in sedimentation rate (e.g., Kusawa Lake, see Gilbert & Desloges 2005). Some authors have assumed a linear sedimentation rate despite evidence for sediment disturbance events in radioisotope or sediment proxy stratigraphies (eg. Stern *et al.* 2009). It is important to consider historical watershed influences when reconstructing mercury accumulation dynamics and evaluating anthropogenic mercury enrichment: Kluane Lake serves as an important case study in this regard, given the demonstrated susceptibility of ΔF metrics to changes in sedimentation rate. It is therefore recommended that: 1) sedimentation rates be determined for each core section instead of assuming a constant sedimentation rate; and, 2) additional paleolimnological variables, such as magnetic susceptibility, become common analyses conducted during paleolimnological reconstructions of mercury dynamics; this will allow practitioners to better understand the historical sediment dynamics and provide context for the reconstructions.

Mercury enrichment metrics are widely used in the paleolimnological literature (e.g., Muir *et al.* 2009, Brazeau *et al.* 2013b, Goodsite *et al.* 2013), but can be influenced by core collection location and historical sediment disturbance events, including landslides and earthquakes. These metrics may be inaccurate indices of pollution especially in large, multi-region or multi-basin lakes, in which mercury accumulation or sediment accumulation dynamics may differ among regions, and/or when lakes are subject to sediment disturbances. Given the topographic setting of many southern Yukon lakes, particularly those in the southwest, it is not unlikely that earthquake events (e.g., Cassidy & Rogers 2004, Hyndman *et al.* 2005, Lamontagne *et al.* 2008) or other sediment disturbances (e.g.,

Lowey 2002) have affected sediment stratigraphies and dry mass accumulation rates. The extent of sediment disturbance events and spatial heterogeneity in mercury dynamics in large lakes has not, to date, been adequately considered in paleolimnological studies, especially those reliant on a single core or site. Future studies should focus on increasing the spatial coverage of studied lakes, analyzing multiple cores from large or multi-region lakes, and utilizing multiple lakes in close proximity to quantify the legacy and characterize the spatial variability of anthropogenic mercury pollution in western subarctic Canada.

4.2 Sediment Disturbance Events in Sediment Stratigraphies from Kluane Lake

Seismic events, such as earthquakes, are known to disturb the surrounding topography and alter the characteristics of lake sediments. As such, lake sediments have been used as 'natural seismographs' to reconstruct historical and past earthquakes globally, especially given the lack of long-term seismographic records (e.g., Doig 1991, Doig 1998, Monecke *et al.* 2004, Bertrand *et al.* 2008, Schwab *et al.* 2009, Doughty *et al.* 2014, Petersen *et al.* 2014). Anomalous layers of sediment formed due to the effects of earthquake events have been called 'turbidites', 'homogenites', or 'seismites' in the literature (Doig 1986, Schilts & Clague 1992, Monecke *et al.* 2004, Bertrand *et al.* 2008, Schwab *et al.* 2009, von Guten *et al.* 2009, Petersen *et al.* 2014; see Shanmugam 2016 for a discussion of terminology). Earthquakes can affect lake sediments in two major ways: by introducing additional sediments from the catchment to the lake, and by redistributing previously deposited lake sediments; generally, both sediment delivery mechanisms occur simultaneously (see Fig. 14, Bertrand *et al.* 2008). Earthquake-induced sediment layers in lakes typically have one of two structures. The first type of structure, called a 'turbidite' *sensu stricto* (Bertrand *et al.* 2008) is a layer characterized by continuous fining of sediments from the bottom (coarser) to the top (finer). The second type of structure is called a 'homogenite' (Bertrand *et al.* 2008; Petersen *et al.* 2014). Homogenite deposits have a characteristic and distinct layered structure, comprised of a coarse-grained (typically sand)

layer on the bottom overlain by a thick and homogenous layer of fine-grained clay sediments capped with a thin layer of fine silt sediments (Bertrand *et al.* 2008; Petersen *et al.* 2014). These layers are often characterized using several methods, including magnetic susceptibility, grain-size, geochemistry, x-ray imaging, and organic matter analysis; rapid identification of earthquake-induced sediment layers can be accomplished using only magnetic susceptibility, geochemistry, and/or sediment density (Doig 1986; Bertrand *et al.* 2008). Identification of earthquakes in sediment records can be strengthened by concomitant occurrence of related deposits in multiple cores collected from different regions of a lake (Bertrand *et al.* 2008). The magnitude of an earthquake and the proximity of the epicenter to the lake in question affect the degree of allochthonous and autochthonous sediment delivery and redistribution in lakes (Ambraseys 1988; Monecke *et al.* 2004). Generally, a larger-magnitude earthquake event will affect a greater area further from the epicenter than a smaller event (Ambraseys 1988).

The earthquakes and other sediment disturbance events identified in Kluane Lake in this study were previously identified by Doig (1998) and Brahney *et al.* (2008b). The Sheep Mountain landslide was a large, catastrophic landslide (or possibly a series of landslides) that occurred between ca. CE 49 (95% credible interval: BCE 58 – CE 179) and ca. CE 1426 (95% credible interval: CE 1324 – CE 1515; Clague 1981). While the ultimate cause is unknown, Clague (1981) identified several factors that may have contributed to the slope failure ultimately causing this landslide, including high seismic activity in the Denali Fault and the occurrence of intense rainstorms. Doig (1998) identified a silt layer in Kluane lake dated to CE 1425 which he attributed to this landslide. The Sheep Mountain landslide was tentatively identified in the sediment core from Middle region, corresponding with a weighted mean core section age of CE 1534 (95% confidence interval: CE 1409 – CE 1627); no peaks were observed in the Talbot Arm which would correspond with this event, however it was not expected to be identified in this region due to the distance between the Talbot Arm and the Sheep

Mountain landslide site. This landslide event likely contributed a large amount of sediment to Kluane Lake, which would have increased sedimentation rate and mineral content in lake sediments. In the Middle region, the inferred landslide event corresponded with increases in magnetic susceptibility, dry density, and dry mass accumulation, as well as mercury concentration and mercury accumulation rate. It is also possible, however, that the peaks observed in numerous proxies were caused by a yet-undescribed earthquake event. Further analysis and additional sediment cores are needed in order to more accurately identify this landslide event and determine its effects on Kluane Lake sediments.

Major hydrological events were also preserved in the lake sediment records and were observed in both sediment cores. The prominent peaks in both cores identified ca. CE 1690 correspond with the previously identified formation of the Kluane River (Clague *et al.* 2006; Brahney *et al.* 2008b). This event resulted in important and rapid changes in the hydrology and sediment characteristics in Kluane Lake (see Brahney *et al.* 2008a,b) that were well-preserved in the sediment cores used in this study. The rapid increase in water level ca. CE 1650 due to the inception of the Ä'äy Chù resulted in decreases in sediment mercury concentrations in Kluane Lake, with parallel increases in dry mass accumulation rate and mercury accumulation rates. The erosion of the Duke River sediment in the Brooks Arm and the formation of the Kluane River ca. CE 1690 (CE 1680 – 1700; Clague *et al.* 2006) resulted in rapid draining of the lake and decreases in dry mass accumulation rates and mercury accumulation rates with increases in mercury concentrations.

In addition to landslides and river formation events, several historical earthquakes were identified in the sediment cores from Kluane Lake. Prominent peaks observed ca. CE 1900 in both cores correspond well with the CE 1899 Yakutat Bay earthquakes, a series of earthquakes that occurred over a six-day period (Lamontage *et al.* 2008), and prominent peaks in ca. CE 1955 in both cores correspond with two localized earthquakes (both $M \geq 5$) in CE 1956 around Kluane Lake (see Clague 1981 Fig. 9): one earthquake was centered near Sheep Mountain and the other was centered just north

of the Gladstone Creek delta. This earthquake was more pronounced and distinct in the Talbot Arm sediment core due to the proximity of this site to the epicenter of the northern earthquake. In both cores, the CE 1899 and CE 1956 events resulted in deposition of a homogenite layer, as evidenced by a three-layer structure where dry density declines immediately prior to a sharp increase in dry density Bertrand *et al.* 2008). Earthquake-induced sediment disturbance events increased sediment mercury concentrations in Kluane Lake, likely dri[ven by the redistribution of sediments, and the concentration of the fine-grained sediments on top of the homogenite layer, sediments that are often associated with mercury (Frenet-Robin & Ottmann 1978; El Bilali *et al.* 2002). Earthquake events also increased mercury contributions from the catchment to lake sediments: concurrent increases in organic matter content and mercury concentration observed in Kluane Lake sediment stratigraphies likely reflect increased catchment contributions.

Over the past 150 years, several other earthquakes have occurred that may have altered the sediments of Kluane Lake and some evidence of these events is present in the stratigraphic record, but these other earthquakes were not identified distinctly in sediment cores. On 27 December CE 1850, an earthquake was felt at Fort Selkirk: this earthquake is suspected to be no greater than magnitude 6 and did not originate nearby the fort but was attributed to the Denali Fault (Jackson 1990). A dense, silty layer of sediment was identified in a sediment core collected from Kluane Lake by Doig (1998) and dated to ca. CE 1865. It is possible that this earthquake affected Kluane Lake as well, which is adjacent to the Denali Fault. There is some evidence in the sediment record for this earthquake, particularly in the Middle region in magnetic susceptibility, dry density, dry mass accumulation, mercury concentration, and mercury accumulation rate; however, a corresponding layer in the Talbot Arm is mostly absent. To positively identify this event, however, additional sediment analysis is required, specifically increasing the sectioning intervals of collected sediment cores. In CE 1920, a local earthquake ($M \geq 5$) occurred near Teepee Peak, approximately 65 km west of the Brooks Arm

(Clague 1981 Fig. 9). This event also likely affected Kluane Lake sediments. It was not identified, however, due to low sedimentation rates and thus low sediment core resolution and the relatively larger effect of the CE 1899 earthquake on the sediment record. Finally, an earthquake ($M \geq 5$) occurred in CE 1940 just east of the Brooks Arm (Clague 1981 Fig. 9). There is some evidence for this earthquake in the sediments collected in the Talbot Arm, however the absence of a corresponding layer in the Middle region and the relative influence of the CE 1956 earthquakes on Talbot Arm sediments make it difficult to conclusively identify this event. In order to better identify these historical earthquakes, additional sediment core analyses and the collection of additional cores nearer to the epicenters are needed. While other earthquakes were not identified distinctly in the collected sediment cores, these events may have affected the sediment stratigraphies and therefore the analysis presented.

4.3 Mercury in Kluane Lake

Hydrological changes have shaped the paleolimnological history of Kluane Lake over the past 1,200 years and resulted in spatiotemporal differences in mercury dynamics throughout the lake. The transition from the Duke River period, when Kluane Lake was supplied by the Duke River in the north and drained via the Ä'äy Chù valley to the south, to the Ä'äy Chù period, when Kluane Lake was supplied glacial meltwater via Ä'äy Chù in the south and drained via the Kluane River in the north, resulted in marked differences in sediment characteristics and mercury dynamics within the lake.

During the Duke River Period (ca. CE 650 – CE 1650), mercury accumulation rates in Kluane Lake were driven by both mercury concentration and dry mass accumulation in the Middle region and the Talbot Arm. Dry mass accumulation was controlled by glacial inputs to the lake and local catchment erosion. During this period, glacial and terrestrial material entering Kluane Lake diluted the incoming

mercury, which likely originated from non-glacial, inorganic sources, such as the surrounding bedrock, based on the results of this study. Similar to controls of dry mass accumulation rate, mercury concentration was controlled by allochthonous inorganic, mineral sediment contributions from the surrounding catchment, and by carbonate-rich glacial sediment contributions from the Duke River acting as diluting agents. Dilution of trace metals, including mercury, was also found in several lakes by Yang & Rose (2005), who suggest that dilution occurs when sediment loading increases from sources that are not contaminated with the trace metal in question. Given the findings of Yang & Rose (2005) and the results of this study, sediment dilution is an important mechanism that controlled mercury dynamics in Kluane Lake, and supports a non-glacial inorganic source of mercury to Kluane Lake during the Duke River period.

Sources of mercury to Kluane Lake during the Duke River period likely included the streams stemming from surrounding mountain ranges, such as Bocks, Nines, and Gladstone creeks, all of which carry eroded materials from the bedrock of the Kluane and Ruby ranges. Many of the streams flowing off the Kluane ranges have channels that have worn through diverse bedrock formations: deposits of gold, gypsum, and lignite have been noted within these mountain ranges (Bostock 1952; Muller 1967), and may have been important sources of mercury to the Middle region of Kluane Lake during the Duke River period. While lignite tends to have lower concentrations of mercury than higher-grade coals, both lignite and gypsum have higher concentrations of mercury than many other minerals (Chu & Porcella 1995; Rytuba 2003; Yudovich & Ketris 2005; Yost *et al.* 2010). Mercury in the Talbot Arm during the Duke River period may have originated from erosion of the gold-bearing gravels found along Gladstone Creek (LeBarge 1996). Gladstone Creek is underlain by the Yukon Group formation, a mixture of metamorphic rocks punctuated by gold-bearing quartz veins (Snow 1936; Bostock 1952; Muller 1967). These veins were likely eroded by fluvial and glaciofluvial processes during the Holocene, and materials were deposited along the creek bed as auriferous gravel

materials (LeBarge 1996). Gold from similar Klondike-region deposits within the Yukon Group formation contain mercury at concentrations ranging from 10 to 90 mg Hg/g Au (Knight *et al.* 1999). Erosion of other bedrock channel creeks that flow into the Talbot Arm may also have contributed mercury to the sediments, as these channels are also underlain by Yukon Group formation bedrock.

The blockage of the Ä'äy Chù drainage that occurred around CE 1520, which caused Kluane Lake to deepen gradually, corresponded with increased mercury concentrations in the core stratigraphy of the Middle region (Brahney *et al.* 2008b; Brahney *et al.* 2010). Mercury concentrations were higher in the Middle region than the Talbot Arm following the blockage, likely owing to an increase in fine glacial sediments being delivered to this region following the valley blockage (Frenet-Robin & Ottmann 1978). Increases in magnetic susceptibility during the transitional period indicated that terrestrial erosion increased as the lake deepened and contributions of glacial meltwater increased over time: both terrestrial and glacial materials likely contributed mercury along with sedimentary materials. The erosion of gold, lignite, and gypsum deposits present along tributary streams of Ä'äy Chù (Bostock 1952; Muller 1967) may have also contributed mercury to the lake after the southern drainage was blocked (Rytuba 2003; Yudovich & Ketris 2005; Yost *et al.* 2010).

During the Ä'äy Chù Period (CE 1650 – CE 2015), mercury accumulation rates were driven primarily by dry mass accumulation rates, which were controlled by the erosion of terrestrial organic matter as well as by glacial contributions to Kluane Lake. Sediment mercury concentration was also an important factor in driving mercury accumulation dynamics in the lake. Evidence from correlations with proxies, including carbonate content and magnetic susceptibility, indicated that mercury in the sediments of the Middle region originates from terrestrial materials and possibly glacial meltwater. Since glaciers accumulate airborne contaminants on their surface but melt at the ablation zone transversely, atmospherically-transported mercury that has accumulated on the surface of the Kaskawulsh Glacier since the Industrial Revolution would be delivered to Kluane Lake, likely

associated with fine sediments suspended in the glacial meltwater. However, glacial meltwater carries an abundance of sediments that would dilute this incoming mercury as well.

Similar to the Middle region in the Ä'äy Chù Period, sediment mercury in the Talbot Arm during the Ä'äy Chù Period originates from terrestrial materials as well, and is likely being diluted by glacial carbonate-rich material or erosion of local carbonate-rich bedrock. In both lake regions, terrestrial mercury is being delivered to the lake primarily in association with allochthonous organic matter, as well as less inputs originating from the gold deposits along Gladstone Creek. The wetland complexes located along the southeastern shores of Kluane Lake may also be important mercury sources, as border wetlands are rich in organic matter and can be important contributors of mercury to lakes (Rudd 1995). However, further investigation into mercury loading from the creeks and inflows around Kluane Lake is required to better characterize the mercury mass balance for the lake.

In May 2016, Kluane Lake abruptly entered into a new hydrological period. The meltwaters of the Kaskawulsh Glacier, which previously fed Ä'äy Chù, were pirated by the Kaskawulsh River. Consequently, flow of Ä'äy Chù decreased significantly (Shugar *et al.* 2017). Based on the elevation differences at the toe of the Kaskawulsh Glacier between Ä'äy Chù and the Kaskawulsh River, this diversion is expected to be a relatively permanent hydrological change (Shugar *et al.* 2017). The diversion of Kaskawulsh Glacier meltwaters away from Ä'äy Chù has several important implications for mercury dynamics in Kluane Lake. First, the decreased discharge of Ä'äy Chù will decrease the overall mass of sediments entering Kluane Lake, and increase the proportion of water and sediments originating from the small tributary creeks along the Ä'äy Chù valley. Deposits of gold, gypsum, and lignite coal have been found within this valley (Bostock 1952; Muller 1967), and erosion of these deposits may be a source of mercury to Kluane Lake (Rytuba 2003; Yudovich & Ketris 2005). An increase in the influence of the tributary sediments relative to Kaskawulsh glacial sediments may result in increased sediment mercury concentrations in Kluane Lake as well as increased sediment

particle size. The loss of fine glacial sediments will decrease the binding capacity of Ä'äy Chù sediments, which may increase mercury bioavailability. However, decreases in glacial contributions will result in increased water clarity and temperature, particularly in the Southern region; the lack of a major water and sediment source may also increase the heterogeneity of environmental controls of mercury accumulation among regions of Kluane Lake, as the relative importance of local contributions will increase. The new hydrological period into which Kluane Lake is entering may be similar to the Duke River period, as lake levels decline. As the lake continues to drain through the Kluane River and water levels decrease, Kluane Lake may become a closed basin (Shugar *et al.* 2017).

Global climate changes and warming are increasing the ice-free period and water temperature in arctic and subarctic lakes across North America (Prowse *et al.* 2006; Schindler & Smol 2006). The Yukon Territory is warming more rapidly than other parts of Canada: winter temperatures have increased 4°C over the past 50 years and are predicted to continue to increase (Streicker 2016). The ice-free season of many lakes has increased in duration, which has also increased lake water temperatures (Prowse *et al.* 2006; Schindler & Smol 2006). In Kluane Lake, this regional warming effect is compounded by the loss of the cold meltwaters from the Kaskawulsh Glacier. It is expected that as the lake level drops, water temperatures in Kluane Lake will increase. Warmer waters paired with increases in terrestrial matter and nutrient export to the lake (Adrian *et al.* 2009), due to increases terrestrial decomposition rates and an increased frequency and severity of precipitation events (Streicker 2016), may result in increased primary production in the lake. Additionally, the decrease in suspended sediments transported by Ä'äy Chù will increase water clarity throughout Kluane Lake, further supporting increased in-lake production. Increased terrestrial export, especially organic matter, due to climate change-related effects, will also increase the rate of mercury loading from the catchment to Kluane Lake, as a strong relationship between mercury accumulation and

autochthonous organic matter was observed during the Ä'äy Chù period in the lake. Increased primary production may result in algal scavenging of mercury, which has been observed in other Yukon lakes (e.g., Stern *et al.* 2009). Further, decreased inputs of glacial meltwater will increase the proportion of groundwater contributions to the lake. In the past, low surface water inputs and high groundwater inputs in Kluane Lake have resulted in meromixis, and possibly anoxic or euxinic (sulphur-rich anoxic) conditions in the lake (Brahney *et al.* 2008a). Clearer, warmer, nutrient-rich water, possible meromictic conditions, increased mercury loading, higher autochthonous primary production, and possible anoxic conditions in lake-bottom sediments will all effect mercury cycling in Kluane Lake, affecting both the biota of the lake and the communities which depend on them.

Brahney *et al.* (2010) suggested that the Duke River could be redirected into Kluane Lake in the event of the loss of the Ä'äy Chù inflow. The past anoxic and meromictic conditions in Kluane Lake (350 BCE – CE 350) were ended by the recapture of the Duke River ca. CE 350 (Brahney *et al.* 2008a, 2010). This also resulted in an increase in water level in the lake (Brahney *et al.* 2008b): however, the Kluane River did not exist during this period. Paleochannels from previous flow paths of the Duke River are evident northwest of Burwash Landing and near the current Duke River delta where it joins the Kluane River. However, the community of Burwash Landing, the Burwash airport, the Alaska Highway, and the Rocking Star Ranch are all located within the Duke River sediment fan, and would be placed at risk if the Duke River were diverted by anthropogenic activities. It is unlikely that the redirection of the Duke River would be a cost-effective and sustainable solution to the loss of meltwater inputs. The Duke River has been shown to move across the landscape repeatedly in the past 5 000 years (Brahney *et al.* 2008a), and maintenance costs associated with controlling this river would likely be immense.

Chapter 5
General Conclusions

5.1 Summary of Research

Using a multi-proxy approach and multiple sediment cores, I investigated mercury accumulation histories in several regions in Kluane Lake, Yukon, and related changes and spatiotemporal variability in mercury accumulation dynamics over a 1 200-year period to previously characterized hydrological changes. Trends in mercury accumulation dynamics were explored in southern Yukon lakes, drawing on previous studies to elucidate spatial patterns in recent sediment mercury enrichment. This study represents the first investigation into regional differences in historical and modern mercury accumulation in sediments in a large, glacial-fed lake.

The dynamic hydrological history of Kluane Lake had marked effects on mercury accumulation in the lake: the loss of the Duke River inflow, the inception of the Ä'äy Chù inflow, and the formation of the Kluane River all resulted in changes in sediment mercury accumulation in Kluane Lake. Additionally, earthquakes in the catchment resulted in increases in sediment mercury concentration and accumulation rate throughout the lake. Overall, sediment mercury concentrations and accumulation rates are declining in much of the lake; however, near the Ä'äy Chù delta, mercury concentrations and accumulation rates are increasing coincident with decreasing dry mass accumulation rates. In general, mercury in Kluane Lake is derived from catchment sources, including soil and bedrock weathering and erosion.

Mercury dynamics in Kluane Lake varied between regions but were generally comparable with other southern Yukon lake. Mercury accumulation rates and concentrations in Kluane Lake sediments were relatively high but within the range of other lakes. Dry mass accumulation rates were also high in Kluane Lake, which drove the high mercury accumulation rates. Differences in mercury accumulation

rate, mercury concentration, and dry mass accumulation rate among lakes were attributed to qualitative topographic differences among lakes and the influence of earthquake events on sediment stratigraphies.

5.2 Significance & Implications of Research

This is one of three studies to reconstruct temporal mercury accumulation dynamics in a large, glacially-fed lake in North America (see Stern *et al.* 2009 & Köck *et al.* 2012), and the only study to investigate regional differences in mercury dynamics in a large, glacially-fed lake. Results have provided insight into the effects of hydrological and climatic changes, earthquake events, and anthropogenic activities on mercury dynamics. This study also contributes valuable baseline information regarding sediment mercury in Kluane Lake, which will provide an important foundation for future monitoring and studies on the lake, especially in light of the recent loss of the Ä'äy Chù inflow (Shugar *et al.* 2017).

In late May 2016, discharge of the Ä'äy Chù inflow into the lake decreased, resulting in a record minimum water level in Kluane Lake during the same month (Shugar et al 2017). Record high river flows in the Alsek River were also recorded during summer 2016 (Shugar *et al.* 2017). Drone surveys indicated that a catastrophic ice wall collapse at the toe of the Kaskawulsh Glacier had drained the lake that fed the Ä'äy Chù; as a result of this collapse, water was diverted into the headwater lake of the Kaskawulsh River (Shugar *et al.* 2017). This resulted in the 'piracy' of the Ä'äy Chù, and Kaskawulsh Glacier meltwater now drains via the Kaskawulsh River (Shugar *et al.* 2017). This drainage change is considered to be permanent, due to the topographic gradient of the Kaskawulsh Glacier terminus (Shugar et al 2017). While dramatic, similar events have occurred in the history of Kluane Lake, with significant changes in drainage occurring during the mid- and late Holocene (Brahney *et al.* 2008b).

Lower water levels have been observed in Kluane Lake since summer 2016 by local community members and Shugar *et al.* (2017). Without meltwaters from the Kaskawulsh Glacier feeding the Ä'äy Chù, flows in this river will decline dramatically, as will the amount of sediment transported into Kluane Lake. The Ä'äy Chù will continue to flow into Kluane Lake, however, only the small streams that originate from the Kluane Ranges, such as Vulcan, Bullion, and Coin creeks will feed it. Water levels in Kluane Lake will continue to fall, ultimately until the Kluane River outlet is lost and the lake becomes a closed basin, which has occurred historically due to drainage shifts in the lake (Brahney *et al.* 2008a; Brahney *et al.* 2010). Previous closed basin periods in Kluane Lake have resulted in sediment hypoxia or anoxia (Brahney *et al.* 2008a), which provide suitable conditions for bacterial methylation of mercury (Pak & Bartha 1998). Inputs of sulphate-rich groundwater to Kluane Lake may further foster increased bacterial mercury methylation (Gilmour *et al.* 1992), resulting in increased concentrations of mercury in aquatic organisms.

Sediment accumulation rates in the southern region will decline sharply with the loss of inflowing glacier meltwaters, while smaller declines in sediment accumulation the middle and northern regions of the lake are likely. This decline in sediment accumulation will likely be paired with an increase in sediment mercury concentration (decreased sediment dilution), as an inverse relationship between sediment accumulation and mercury concentration was found in this study. Further, water column turbidity will decrease throughout the lake, and water temperatures will slowly increase, due to both the loss of cold glacial meltwaters and regional climate warming, likely resulting in increases in algal primary productivity (see Whitehead *et al.* 2009). This increase in primary production may result in increased mercury scavenging by algal matter, and increased sediment mercury concentrations throughout the lake (see Stern *et al.* 2012). The loss of the fine glacial materials may also result in higher mercury concentrations in aquatic organisms, as these fine sediments have a high affinity for mercury (Desauziers *et al.* 1997) and retain mercury in a relatively non-bioavailable form (Ullrich *et*

al. 2001) in the oxic sediments throughout Kluane Lake. Lower concentrations of fine sediment will decrease this sorption, and increase the proportion of mercury that may be biologically accessible for mercury methylation and bioaccumulation though the lake food chain (Ullrich *et al.* 2001).

Brahney *et al.* (2010) suggested that the Duke River could be redirected into Kluane Lake to compensate for the loss of the Ä'äy Chù if it should occur; the Duke River currently flows into the Kluane River approximately 4 km from Kluane Lake. However, the redirection of the Duke River is an unlikely and infeasible alternative, due to the sheer cost of a river diversion project, the dynamic nature of glacially-fed rivers making them difficult to manage, and the high level of uncertainty in short- and long-term effects of diversion on the aquatic communities and hydrological regimes of Kluane Lake, the Kluane River, and the Duke River.

It can be concluded that the loss of the glacial inputs from the Ä'äy Chù and the anticipated effects of global climate change together will result in lower water levels, warmer water temperatures, and increased mercury concentrations in the aquatic organisms in Kluane Lake. The piracy of the Ä'äy Chù may represent the beginning of a new hydrological period for Kluane Lake, if the loss of Kaskawulsh Glacier inputs is indeed permanent.

5.3 Future Directions

Future research on Kluane Lake should continue to investigate the spatiotemporal variation in mercury accumulation dynamics among regions, expanding on both the spatial and temporal dimensions of paleolimnological mercury reconstruction. The Talbot and Brooks arms differ from the main regions of Kluane Lake in water temperature, turbidity, and algal productivity (E. McKnight, personal communication), and have water sources that flow through lowland wetland complexes. These factors are known to influence mercury accumulation, but to date, the Talbot and Brooks arms of Kluane Lake have received little scientific study of any kind. While one core from this study was

collected in the Talbot Arm, it was collected from the southern end of the arm where it joins with the main region of Kluane Lake. The Talbot Arm is approximately 35 km long, and may have been a separate lake in the past (Clague *et al.* 2006). Additionally, the Brooks Arm has received no scientific attention, despite the shallow, warm, and productive waters found there (E. McKnight, unpubl. data). This arm was where the Duke River historically flowed into Kluane Lake: the sediment fan deposited by this river is evident in the bathymetric profile of Kluane Lake today. However, north of this sediment fan, the Brooks Arms narrows and deepens. Additional core collection in the northern ends of the Talbot and Brooks arms would provide additional insight into spatial variations in mercury dynamics and help to better characterize the hydrological history of Kluane Lake. Due to the high sedimentation rate in the southern end of Kluane Lake, the core collected for this study provided only approximately 100 years of sediment accumulation history. A longer sediment core, perhaps collected using a piston corer, would provide greater historical insight into mercury accumulation dynamics in the southern end of Kluane Lake, hopefully capturing the drainage reversal and inception of the Ä'äy Chù. This would allow for greater understanding of the spatial variability of mercury accumulation in Kluane Lake during the Duke River period. Finally, collecting a sediment core from a small lake, such as the kettle lakes near Christmas Bay, would provide a clearer quantification of atmospheric mercury loading to this region.

As was previously discussed, disentangling geological and natural inputs of mercury, anthropogenic mercury deposition, and influence of algal scavenging on recent increases of mercury delivery to sediment is necessary to accurately understand the complex nature of mercury cycling in northern lake ecosystems. Previous studies have used RockEval®, a method for characterizing organic matter using thermal devolatilization (see Sanei & Goodarzi 2006), and stable carbon isotopes to characterize and classify sediment organic matter, and to evaluate algal-mercury scavenging as a mechanism for increased mercury concentrations (e.g., Cooke *et al.* 2012, Outridge *et al.* 2017).

Trace metals, such as titanium, calcium, and aluminum, have been used as geochemical tracers for geological mercury sources to lake sediments (e.g., Carrie *et al.* 2010, Outridge *et al.* 2017). These proxies and tracers would provide additional insight into sediment mercury dynamics in Kluane Lake and help to determine the relative contribution of natural and anthropogenic mercury to the lake. To complement these methods, the inflows to Kluane Lake and to the Ä'äy Chù should be sampled for mercury, other trace metals, and sediments, which would allow for further quantification of relative contributions of geologically- and catchment-derived mercury with respect to the diverse topography of the Kluane Lake catchment.

Future paleolimnological mercury reconstruction studies on lakes globally should incorporate analysis to determine the occurrence and possible influence of catchment disturbance events, such as earthquakes, landslides, and human activities, on sediment stratigraphies. I showed that earthquake events can affect mercury accumulation rates and mercury concentration, as well as other commonly-used paleolimnological proxies, such as magnetic susceptibility and dry density, and that these effects can confound the use and interpretation of mercury enrichment metrics, such as enrichment factors, flux ratios, and anthropogenic mercury flux. Methods for the identification of these events include sediment density determination, LOI, and magnetic susceptibility, which are affordable, quick, and non-destructive or require very small sediment subsamples. High-resolution sediment sectioning and analysis, as well as multimethod age-depth models can help identify these possible disturbances, which may be frequent in seismically-active or montane areas, such as Kluane Lake, and contribute to more accurate reconstructions of mercury accumulation dynamics in lakes (see Cooke *et al.* 2010).

The loss of the Ä'äy Chù glacial meltwaters and this research provide an excellent incentive to begin environmental monitoring of Kluane Lake. Annual or biannual monitoring of aquatic organisms and sediment mercury concentrations throughout the lake will help track ecological and biogeochemical changes as they occur in the lake. As the anticipated effects of inflow loss and climate change are

expected to increase mercury concentrations in aquatic organisms, which may increase the risk to communities that harvest fish from Kluane Lake, monitoring of mercury is essential to quantifying the risk, if it exists, of consuming fish from Kluane Lake. Lake surface sediment monitoring throughout the lake will also provide insight into the changes that may occur in the lake in light of recent hydrological changes, and provide insight into spatial variability of anticipated effects. As climate change is considered to be the root cause of the loss of the Ä'äy Chù and is anticipated to have continued effects on the ecosystem of Kluane Lake, environmental monitoring of Kluane Lake is essential to quantify future effects of climate change on the lake. Kluane Lake is also an ideal model ecosystem for predicting effects of climate change-related effects on other subarctic lakes, especially in light of the loss of the primary water and sediment source to the lake.

Bibliography

Adrian, R., O'Reilly, C. M., Zagarese, H., Baines, S. B., Hessen, D. O., Keller, W., ... & Weyhenmeyer, G. A. (2009). Lakes as sentinels of climate change. *Limnology & Oceanography, 54*(6), 2283 – 2297.

Allen-Gil, S. M., Gubala, C. P., Landers, D. H., Lasorsa, B. K., Crecelius, E. A., & Curties, L. R. (1997). Heavy metal accumulation in sediment and freshwater fish in U.S. Arctic lakes. *Environmental Toxicology & Chemistry 16*(4), 733 – 741.

Ambraseys, N.N. (1988). Engineering seismology. Part I. *Earthquake Engineering & Structural Dynamics 17*, 1–105.

Appleby, P. G. (2001). Chronostratigraphic techniques in recent sediments. In W. M. Last & J. P. Smol (Eds.), *Tracking Environmental Change Using Lake Sediments. Volume 1: Basin Analysis, Coring, and Chronological Techniques* (pp. 73 – 105). Dordrecht, Netherlands: Kluwer Academic Publishers.

Arctic Monitoring and Assessment Programme (AMAP). (2011). AMAP Assessment 2011: Mercury in the Arctic. AMAP: Oslo, Sweden.

Arias, M., Barral, M. T., Da Silva-Carvalhal, J., Mejuto, J. C., & Rubinos, D. (2004). Interaction of Hg(II) with kaolin-humic acid complexes. *Clay Mineral 39,* 35 – 45.

Bertrand, S., Charlet, F., Chapron, E., Fagel, N., & de Batist, M. (2008). Reconstruction of the Holocene seismotectonic activity of the Southern Andes from seimites recorded in Lago Icalma, Chile, 39°S. *Palaeogeography, Palaeoclimatology, Palaeoecology 259,* 301 – 322.

Biester, H., Bindler, R., Martin-Cortizas, A., & Engstrom, D. R. (2007). Modeling the past atmospheric deposition of mercury using natural archives. *Environmental Science & Technology 41,* 4851 – 4860.

Blaauw, M. & Christen, J. A. (2013). Bacon Manual – v2.2. Accessed from http://www.chrono.qub.ac.uk/blaauw/bacon.html. Last access on 1 May 2017.

Blaauw, M., & Christen, J. A. (2011). Flexible Paleoclimate Age-Depth Models Using an Autoregressive Gamma Process. *Bayesian Analysis 6*(3), 457 – 474.

Bostock, H. S. (1952). Geology of Northwest Shakwak Valley, Yukon Territory. *Geological Survey of Canada* Memoir 267.

Braaten, H. F. V., de Wit, H. A., Fjeld, E., Rognerud, S., Lydersen, E., & Larssen, T. (2014). Environmental factors influencing mercury speciation in subarctic and boreal lakes. *Science of the Total Environment 476-477*, 336 – 345.

Brahney, H. L. (2007). *Paleolimnology of Kluane Lake.* (Master's thesis). Simon Fraser University, Burnaby, British Columbia, Canada,

Brahney, J., Clague, J. J., Edwards, T. W. D., & Menounos, B. (2010). Late Holocene paleohydrology of Kluane Lake, Yukon Territory, Canada. *Journal of Paleolimnology 44*, 873 – 885.

Brahney, J., Clague, J. J., Menounos, B., & Edwards, T. W. D. (2008a). Geochemical reconstruction of late Holocene drainage and mixing in Kluane Lake, Yukon Territory. *Journal of Paleolimnology 40*, 489 – 505.

Brahney, J., Clague, J. J., Menounos, B., & Edwards, T. W. D. (2008b). Timing and cause of water level fluctuations in Kluane Lake, Yukon Territory, over the past 5000 years. *Quaternary Research 70*, 213 – 227.

Braune, D., Muir, D., DeMarch, B., Gamberg, M., Poole, K., Currie, R., Dodd, M., Duschenko, W., Eamer, J., Elkin, B., Evans, M., Grundy, S., Hebert, C., Johnstone, R., Kidd, K., Koenig, B., Lockhart, L., Marshall, H., Reimer, K., Sanderson, J., & Shutt, L. (1999). Spatial and temporal trends of contaminants in Canadian Arctic freshwater and terrestrial ecosystems: a review. *The Science of the Total Environment 230*, 145 – 207.

Brazeau, M. L., Blais, J. M., Paterson, A. M., Keller, W., & Poulain, A. J. (2013a). Evidence for microbially mediated production of elemental mercury (Hg^0) in subarctic lake sediments. *Applied Geochemistry 37*, 142 – 148.

Brazeau, M. L., Poulain, A. J., Paterson, A. M., Keller, W., Sanei, H., & Blais, J. M. (2013b). Recent changes in mercury deposition and primary productivity inferred from sediments of lakes from the Hudson Bay Lowlands, Ontario, Canada. *Environmental Pollution 173*, 52 – 60.

Bunbury, J., & Gajewski, K. (2009). Variations in the depth and thickness of the White River Ash in lakes of the southwest Yukon. In L.H. Weston, L.R. Blackburn & L.L. Lewis (eds.), *Yukon*

Exploration and Geology 2008 (pp. 77 – 84). Whitehorse, Canada: Yukon Geological Survey.

Canadian Council of Ministers of the Environment (CCME). (1999). Canadian sediment quality guidelines for the protection of aquatic life: Mercury. In: *Canadian environmental quality guidelines*. Canadian Council of Ministers of the Environment: Winnipeg, Canada.

Carrie, J., Wang, F., Sanei, H., Macdonald, R. W., Outridge, P. M., & Stern, G. A. (2010). Increasing contaminant burdens in an Arctic fish, Burbot (*Lota lota*), in a warming climate. *Environmental Science & Technology 44*, 316 – 322.

Cassidy, J. F. & Rogers, G. C. (2004). The M_W 7.9 Denali Fault earthquake of 3 November 2002: felt reports and unusual effects across western Canada. *Bulletin of the Seismological Society of America 94*(6B), S53 – S57.

Chakraborty, K., Finkelstein, S. A., Desloges, J. R., & Chow, N. A. (2010). Holocene paleoenvironmental changes inferred from diatom assemblages in sediments of Kusawa Lake, Yukon Territory, Canada. *Quaternary Research 74*, 15 – 22.

Chételat, J., Amyot, M., Arp, P., Blais, J. M., Depew, D., Emmerton, C. A., …, & van der Velden, S. (2015). Mercury in freshwater ecosystems of the Canadian Arctic: recent advances on its cycling and fate. *Science of the Total Environment 509-510*, 41 – 66.

Chu, P. & Porcella, D. B. (1995). Mercury stack emissions from U.S. electric utility power plants. *Water, Air, and Soil Pollution 80*, 135 – 144.

Clague, J. J. (1981). Landslides at the south end of Kluane Lake, Yukon Territory. *Canadian Journal of Earth Sciences 18*, 959 – 971.

Clague, J. J., Evans, S. G., Rampton, V. N., & Woodworth, G. J. (1995). Improved age estimates for the White River and Bridge River tephras, western Canada. *Can. J. Earth Sci. 32*, 1172 – 1179.

Clague, J. J., Luckman, B. H., Van Dorp, R. D., Gilbert, R., Froese, D., Jensen, B. J. L., & Reyes, A. V. (2006). Rapid changes in the level of Kluane Lake in Yukon Territory over the last millennium. *Quaternary Research 66*, 342 – 355.

Cohen, A. S. (2004). *Paleolimnology: The history and evolution of lake systems.* Oxford, England: Oxford University Press.

Cooke, C. A., Hobbs, W. O., Michelutti, N., & Wolfe, A. P (2010). Reliance on ^{210}Pb chronology can compromise the inference of preindustrial Hg flux to lake sediments. *Environmental Science & Technology 44*, 1998 – 2003.

Cooke, C. A., Wolfe, A. P., Michelutti, N., Balcom, P. H., & Briner, J. P. (2012). A Holocene perspective on algal mercury scavenging to sediments of an arctic lake. *Environmental Science & Technology 46*, 7135 – 7141.

Crann, C. A., Patterson, R. T., Macumber, A. L., Galloway, J. M., Roe, H. M., Blaauw, M., Swindles, G. T., & Falck, H. (2015). Sediment accumulation rates in subarctic lakes: Insights into age-depth modeling from 22 dated lake records from the Northwest Territories, Canada. *Quaternary Geology 27*, 131 – 144.

Danby, R. K., Williams, A., & Hik, D. S. (2014). Fifty years of science at the Kluane Lake Research Station. *Arctic 67* (Suppl. 1), iii – viii.

Deison, R., Smol, J. P., Kokelj, S. V., Pisaric, M. F. J., Kimpe, L. E., Poulain, A. J., Sanei, H., Thienpont, J. R., & Blais, J. M. (2012). Spatial and temporal assessment of mercury and organic matter in thermokarst affected lakes of the Mackenzie Delta Uplands, NT, Canada. *Environmental Science & Technology 46*, 8748 – 8755.

Desauziers, V., Castre, N., & Le Cloirec, P. (1997). Sorption of methylmercury by clays and mineral oxides. *Environmental Technology 18*, 1009 – 1018.

Dodds, C. J., & Campbell, R. B. (1992). *Geology, SW Kluane Lake map area [115G & F[E1/2]], Yukon Territory* [map]. 1:250,000. Geological Survey of Canada, Open File 2188.

Doig, R. (1986). A method for determining the frequency of large-magnitude earthquakes using lake sediments. *Canadian Journal of Earth Sciences 23*, 930 – 937.

Doig, R. (1991). Effects of strong seismic shaking in lake sediments, and earthquake recurrence interval, Témiscaming, Québec. *Canadian Journal of Earth Sciences 28*, 1349 – 1352.

Doig, R. (1998). Paleoseismological evidence from lake sediments from recent movement on the Denali and other faults, Yukon Territory, Canada. *Tectonophysics 296*, 363 – 370.

Dórea, J. G. (2008). Persistent, bioaccumulative and toxic substances in fish: human health considerations. *Science of the Total Environment 400*, 93 – 114.

Doughty, M., Eyles, N., Eyles, C. H., Wallace, K., & Boyce, J. I. (2014). Lake sediments as natural seismographs: earthquake-related deformations (seismites) in central Canadian lakes. *Sedimentary Geology 313*, 45 – 67.

Drevnick, P. E., Cooke, C. A., Barraza, D., Blais, J. M., Coale, K. H., Cumming, B. F., Curtis, C. J., …, Wolfe, B. B. (2016). Spatiotemporal patterns of mercury accumulation in lake sediments of western North America. *Science of the Total Environment 568,* 1157 – 1170.

Drevnick, P. E., Engstrom, D. R., Driscoll, C. T., Swain, E. B., Balogh, S. J., Kamman, N. C., Long, D. T., Muir, D. C. G., Parsons, M. J., Rolfhus, K. R., & Rossmann, R. (2012). Spatial and temporal patterns of mercury accumulation in lacustrine sediments across the Laurentian Great Lakes region. *Environmental Pollution 161*, 252 – 260.

Driscoll, C. T., Blette, V., Yan, C., Schofield, C. L., Munson, R., & Holsapple, J. (1995). The role of dissolved organic carbon in the chemistry and bioavailaibility of mercury in remote Adirondak lakes. *Water, Air, and Soil Pollution 80*, 499 – 508.

El Bilali, L., Rasmussen, P. E., Hall, G. E. M., & Fortin, D. (2002). Role of sediment composition in trace metal distribution in lake sediments. *Applied Geochemistry 17*, 1171 – 1181.

Engstrom, D. R., Swain, E. B., Henning, T. A., Brighma, M. E., & Brezonik, P. L. (1994). Atmospheric mercury deposition to lakes and watersheds: a quantitative reconstruction from multiple sediment cores. In: Baker, L. A. (ed). *Environmental Chemistry of Lakes and Reservoirs.* American Chemical Society. Pg. 33 – 66.

Environment Yukon. (2010). *Status of Yukon Fisheries 2010: An overview of the state of Yukon fisheries and the health of fish stocks, with special reference to fisheries management programs.* Yukon Fish and Wildlife Branch Report MR-10-01.

Ficke, A. D., Myrick, C. A., & Hansen, L. J. (2007). Potential impacts of global climate change on freshwater fisheries. *Reviews in Fish Biology and Fisheries 17*, 581 – 613.

Fitzgerald, W. F., Engstrom, D. R., Lamborg, C. H., Tseng, C.-M., Balcom, P. H., & Hammerschmidt, C. R. (2005). Modern and historic atmospheric mercury fluxes in northern Alaska: global sources and Arctic depletion. *Environmental Science & Technology 39*, 557 – 568.

Fitzgerald, W. F., Engstrom, D. R., Mason, R. P., & Nater, E. A. (1998). The case for atmospheric mercury contamination in remote areas. *Environmental Science & Technology 32*(1), 1 – 7.

Frenet-Robin, M., & Ottmann, F. (1978). Comparative study of the fixation of inorganic mercury on the principal clay minerals and the sediments of the Loire estuary. *Estuarine and Coastal Marine Research 7*, 425 – 436.

Gabriel, M. C. & Williamson, D. G. (2004). Principal biogeochemical factors affecting the speciation and transport of mercury through the terrestrial environment. *Environmental Geochemistry & Health 26*(4), 421 – 434.

Gilbert, R., & Desloges, J. R. (2005). The record of Glacial Lake Champagne in Kusawa Lake, southwestern Yukon Territory. *Canadian Journal of Earth Sciences 42*: 2127 – 2140.

Gilmour, C. C., Henry, E. A., & Mitchell, R. (1992). Sulfate stimulation of mercury methylation in freshwater sediments. *Environmental Science & Technology 26*(11), 2281 – 2287.

Glew, J. R. (1988). A portable extruding device for close interval sectioning of unconsolidated core samples. *Journal of Paleolimnology 1*, 235 – 239.

Glew, J. R., Smol, J. P., & Last, W. M. (2001). Sediment core collection and extrusion. In W. M. Last & J. P. Smol (Eds.), *Tracking Environmental Change Using Lake Sediments. Volume 1: Basin Analysis, Coring, and Chronological Techniques* (pp. 73 – 105). Dordrecht, Netherlands: Kluwer Academic Publishers.

Goodsite, M. E., Outridge, P. M., Christensen, J. H., Dastoor, A., Muir, D., Travikov, O., & Wilson, S. (2013). How well to environmental archives of atmospheric mercury deposition in the Arctic reproduce rates and trends depicted by atmospheric models and measurements?. *Science of the Total Environment 453-453*, 196 – 207.

Greenfield, B. K., Hrabik, T. R., Harvey, C. J., & Carpenter, S. R. (2001). Predicting mercury levels in yellow perch: use of water chemistry, trophic ecology, and spatial traits. *Canadian Journal of Fisheries and Aquatic Sciences 58*, 1419 – 1429.

Grigal, D. F. (2002). Inputs and outputs of mercury from terrestrial watersheds: a review. *Environmental Reviews 10*, 1 – 39.

Gupta, S. K., & Polach, H. A. (1985). Radiocarbon dating practices at ANU. Handbook, Radiocarbon Laboratory, Research School of Pacific Studies, ANU, Canberra.

Harrell, F. E. Jr. (2017). Hmisc, R package version (4.0-3). (https://cran.r-project.org/package=Hmisc).

Hart, B. (1982). Uptake of trace metals by sediments and suspended particulates: a review. *Hydrobiologia 91-92*, 399 – 313.

Heiri, O., Lotter, A. F., & Lemcke, G. (2001). Loss on ignition as a method for estimating organic and carbonate content in sediments: reproducibility and comparability of results. *Journal of Paleolimnology 25*, 101 – 110.

Hermanson, M. H. & Brozowski, J. R. (2005). History of Inuit community exposure to lead, cadmium, and mercury in sewage lake sediments. *Environmental Health Perspectives 113*(10), 1308 – 1312.

Hermanson, M. H. (1993). Historical accumulation of atmospherically derived pollutant trace metals in the Arctic measured in dated sediment cores. *Water Science & Technology 28(8-9), 33 – 41*.

Hermanson, M. H. (1998). Anthropogenic mercury deposition to arctic lake sediments. *Water, Air, and Soil Pollution 101*, 309 – 321.

Hyndman, R. D., Cassidy, J. F., Adams, J., Rogers, G. C., & Mazzotti, S. (2005). Earthquakes and seismic hazard in the Yukon-Beaufort-Mackenzie. *Canadian Society of Exploration Geophysicists Recorder 30*(5), 32 – 66.

Jaakkola, T., Tolonen, K., Huttunen, P., & Leskinen, S. (1983). The use of fallout of ^{137}Cs and ^{239,240}Pu for dating of lake sediments. *Hydrobiologia 103*, 15 – 19.

Jackson, L. E. Jr. (1990). Oldest dated earthquake in Yukon Territory, Canada. *Canadian Journal of Earth Sciences 27*, 818 – 819.

Johansson, K., Aastrup, M., Andersson, A., Bringmark, L., & Iverfeldt, A. (1991). Mercury in Swedish forest soils and waters – assessment of critical load. *Water, Air, & Soil Pollution 56*(1), 267 – 281.

Juggins, S. (2015). rioja: Analysis of Quaternary Science Data, R package version (0.9-9). (http://cran.r-project.org/package=rioja).

Kainz, M., Lucotte, M., & Parrish, C. C. (2003). Relationships between organic matter composition and methyl mercury content of offshore and carbon-rich littoral sediments in an oligotrophic lake. *Canadian Journal of Fisheries and Aquatic Sciences 60*(7), 888 – 896.

Kirk, J. L., Muir, D. C. M., Antoniades, D., Douglas, M. S. V., Jackson, T. A., Kling, H., Lamoureux, S., Lim, D. S. S., Pienitz, R., Smol, J. P., Stewart, K., Wang, X., & Yang, F. (2011). Climate change and mercury accumulation in Canadian high and subarctic lakes. *Environmental Science & Technology 45*, 964 – 970.

Kluane First Nation (KFN). (2014). Nourishing Our Future: An Adaptive Food Security Strategy to Ensure the Cultural and Physical Well-Being of the Kluane First Nation Against the Impacts of Climate Change in the Yukon.

Knight, J. B., Mortensen, J. K., & Morison, S. R. (1999). Lode and placer gold composition in the Klondike District, Yukon Territory, Canada: Implications for the nature and genesis of Klondike placer and lode gold deposits. *Economic Geology 94*, 649 – 664.

Köck, G., Muir, D, Yang, F., Wang, X., Talbot, C., Gantner, N., & Moser, D. (2012). Bathymetry and sediment geochemistry of Lake Hazen (Quttinirpaaq National Park, Ellesmere Island, Nunavut). *Arctic 65*(1), 56 – 66.

Korosi, J. B., McDonald, J., Coleman, K. A., Palmer, M. J., Smol, J. P., Simpson, M. J., & Blais, J. M. (2015). Long-term changes in organic matter and mercury transport to lakes in the sporadic discontinuous permafrost zone related to peat subsidence. *Limnology & Oceanography 60*, 1550 – 1561.

Kuhnlein, H. V., & Chan, H. M. (2000). Environment and contaminants in traditional food systems of northern indigenous peoples. *Annual Review of Nutrition, 20*(1), 595-626.

Lamontagne, M., Halchuk, S., Cassidy, J. F., & Rogers, G. C. (2008). Significant Canadian Earthquakes of the Period 1600 – 2006. *Seismological Research Letters 79*(2), 211 – 223.

Landers, D. H., Gubala, C., Verta, M., Lucotte, M., Johansson, K., Vlasova, T., & Lockhart, W. L. (1998). Using lake sediment mercury flux ratios to evaluate the regional and continental dimensions of mercury deposition in Arctic and boreal environments. *Atmospheric Environment 32*(5), 919 – 928.

Laperrière, L., Fallu, M.-A., Hausmann, S., Pienitz, R., & Muir, D. (2008). Paleolimnological evidence of mining and demographic impacts on Lac Dauriat, Schefferville (subarctic Québec, Canada). *Journal of Paleolimnology 40*, 309 – 324.

LeBarge, W. P. (ed). (1996). Yukon Quaternary Geology Volume 1. Exploration and Geological Services Division, Indian and Northern Affairs Canada, Yukon Region. 84 pg.

Lehnherr, I. (2014). Methymercury biogeochemistry: a review with special reference to Arctic aquatic ecosystems. *Environmental Reviews 22*, 229 – 243.

Lindsey, C. C., Patalas, K., Bodaly, R. A., & Archibald, C. P. (1981). Glaciation and the physical, chemical and biological limnology of Yukon lakes. Canadian Technical Report of Fisheries and Aquatic Sciences 966. Winnipeg, Manitoba: Department of Fisheries and Oceans.

Liu, G., Li, Y., & Cai, Y. (2012). Adsorption of mercury on solids in the aquatic environment. In Liu, G., Cai, Y., & O'Driscoll (Eds)., *Environmental Chemistry and Toxicology of Mercury* (pp. 367 – 387). Hoboken, USA: John Wiley & Sons, Inc.

Lockhart, W. L., Macdonald, R. W., Outridge, P. M., Wilkinson, P., DeLaronde, J. B., & Rudd, J. W. M. (2000). Tests of the fidelity of lake sediment core records of mercury deposition to known histories of mercury contamination. *The Science of the Total Environment 260*, 171 – 180.

Lockhart, W. L., Stern, G. A., Low, G., Hendzel, M., Boila, G., Roach, P., Evans, M. S., Billeck, B. N., DeLaronde, J., Friesen, S., Kidd, K., Atkins, S., Muir, D. C. G., Stoddart, M., Stephens, G., Stephenson, S., Harbicht, S., Snowshoe, N., Grey, B., Thompson, S., & DeGraff, N. (2005). A history of total mercury in edible muscle of fish from lakes in northern Canada. *Science of the Total Environment 351-352*, 427 – 463.

Lockhart, W. L., Wilkinson, P., Billeck, B. N., Danell, R. A., Hunt, R. V., Brunskill, G. J., DeLaronde, J., & St. Louis, V. (1998). Fluxes of mercury to lake sediments in central and northern Canada inferred from dated sediment cores. *Biogeochemistry 40*, 163 – 173.

Lockhart, W. L., Wilkinson, P., Billeck, B. N., Hunt, R. V., Wagemann, R., & Brunskill, G. J. (1995). Current and historical inputs of mercury to high-latitude lakes in Canada and to Hudson Bay. *Water, Air, and Soil Pollution 80*, 603 – 610.

Lowey, G. W. (2002). Sedimentary processes of the Kusawa Lake torrent system, Yukon, Canada, as revealed by the September 16, 1982 flood event. *Sedimentary Geology 151*(3-4), 293 – 312.

Luckman, B. H. (2000). The Little Ice Age in the Canadian Rockies. *Geomorphology 32*, 357 – 384.

Lucotte, M., Mucci, A., Hillaire-Marcel, C., Pichet, P., & Grondin, A. (1995). Anthropogenic mercury enrichment in remote lakes of northern Quebec (Canada). *Water, Air, and Soil Pollution 80*, 467 – 476.

Luo, Y., Duan, Y., Xu, G., & Hao, J. (2015). Inhibition of mercury release from forest soil by atmospheric deposition of Ca^{2+} and SO_4^{2-}. *Chemosphere 134*, 113 – 119.

MacDonald, L. A., Wiklund, J. A., Elmes, M. C., Wolfe, B. B., & Hall, R. I. (2016). Paleolimnological assessment of riverine and atmospheric pathways and sources of metal deposition at a floodplain lake (Slave River Delta, Northwest Territories, Canada). *Science of the Total Environment 544*, 811 – 823.

Mason, R. P., Fitzgerald, W. F., & Morel, F. M. M. (1994). The biogeochemical cycling of elemental mercury: Anthropogenic influences. *Geochimica et Cosmochimica Acta 58*(15), 3191 – 3198.

Mergler, D., Anderson, H. A., Chan, L. H. M., Mahaffey, K. R., Murray, M., Sakamoto, M., & Stern, A. H. (2007). Methylmercury exposure and health effects in humans: a worldwide concern. *Ambio 36*(1), 3 – 11.

Michelutti, N., Blais, J. M., Cumming, B. F., Paterson, A. M., Rühland, K., Wolfe, A. P., & Smol, J. P. (2010). Do spectrally inferred determinations of chlorophyll a reflect trends in lake trophic status? *Journal of Paleolimnology 43*, 205 – 217.

Michelutti, N., Hermanson, M. H., Smol, J. P., Dillon, P. J., & Douglas, M. S. V. (2007). Delayed response of diatom assemblages to sewage inputs in an Arctic lake. *Aquatic Science 69*, 523 – 533.

Monecke, K., Anselmetti, F. S., Becker, A., Sturm, M., & Giardini, D. (2004). The record of historic earthquakes in lake sediments of central Switzerland. *Tectonophysics 394*, 21 – 40.

Moore, R. D., Fleming, S. W., Menounos, B., Wheate, R., Fountain, A., Stahl, K., Holm, K., & Jakob, M. (2009). Glacier change in western North America: influences on hydrology, geomorphic hazards and water quality. *Hydrological Processes 23*, 42 – 61.

Muir, D. C. G., Wang, X., Yang, F., Nguyen, N., Jackson, T. A., Evans, M. S., Douglas, M., Kock, G., Lamoureux, S., Pienitz, R., Smol, J. P., Vincent, W. F., & Dastoor, A. (2009). Spatial

trends and historical deposition of mercury in eastern and northern Canada inferred from lake sediment cores. *Environmental Science & Technology 43*, 4802 – 4809.

Muller, J. E. (1967). Kluane Lake Map-Area, Yukon Territory (115G, 115F E½). *Geological Survey of Canada* Memoir 340.

Northrup, S., Connor, M., & Taylor, E. B. (2010). Population structure of lake trout (*Salvelinus namaycush*) in a large glacial-fed lake inferred from microsatellite DNA and morphological analysis. *Canadian Journal of Fisheries & Aquatic Sciences 67*, 1171 – 1186.

Oldfield, F., Barnosky, C., Leopold, E. B., & Smith, J. P. (1983). Mineral magnetic studies of lake sediments. A brief review. *Hydrobiologia 103*, 37 – 44.

Outridge, P. M., Sanei, H., Courtney Mustaphi, C. J., & Gajewski, K. (2017). Holocene climate change influences on trace metal and organic matter geochemistry in the sediments of an Arctic lake over 7 000 years. *Applied Geochemistry 78*, 35 – 48.

Outridge, P. M., Sanei, H., Stern, G. A., Goodsite, M., Hamilton, P. B., Carrie, J., Goodarzi, F., & MacDonald, R. W. (2011). Comment on climate change and mercury accumulation in Canadian high and subarctic lakes. *Environmental Science & Technology 45*, 6703 – 6704.

Outridge, P. M., Sanei, H., Stern, G. A., Hamilton, P. B., & Goodarzi, F. (2007). Evidence for Control of Mercury Accumulation Rates in Canadian High Arctic Lake Sediments by Variations of Aquatic Primary Productivity. *Environmental Science & Technology 41*, 5259 – 5265.

Outridge, P. M., Stern, G. A., Hamilton, P. B., Percival, J. B., McNeely, R., & Lockhart, W. L. (2005). Trace metal profiles in the varved sediment of an Arctic lake. *Geochimica et Cosmochimica Acta 69*(2), 4881 – 4894.

Outridge, P., M., Sanei, H., Courtney Mustaphi, C. J., & Gajewski, K. (2017). Holocene climate change influences on trace metal and organic matter geochemistry in the sediments of an Arctic lake over 7,000 years. *Applied Geochemistry 78*, 35 – 48.

Paranjape, A. R., & Hall, B D. (2017). Recent advances in the study of mercury methylation in aquatic systems. *FACETS 2*, 85 – 119.

Pak, K.-R. & Bartha, R, (1998). Mercury methylation and demethylation in anoxic lake sediments and by strictly anaerobic bacteria. *Applied Environmental Microbiology 64*(3), 1013 – 1017.

Permaki, L., & Stone, M. (2007). Fluxes of As, Cu, Hg, Pb, in lake sediments in the Coppermine River basin, Canada. *Nordic Hydrology 38*(2), 177 – 185.

Perry, E., Norton, S. A., Kamman, N. C., Lorey, P. M., & Driscoll, C. T. (2005). Deconstruction of historic mercury accumulation in lake sediments, northeastern United States. *Ecotoxicology 14*, 85 – 99.

Petersen, J., Wilhelm, B., Revel, M., Rolland, Y., Crouzet, C., Arnaud, F., Brisset, E., Chaumillon, E., & Magand, O. (2014). Sediments of Lake Vens (SW European Alps, France) record large-magnitude earthquake events. *Journal of Paleolimnology 51*, 343 – 355.

Prowse, T. D., Wrona, F. J., Reist, J. D., Gibson, J. J., Hobbie, J. E., Lévesque, L. M. J., & Vincent, W. F. (2006). Climate change effects on hydroecology of Arctic freshwater ecosystems. *Ambio 35*(7), 347 – 358.

R Core Team (2016) – R: A language and environment for statistical computing. R Foundation for Statistical Computing, Vienna, Austria.

Rampton, V. N., & Shearer, J. M. (1978). The geology and limnology of Kluane Lake, Yukon Territory, I preliminary assessment. Terrain Analysis Mapping Service, Stittsville.

Rasmussen, P. E., Villard, D. J., Gardner, H. D., Fortescue, J. A. C., Schiff, S. L., & Shilts, W. W. (1998). Mercury in lake sediments of the Precambrian Shield near Huntsville, Ontario, Canada. *Environmental Geology 33*(2/3), 170 – 182.

Ravichandran, M. (2004). Interactions between mercury and dissolved organic matter—a review. *Chemosphere 55*(3), 319 – 331.

Rawn, D. F. K., Lockhart, W. L., Wilkinson, P., Savoie, D. A., Rosenberg, G. B., & Muir, D. C. G. (2001). Historical contamination of Yukon Lake sediments by PCBs and organochlorine pesticides: influence of local sources and watershed characteristics. *Science of the Total Environment 280*, 17 – 37.

Receveur, O., Kassi, N., Chan, H. M., Berti, P. R., & Kuhnlein, V. (1998). *Yukon First Nations' assessment of dietary benefit/risk*. Centre for Indigenous Peoples' Nutrition and Environment, McGill University. 178 pp.

Reimer, P.J., Bard, E., Bayliss, A., Beck, J.W., Blackwell, P.G., Bronk Ramsey, …, & van der Plicht, J. (2013). IntCal13 and Marine13 radiocarbon age calibration curves, 0-50,000 years cal BP. *Radiocarbon* 55, 1869 - 1887.

Reimers, R. S., & Krenkel, P. A. (1974). Kinetics of mercury adsorption and desorption in sediments. *Journal (Water Pollution Control Federation) 46*(2), 352 – 365.

Reist, J. D., Wrona, F. J., Prowse, T. D., Power, M., Dempson, J. B., Beamish, R. J., King, J. R., Carmichael, T. J., & Sawatzky, C. D. (2006). General effects of climate change on Arctic fishes and fish populations. *Ambio 35*(7), 370 – 380.

Reyes, A. V., Luckman, B. H., Smith, D. J., Clague, J. J., & Van Dorp, R. (2006). Tree-ring dates for the maximum Little Ice Age advance of Kaskawulsh Glacier, St. Elias mountains, Canada. *Arctic 59*(1), 14 – 20.

Rudd, J. W. M. (1995). Sources of methyl mercury to freshwater ecosystems: a review. *Water, Air, and Soil Pollution 80*, 697 – 713.

Rydberg, J., Klaminder, J., Rosén, P., & Bindler, R. (2010). Climate driven release of carbon and mercury from permafrost mires increases mercury loading to sub-arctic lakes. *Science of the Total Environment 408*, 4778 – 4783.

Rytuba, J. J. (2003). Mercury from mineral deposits and potential environmental impact. *Environmental Geology 43*, 326 – 338.

Sandgren, P. & Snowball, I. (2001). Application of mineral magnetic techniques to paleolimnology. In: Last, W. M. & Smol, J. P. (eds). *Tracking Environmental Change using Lake Sediments. Volume 2: Physical and Geochemical Methods*. (pp. 217 – 237). Dordrecht, Netherlands: Kluwer Academic Publishers.

Sanei, H., & Goodarzi, F. (2006). Relationship between organic matter and mercury in recent lake sediment: the physical-geochemical aspects. *Applied Geochemistry 21*, 1900 – 1912.

Sanei, H., Outridge, P. M., Dallimore, A., & Hamilton, P. B. (2012). Mercury-organic matter relationships in pre-pollution sediments of thermokarst lakes from the Mackenzie River delta, Canada: the role of depositional environment. *Biogeochemistry 107*, 149 – 164.

Scherbatskoy, T., Shanely, J. B., & Keeler, G. J. (1998). Factors controlling mercury transport in an upland forested catchment. *Water, Air, and Soil Pollution 105*, 427 – 438.

Schindler, D. W. & Smol, J. P. (2006). Cumulative effects of climate warming and other human activities on freshwaters of Arctic and subarctic North America. *Ambio 35*(4), 160 – 168.

Schindler, D. W. (2009). Lakes as sentinels and integrators for the effects of climate change on watersheds, airsheds, and landscapes. *Limnology & Oceanography 54*(6 part 2), 2349 – 2358.

Schuster, P. F., Krabbenhoft, D. P., Naftz, D. L., Cecil, D., Olson, M. L., Dewild, J. F., Susong, D. D., Green, J. R., & Abbott, M. L. (2002). Atmospheric mercury deposition and during the last 270 years: a glacial ice core record of natural and anthropogenic sources. *Environmental Science & Technology 36*(11), 2303 – 2310.

Schwab, M. J., Werner, P., Dulshi, P., McGee, E., Nowaczyk, N. R., Bertrand, S., & Leroy, S. A. G. (2009). Paleolimnology of Lake Sapanca and identification of historic earthquake signals, northern Anatolian Fault Zone (Turkey). *Quaternary Science Reviews 28*, 991 – 1005.

Selin, N. E. (2009). Global biogeochemical cycling of mercury: a review. *Annual Review of Environment and Resources 34*, 43 – 63.

Shanmugam, G. (2016). The seismite problem. *Journal of Palaeogeography 5*(4), 318 – 362.

Shilts, W. W., & Clague, J. J. (1992). Documentation of earthquake-induced disturbance of lake sediments using subbottom acoustic profiling. *Canadian Journal of Earth Sciences 29*, 1018 – 1042.

Shugar, D. H., Clague, J. J., Best, J. L., Schoof, C., Willis, M. J., Copland, L., & Roe, G. H. (2017). River piracy and drainage basin reorganization led by climate-driven glacier retreat. *Nature Geoscience* (Advance Online Publication), 1 – 7.

Smith, J. G. (2003). Aspects of the loss-on-ignition (LOI) technique in the context of clay-rich, glaciolacustrine sediments. *Geografiska Annaler 85A*(1), 91 – 97.

Smol, J. P., & Douglas, M. S. V. (2007). From controversy to consensus: making the case for recent climate change in the Arctic using lake sediments. *Frontiers in Ecology and the Environment 5*(9), 466 – 474.

Snow, W. E. (1936). *The ore deposits of Alaska and the Yukon*. (Unpublished master's thesis). The University of British Columbia, Vancouver, British Columbia, Canada.

St. Louis, V., Rudd, J. W. M., Kelly, C. A., Beaty, K. G., Bloom, N. S., & Flett, R. J. (1994). Importance of wetlands as sources of methyl mercury to boreal forest ecosystems. *Canadian Journal of Fisheries and Aquatic Sciences 51*(5), 1065 – 1076.

Stenström, K. E., Skog G., Georgiadou, E., Genberg, J., & Johansson, A. (2011). A guide to radiocarbon units and calculations. Lund University, Lund, Sweden.

Stern, G. A. (2013). Trace metals and organohalogen contaminants in fish from selected Yukon lakes: a temporal and spatial study. In*: Synopsis of Research Conducted under the 2013-2014 Northern Contaminants Program*. Aboriginal Affairs and Northern Development Canada. 472 pp.

Stern, G. A., Macdonald, R. W, Outridge, P. M., Wilson, S., Chételat, J., Cole, A., Hintelmann, H., Loseto, L. L., Steffen, A., Wang, F., & Zdanowicz, C. (2012). How does climate change influence arctic mercury?. *Science of the Total Environment 414*, 22 – 42.

Stern, G. A., Sanei, H., Roach, P., DeLaronde, J., & Outridge, P. M. (2009). Historical interrelated variations of mercury and aquatic organic matter from a subarctic lake in Yukon, Canada: Further evidence toward the algal-mercury scavenging hypothesis. *Environmental Science & Technology 43*, 7684 – 7690.

Stern, G.A., Macdonald, R. W., Outridge, P. M., Wilson, S., Chetelat, J., Cole, A., …, & Zdanowicz, C. (2012). How does climate change influence Arctic mercury?. *Science of the Total Environment 414*, 22 – 42.

Stoermer, E. F., Schelske, C. L., & Wolin, J. A. (1990). Siliceous microfossil succession in the sediments of McLeod Bay, Great Slave Lake, Northwest Territories. *Canadian Journal of Fisheries and Aquatic Sciences 47*, 1865 – 1974.

Streicker, J. (2016). Yukon climate change indicators and key findings 2015. Northern Climate ExChange, Yukon Research Centre. 84 pp.

Thompson, R., & Oldfield, F. (1986). *Environmental Magnetism*. London, England: George Allen and Unwin.

Ullrich, S. M., Tanton, T. W., & Abdrashitova, S. A. (2001). Mercury in the Aquatic Environment: A Review of Factors Affecting Methylation. *Critical Reviews in Environmental Science and Technology 31*(3), 241 – 293.

Van Loon, S. & Bond, J. D. (2014). Yukon Placer Mining Industry 2010 – 2014. Yukon Geological Survey. 230 pp.

van Metre, P.C. & Fuller, C. C. (2009). Dual-core mass-balance approach for evaluating mercury and ^{210}Pb atmospheric fallout and focusing to lakes. *Environmental Science & Technology 43,* 26 – 32.

Van Oostdam, J., Donaldson, S. G., Feeley, M., Arnold, D., Ayotte, P., Bondy, G., …, & Kalhok, S. (2005). Human health impacts of environmental contaminants in Arctic Canada: A review. *Science of the Total Environment 351-352,* 165 – 246.

Verosub, K. L., & Roberts, A. P. (1995). Environmental magnetism: Past, present, and future. *Journal of Geophysical Research 100*(B2), 2175 – 2192.

von Guten, L., Grosjean, M., Beer, J., Grob, P., Morales, A., & Urrutia, R. (2009). Age modeling of young non-varved lake sediments: methods and limits. Examples from two lakes in Central Chile. *Journal of Paleolimnology 42,* 401 – 412.

Wein, E. E., & Freeman, M. M. R. (1995). Frequency of traditional food use by three Yukon First Nations living in four communities. *Arctic 48*(2), 161 – 171.

Whitehead, P.G., Wilby, R. L., Battarbee, R. W., Kernan, M., & Wade, A. J. (2009). A review of the potential impacts of climate change on surface water quality. *Hydrological Sciences Journal 54*(1), 101 – 123.

Wiener, J. G., Knights, B. C., Sandheinrich, M. B., Jeremiason, J. D., Brigham, E., Engstrom, D. R., …, & Balogh, S. J. (2006). Mercury in soils, lakes, and fish in Voyageurs National Park (Minnesota): importance of atmospheric deposition and ecosystem factors. *Environmental Science & Technology 40,* 6261 – 6268.

Wolfe, A. P., Vinebrooke, R. D., Michelutti, N., Rivard, B., & Das, B. (2006). Experimental calibration of lake-sediment spectral reflectance to chlorophyll a concentrations: methodology and paleolimnological validation. *Journal of Paleolimnology 36,* 91 – 100.

Wolfenden, S., Charnock, J. M., Hilton, J., Livens, F. R., & Vaughan, D. J. (2005). Sulfide species as a sink for mercury in lake sediments. *Environmental Science & Technology 39,* 6644 – 6648.

Yang, H. & Rose, N. (2005). Trace element pollution records in some UK lake sediments, their history, influence factors and regional differences. *Environment International 31,* 63 – 75.

Yost, L. J., Shock, S. S., Holm, S. E., Lowney, Y. W., & Noggle, J. J. (2010). Lack of complete exposure pathways for metals in natural and FGD gypsum. *Human and Ecological Risk Assessment 16*, 317 – 339.

Yudovich, Y. E. & Ketris, M. P. (2005). Mercury in coal: a review. Part 1. Geochemistry. *International Journal of Coal Geology 62*, 107 – 134.

Yukon Geological Survey. (2017*). Bedrock Geology* (file CSW_GEOLOGY.BEDROCK_GEOLOGY_POLY). GeoYukon. Created by Geomatics Yukon using Geocortex Essentials (Esri ArcGIS). < http://mapservices.gov.yk.ca/GeoYukon/>

Zhu, D. & Zhong, H. (2015). Potential bioavailability of mercury in humus-coated clay minerals. *Journal of Environmental Sciences 36*, 48 – 55.

Appendix A

Age-Depth Model Development using BACON

Age-depth models were developed for cores used in this study using a Bayesian approach, which allows for the combination of multiple dating proxies in order to depth a more robust model. These models incorporated radioisotope dating (^{210}Pb, ^{137}Cs, ^{14}C) as well as known marker layers (White River Tephra, Yakutat Bay earthquakes) identified within pairs of sediment cores from each site.

A1. 'Wiggle Matching'

First, sediment core pairs were aligned using loss-on-ignition (LOI) data by 'wiggle matching', in order to use dating information from both cores. This matching process is conducted by using a constant modifier of depth for one sediment core, in order to achieve parallel stratigraphic trends in LOI data with respect to the other core of the pair. Due to the variable nature of sedimentation rates in Kluane Lake, multiple, depth-specific constants were used in some cases, in order to better align sediment cores. Presented below are the 'wiggle matched' LOI stratigraphies for cores 3A & 3B, and 4A & 4B (Figures A.1, A.2, A.3).

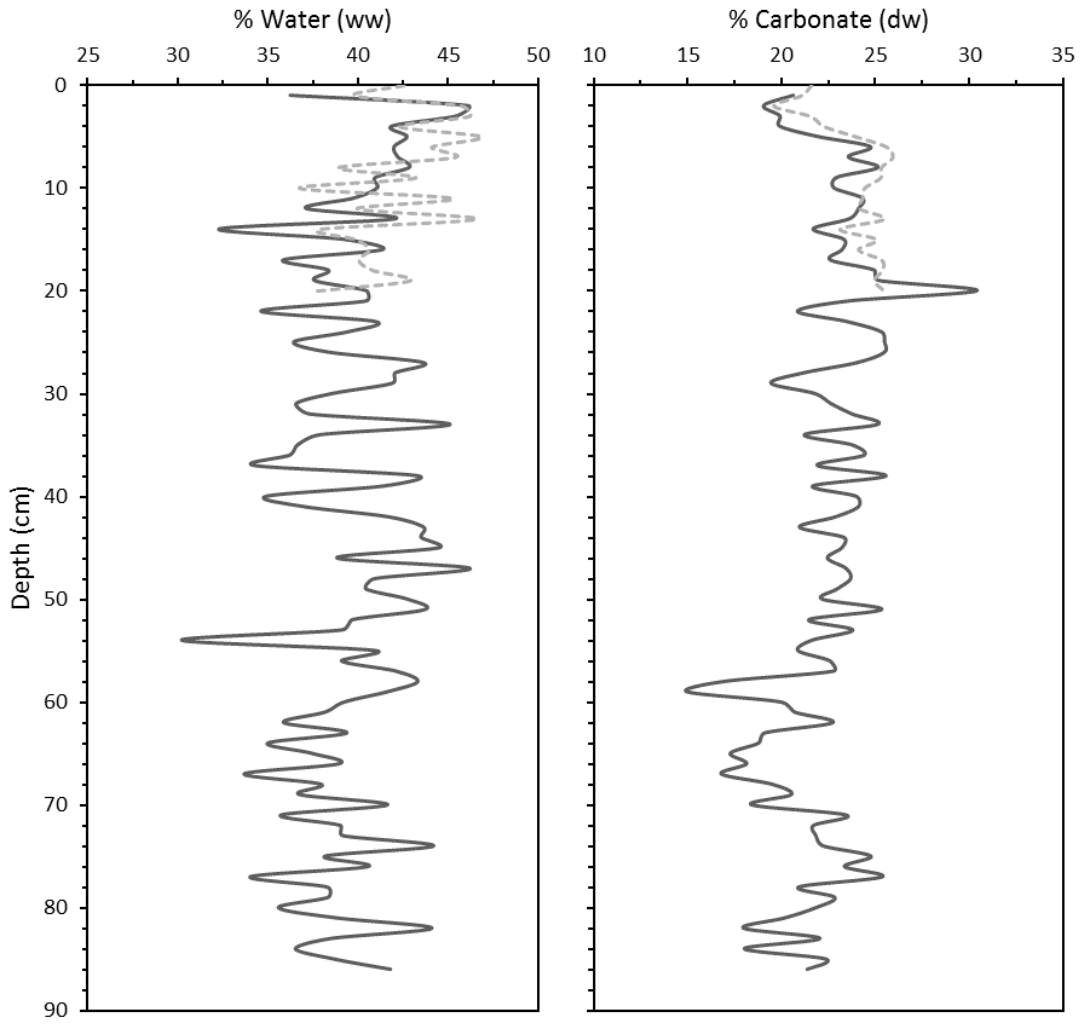

Figure A.1. Water and carbonate content stratigraphies for cores collected at site 1 used in 'wiggle matching'. These cores were aligned by shifting the depth values for core 1A (dark grey solid) down by 1 cm with respect to core 1B (light grey dashed), as the surface sediment section was lost during core collection.

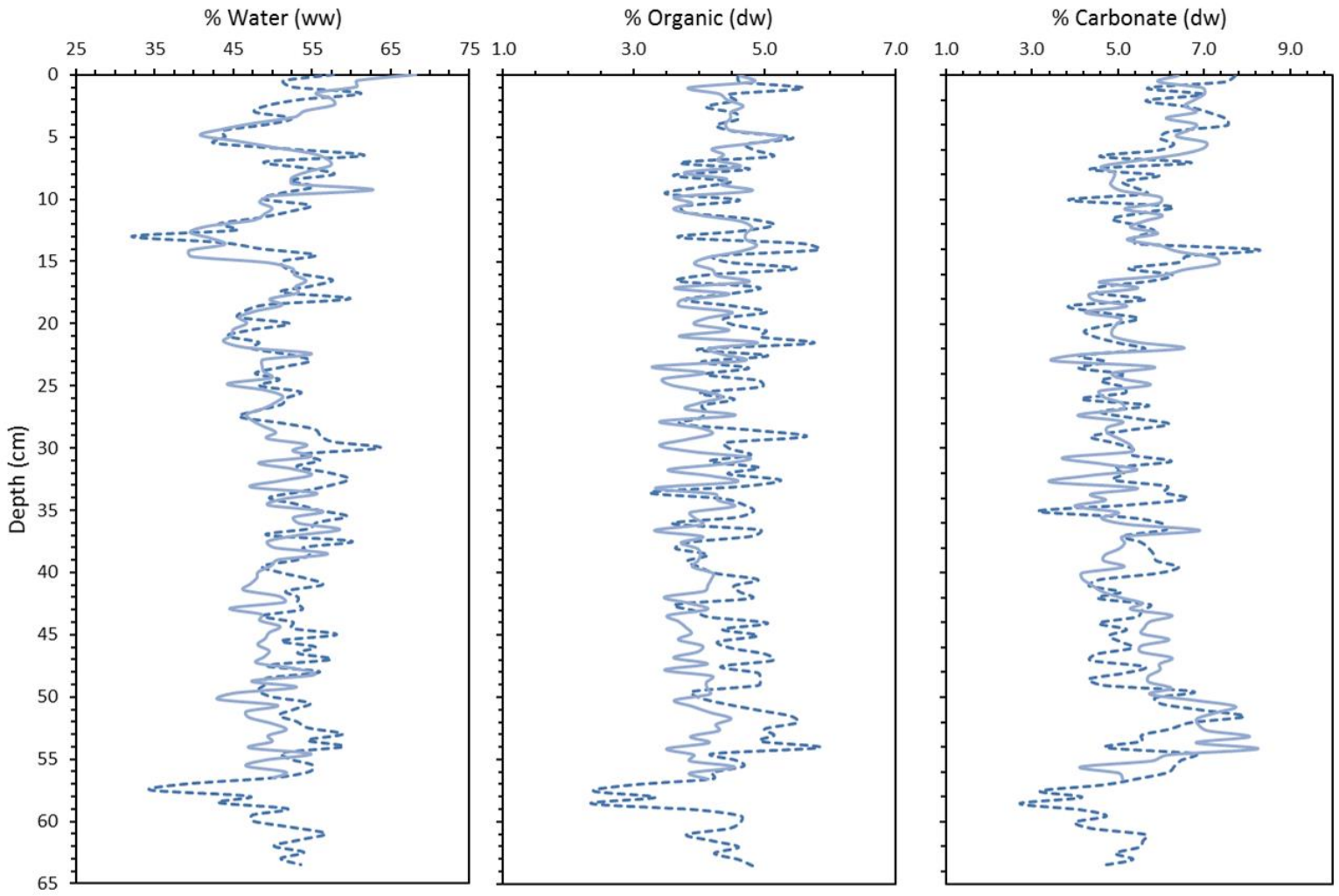
% Water (ww)
25
35
45
55
65
75
% Organic (dw)
1.0
3.0
5.0
7.0
% Carbonate (dw)
1.0
3.0
5.0
7.0
9.0
Depth (cm)
0
5
10
15
20
25
30
35
40
45
50
55
60
65

Figure A.2. Loss-on-ignition stratigraphies for cores collected at site 3. These cores were aligned using one multiplicative constant: core 3B (light blue solid) was matched with respect to core 3A (dark blue dashed) using the following formula: $d_w^{3B} = 0.975 \times d^{3A}$, where d_w^{3B} is the 'wiggle matched' section depth for core 3B with respect to core 3A and d^{3A} is the section depth for core 3A.

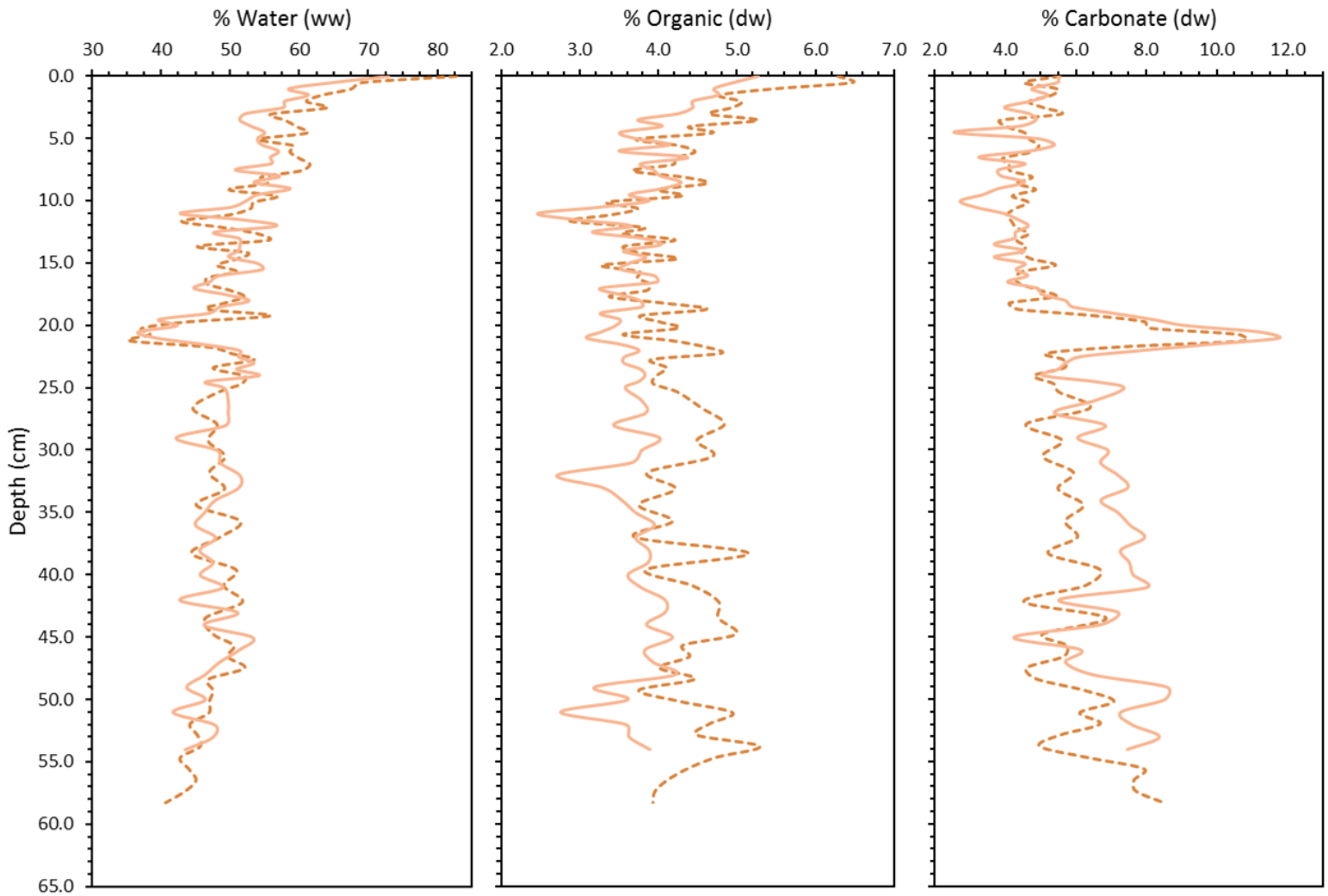
% Water (ww)
30
40
50
60
70
80
% Organic (dw)
2.0
3.0
4.0
5.0
6.0
7.0
% Carbonate (dw)
2.0
4.0
6.0
8.0
10.0
12.0
Depth (cm)
0.0
5.0
10.0
15.0
20.0
25.0
30.0
35.0
40.0
45.0
50.0
55.0
60.0
65.0

Figure A.3. Loss-on-ignition stratigraphies for cores collected at site 4. Core 4A (dark orange dashed) was aligned with core 4B (light orange solid) using several depth-specific constants due to the notable differences in sedimentation rates throughout this core. For depths 0.0 to 22.5 cm (in core 4B), the 'wiggle' formula used was: $d_w^{4A} = 1.01 \times d^{4B}$, where d_w^{4A} is the 'wiggle matched' section depth for core 4A with respect to core 4B and d^{4B} is the section depth for core 4B. For depths 22.5 to 39.0 cm (in core 4B), the 'wiggle' formula used was: $d_w^{4A}{}_n = d_w^{4A}{}_{n-1} + 0.6475$, where $d_w^{4A}{}_n$ is the 'wiggle matched' section depth for section *n* of core 4A and $d_w^{4A}{}_{n-1}$ is the 'wiggle matched' section depth of the previous section. For depths 39.0 to 54.0 cm (in core 4B), the 'wiggle formula used was: $d_w^{4A}{}_n = d_w^{4A}{}_{n-1} + 0.9$.

A2. Radioisotope Chronologies

Initial sediment chronologies were developed using ^{210}Pb and ^{137}Cs radioisotope dating. Cores 1B, 3B, and 4A were used for radioisotope analysis. The radioisotope activity stratigraphies were used in the CRS model to develop sediment chronologies. The chronologies and measured radioisotope activities are presented for core 1B (Table A.1), core 3B (Table A.2), and core 4A (Table A.3). These data were used in the development of Bayesian age-depth models.

Table A.1. Radioisotope activities and CRS model sediment chronology for core 1B. (Note: *nd* represents values below the detection limit, which were treated as zero).

Section Top Depth (cm)	Year (SD)	^{210}Pb Activity (SD) (dpm g^{-1})	^{137}Cs Activity (SD) (dpm g^{-1})	^{226}Ra Activity (SD)* (dpm g^{-1})
0.0	2015 (n/a)	3.1913 (0.2760)	*nd*	2.0845 (0.1635)
2.0	2012 (1.05)	3.0946 (0.2625)	*nd*	2.2472 (0.1611)
4.0	2010 (1.46)	2.6608 (0.2409)	*nd*	1.9287 (0.1498)
6.0	2007 (1.91)	3.0044 (0.2349)	*nd*	2.0439 (0.1458)
8.0	2004 (2.44)	2.8347 (0.2411)	0.0543 (0.0276)	1.9455 (0.1468)
10.0	2001 (3.06)	2.3447 (0.2142)	0.0499 (0.0254)	1.9293 (0.1393)
12.0	1999 (3.54)	2.6659 (0.2271)	0.0447 (0.0247)	1.8484 (0.1451)
14.0	1996 (4.21)	2.3499 (0.2263)	0.0548 (0.0280)	2.0893 (0.1505)
16.0	1995 (4.62)	2.3543 (0.2072)	0.0602 (0.0254)	1.8586 (0.1379)
18.0	1992 (5.27)	2.3833 (0.2010)	0.0459 (0.0238)	1.9834 (0.1450)
20.0	1990 (5.96)	2.4714 (0.2152)	0.0557 (0.0265)	1.9367 (0.1426)

* calculated as the weighted mean of ^{214}Bi and ^{214}Pb

Table A.2. Radioisotope activities and CRS model sediment chronology for core 3B. (Note: *nd* represents values below the detection limit, which were treated as zero).

Section Top Depth (cm)	Year (SD)	^{210}Pb Activity (SD) (dpm g^{-1})	^{137}Cs Activity (SD) (dpm g^{-1})	^{226}Ra Activity (SD)* (dpm g^{-1})
0.0	2015 (n/a)	7.8994 (0.4869)	0.0858 (0.0475)	2.4309 (0.2387)
0.5	2004 (1.43)	5.6510 (0.4706)	0.1650 (0.0610)	2.4015 (0.2506)
1.0	1995 (2.35)	5.0046 (0.3828)	0.3520 (0.0562)	2.2020 (0.2090)
1.5	1985 (3.71)	4.0390 (0.3416)	0.7983 (0.0633)	2.1839 (0.2055)
2.0	1973 (5.41)	3.6546 (0.3337)	1.2237 (0.0730)	2.3131 (0.2266)
2.5	1963 (7.29)	3.1503 (0.2583)	1.6719 (0.0594)	2.0070 (0.1766)
3.0	1949 (10.96)	2.4651 (0.2136)	1.3697 (0.0497)	1.9742 (0.1656)
3.5	1938 (13.89)	1.9559 (0.1929)	0.4433 (0.0420)	1.9123 (0.1740)
4.0	1937 (12.20)	2.4627 (0.2029)	0.2551 (0.0357)	2.0051 (0.1661)
4.5	1920 (15.68)	1.8583 (0.1825)	0.0190 (0.0312)	1.7405 (0.1556)
5.0	1916 (n/a)	1.6402 (0.1691)	*nd*	1.8249 (0.1564)
6.0	1887 (n/a)	1.9459 (0.1972)	*nd*	1.8553 (0.1683)
8.0	1850 (n/a)	2.3180 (0.2137)	*nd*	2.2034 (0.1692)

* calculated as the weighted mean of ^{214}Bi and ^{214}Pb

Table A.3. Radioisotope activities and CRS model sediment chronology for core 4A. (Note: *nd* represents values below the detection limit, which were treated as zero).

Section Top Depth (cm)	Year (SD)	^{210}Pb Activity (SD) (dpm g^{-1})	^{137}Cs Activity (SD) (dpm g^{-1})	^{226}Ra Activity (SD)* (dpm g^{-1})
0.0	2015 (n/a)	13.5144 (0.6909)	0.3776 (0.0667)	2.3716 (0.2557)
0.5	2011 (0.38)	13.7330 (0.7924)	0.3454 (0.0771)	2.0478 (0.2385)
1.0	2001 (1.04)	8.3621 (0.4877)	0.6094 (0.0570)	2.0803 (0.1880)
1.5	1995 (1.45)	5.3523 (0.4040)	1.0504 (0.0667)	2.1001 (0.1862)
2.0	1990 (1.84)	5.7896 (0.3971)	1.4339 (0.0698)	1.9694 (0.1769)
2.5	1983 (2.49)	5.2849 (0.3527)	2.2053 (0.0715)	1.6252 (0.1596)
3.0	1975 (3.38)	3.5661 (0.3156)	2.2132 (0.0764)	2.4293 (0.2004)
3.5	1971 (3.83)	2.2897 (0.2347)	0.7267 (0.0473)	1.7055 (0.1531)
4.0	1968 (4.09)	2.5135 (0.2346)	0.2474 (0.0390)	2.2568 (0.1707)
4.5	1968 (4.14)	2.6261 (0.2322)	0.0789 (0.0317)	1.9753 (0.1605)
5.0	1965 (4.44)	2.6705 (0.2217)	0.0659 (0.0280)	1.7190 (0.1497)
5.5	1960 (5.12)	2.4992 (0.2289)	*nd*	2.4072 (0.1715)
6.0	1960 (5.05)	2.4435 (0.2350)	*nd*	1.3942 (0.1438)
6.5	1951 (6.41)	2.5229 (0.2374)	*nd*	2.0244 (0.1675)
7.0	1948 (6.83)	2.1385 (0.1960)	*nd*	1.9494 (0.1577)
7.5	1947 (6.89)	2.4642 (0.2228)	*nd*	1.8352 (0.1594)
8.5	1935 (8.25)	2.2738 (0.2073)	*nd*	1.7786 (0.1486)
9.5	1916 (9.85)	2.1563 (0.2080)	*nd*	1.4610 (0.1313)

* calculated as the weighted mean of ^{214}Bi and ^{214}Pb

A3. Radiocarbon Dating

Two wood fragments were recovered during core sectioning from cores 3B and 4A, respectively. These samples were used for carbon-14 dating analysis. Table A.4 (below) presents radiocarbon ages for the samples as well as calibrated ages and credible intervals. Uncalibrated ages were calibrated during age-depth model development: calibrated ages are presented as additional information for the reader.

Table A.4. Radiocarbon and calibrated ages for wood fragments recovered from cores 3B and 4A, respectively. Radiocarbon ages were calibrated using IntCal13 in Bacon. Age-depth model development utilized the ^{14}C ages, as radiocarbon age calibration is built-in to the modeling function.

Core	Depth (cm)	Material	^{14}C Age (SD) (^{14}C years BP)	Calibrated Age (95% Credible Interval) (Year CE)
3B	52.0	Wood	1108.43 (25.83)	938 (890 – 986)
4A	38.0	Wood	576.67 (25.06)	1356 (1308 – 1412)

A4. Sediment Marker Layers

Sediment marker layers have been previously used in age-depth model development in Kluane Lake (see Brahney *et al.*, 2008a,b and Brahney *et al.* 2010). The White River Tephra (Clague *et al.* 1995) and the 1899 Yakutat Bay Earthquakes (Lamontagne *et al.* 2008) were identified in several sediment cores. The formation of the Kluane River had been previous shown to be a marker layer in Kluane Lake sediment stratigraphies (Brahney *et al.* 2008b) and was also used in age-depth model development. The occurrence of these events in collected sediment cores is presented in Table A.5.

Table A.5. Sediment marker layers used in age-depth model development for select sediment cores in Kluane Lake. Error was assigned based on previous literature (White River Tephra: Clague *et al.* 1995; Kluane River formation: Brahney *et al.* 2008b) or based on the depth span in which the event was identified (Yakutat Bay earthquakes). If an event spanned several sediment sections, the mean depth was used in model development.

Event	Year	Core: Depth (cm)
Yakutat Bay Earthquakes	1899	3B: 5.5 4A: 10.5
Kluane River Formation	1690 (1680 – 1700)	3B: 14.25 4A: 21.0
White River Tephra	803 (1 SD: 60.5)	3A: 60.5

A5. Bayesian Age-Depth Modeling

The radioisotope chronologies, radiocarbon samples, and sediment marker layers were all used to develop Bayesian age-depth models using Bacon (Bayesian ACcumulatiON; Blaauw & Christen 2011) in R statistical language (R Core Team 2016).

A5.1 User-supplied dating information

For cores in which age-depth information was characterized from the other paired core, the 'wiggle matched' depth was used in model development. For cores that had chronologies developed directly and/or marker layers identified within the core, true sediment depths were used. Presented below are the input data, including radioisotope chronologies, radiocarbon dating information, and marker sediment layers, used to develop age-depth models for core 1A (Table A.6), core 3B (Table A.7), and core 4A (Table A.8).

Table A.6. Input data used in Bacon for Bayesian age-depth model development for core 1A. *datedID* is a unique identifier for dating information, and *cc* is a binary operator for radiocarbon age calibration. Age is supplied as years before CE 1950 (ybp). As radioisotope chronologies were developed using core 1B, the *dateID* and *Depth* values were labelled and adjusted accordingly.

dateID	Age (ybp)	Error (SD)	Depth (cm)	cc
surface	-65.33	0.10	-1.0	0
1b1	-64.05	0.43	0.0	0
1b2	-62.33	1.05	1.0	0
1b3	-61.22	1.22	2.0	0
1b4	-60.12	1.46	3.0	0
1b5	-58.99	1.65	4.0	0
1b6	-57.66	1.91	5.0	0
1b7	-56.36	2.13	6.0	0
1b8	-54.83	2.44	7.0	0
1b9	-53.06	2.79	8.0	0
1b10	-51.83	3.06	9.0	0
1b11	-50.85	3.28	10.0	0
1b12	-49.73	3.54	11.0	0
1b13	-47.95	3.95	12.0	0
1b14	-46.90	4.21	13.0	0
1b15	-46.27	4.37	14.0	0
1b16	-45.27	4.62	15.0	0
1b17	-44.05	4.94	16.0	0
1b18	-42.82	5.27	17.0	0
1b19	-41.69	5.58	18.0	0
1b20	-40.32	5.96	19.0	0
1b21	-39.14	6.31	20.0	0

Table A.7. Input data used in Bacon for Bayesian age-depth model development for core 3B. *datedID* is a unique identifier for dating information, and *cc* is a binary operator for radiocarbon age calibration. Age is input as years before CE 1950 (ybp).

dateID	Age (ybp)	Error (SD)	Depth (cm)	cc
surface	-65.33	0.10	0.0	0
3b1	-56.11	1.00	0.5	0
3b2	-45.33	2.52	1.0	0
3b3	-34.55	4.04	1.5	0
3b4	-23.76	5.57	2.0	0
3b5	-12.98	7.09	2.5	0
3b6	-2.20	8.61	3.0	0
3b7	8.58	10.13	3.5	0
3b8	19.37	11.66	4.0	0
3b9	30.15	13.18	4.5	0
earthquake-1899	51.00	1.00	5.5	0
14C-52	1108.00	26.00	52.0	1
WR-tephra	1147.00	60.50	59.0	0
KLR-form	260.00	5.00	14.3	0

Table A.8. Input data used in Bacon for Bayesian age-depth model development for core 4A. *datedID* is a unique identifier for dating information, and *cc* is a binary operator for radiocarbon age calibration. Age is input as years before CE 1950 (ybp).

dateID	Age (ybp)	Error (SD)	Depth (cm)	cc
surface	-65.33	0.10	0.0	0
4A1	-59.93	0.48	0.5	0
4A2	-47.46	1.46	1.0	0
4A3	-39.37	2.22	1.5	0
4A4	-32.25	3.03	2.0	0
4A5	-20.84	4.74	2.5	0
4A6	-6.07	8.11	3.0	0
4A7	3.99	10.94	3.5	0
4A8	11.07	13.41	4.0	0
4A9	13.82	14.32	4.5	0
4A10	22.70	18.67	5.0	0
4A11	28.30	20.40	5.5	0
4A12	29.97	20.72	6.0	0
4A13	38.26	20.46	6.5	0
4A14	49.96	28.33	7.0	0
earthquake-1899	51.00	2.00	10.5	0
KLR-form	260.00	2.00	21.0	0
14C-38	577.00	25.00	38.0	1

A5.2 User-defined Priors

Users are also able to determine the number of sections in which a core should be divided in Bacon in order to model accumulation rates, which are used to then determine interval ages (interval size is user-defined). The number of sections used in age-depth model development was selected to minimize error in ages and was core-specific: for core 1A, 44 sections (2-cm each) were used; for core 3B, 32 sections (2-cm each) were used; and for core 4A, 19 sections (3-cm each) were used.

Prior information can be incorporated into Bayesian age-depth models, based on existing knowledge about the lake. In Bacon, this prior information can be input as accumulation rates (as *acc.mean* and *acc.shape*) and accumulation rate memory or coherence (as *mem.mean* and *mem.strength*). The shape of the accumulation rate prior determines how much influence accumulation rate will have on the model: a lower shape value allows for freedom for the age-depth model to adapt to supplied data. Accumulation rate priors were based on the radioisotope chronologies and previous literature (Brahney *et al.* 2008b). Memory is a parameter which based on the dependence of the accumulation rate in a particular section on the previous section. Accumulation rate memory in lake sediments tends to be lower than in other systems, such as peat bogs (Crann *et al.* 2015). Memory priors used were relatively low, in order to accommodate for variability in sediment accumulation rates previously noted (Brahney *et al.* 2008b). Priors used for age-model development for each sediment core are presented in Table A.9.

Table A.9. Accumulation rate and accumulation memory priors used in age-depth model development for cores 1A, 3B, and 4A from Kluane Lake.

Core	Accumulation Rate		Memory	
	acc.mean	*acc.shape*	*mem.mean*	*mem.strength*
1A	1	1.5	0.2	4
3B	25	1.5	0.2	10
4A	20	1.5	0.4	4

A5.3 Model Output

Using millions of Markov Chain Monte Carlo iterations, BACON generates an age-depth model, outputting median section ages and weighted mean ages with 95% confidence intervals. This program produces age-depth plots, which identifying the input data as two-dimensional distributions (radiocarbon data in blue and other data in teal), as well as MCMC iteration plots, and prior and posterior distributions for accumulation rate and memory, two parameters used when developing the

models. These plots are presented for core 1A (Figure A.4), core 3B (Figure A.5), and core 4B (Figure A.6). The weighted mean age-depth model is plotted with a red dashed line, 95% confidence intervals are plotted in grey dotted lines, and the density of MCMC iterations are plotted as a black cloud about the mean age-depth relationship. Weighted mean section ages were selected and used during all analysis.

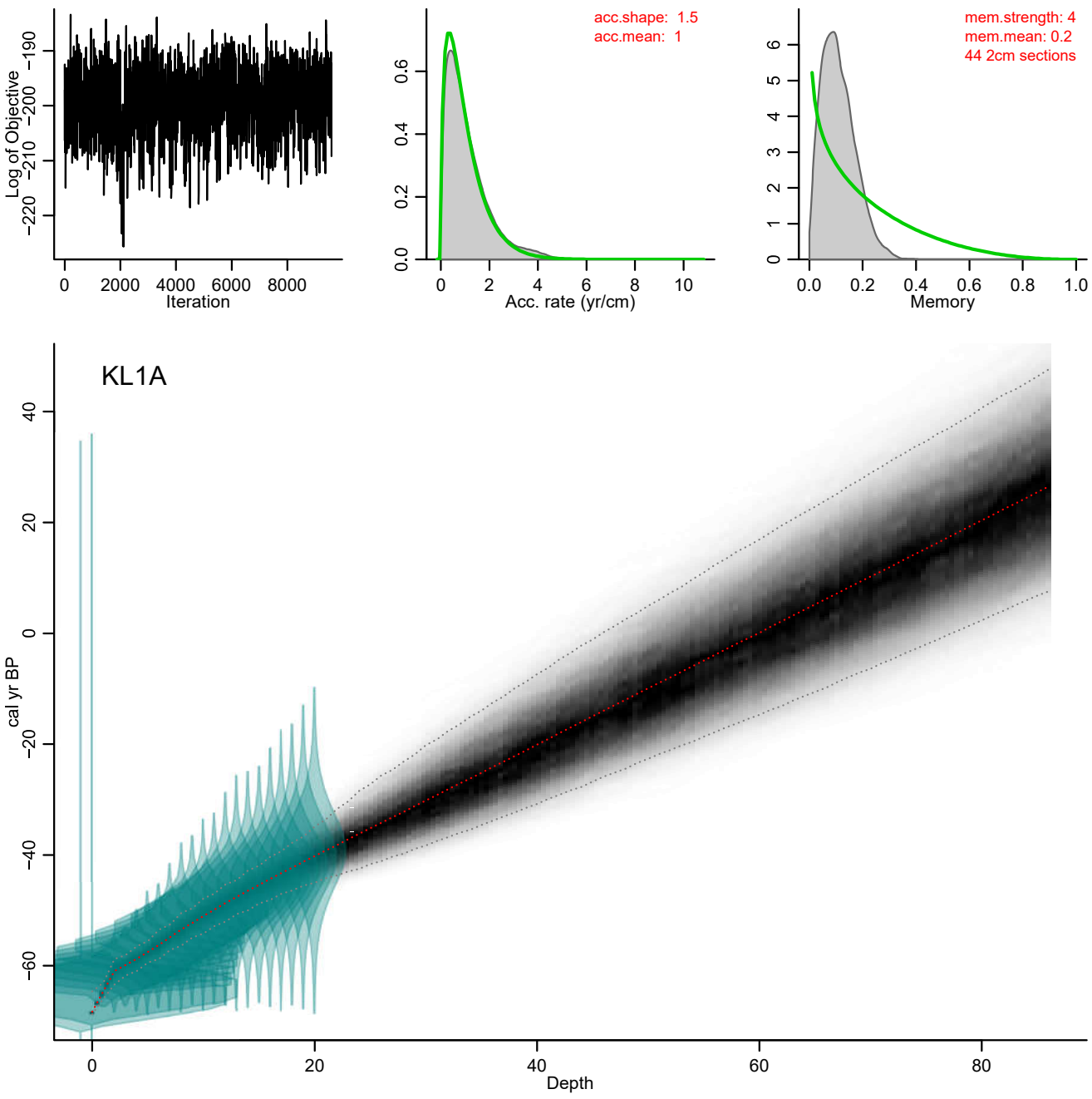
Log of Objective
−190
−200
−210
−220
0
2000
4000
6000
8000
Iteration
acc.shape: 1.5
acc.mean: 1
0.0
0.2
0.4
0.6
0
2
4
6
8
10
Acc. rate (yr/cm)
mem.strength: 4
mem.mean: 0.2
44 2cm sections
0
1
2
3
4
5
6
0.0
0.2
0.4
0.6
0.8
1.0
Memory
KL1A
cal yr BP
40
20
0
−20
−40
−60
0
20
40
60
80
Depth

Figure A.4. The Bayesian age-depth model for core 1A. The lower plot depicts the age-depth model: user-supplied data are shown as a distribution in teal, the weighted mean age-depth relationship is shown with a red dotted line, the 95% confidence intervals are shown in grey dashed lines, and the MCMC iterations are shown as densities in black. The upper-left plot depicts the MCMC iterations. The upper-middle and upper-right plots depict the prior and posterior distributions for accumulation rate (middle) and memory (right). See Blaauw & Christen (2013) for further information.

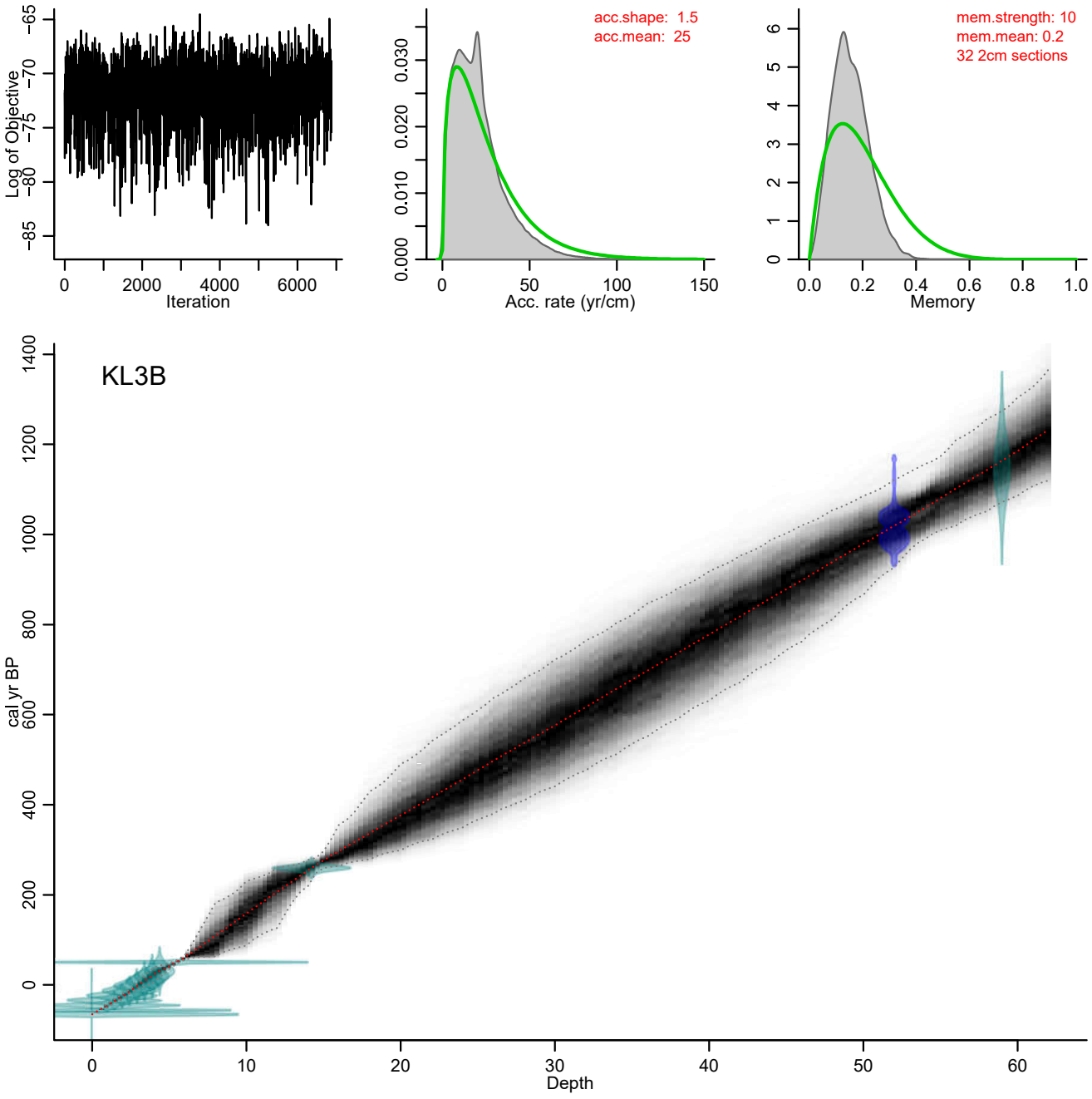
Log of Objective
−65
−70
−75
−80
−85
0
2000
4000
6000
Iteration
acc.shape: 1.5
acc.mean: 25
0.000
0.010
0.020
0.030
0
50
100
150
Acc. rate (yr/cm)
mem.strength: 10
mem.mean: 0.2
32 2cm sections
0
1
2
3
4
5
6
0.0
0.2
0.4
0.6
0.8
1.0
Memory
KL3B
cal yr BP
0
200
400
600
800
1000
1200
1400
0
10
20
30
40
50
60
Depth

Figure A.5. The Bayesian age-depth model for core 3B. The lower plot depicts the age-depth model: user-supplied data are shown as a distribution in teal, radiocarbon dates are shown as a blue distribution, the weighted mean age-depth relationship is shown with a red dotted line, the 95% confidence intervals are shown in grey dashed lines, and the MCMC iterations are shown as densities in black. The upper-left plot depicts the MCMC iterations. The upper-middle and upper-right plots depict the prior and posterior distributions for accumulation rate (middle) and memory (right). See Blaauw & Christen (2013) for further information.

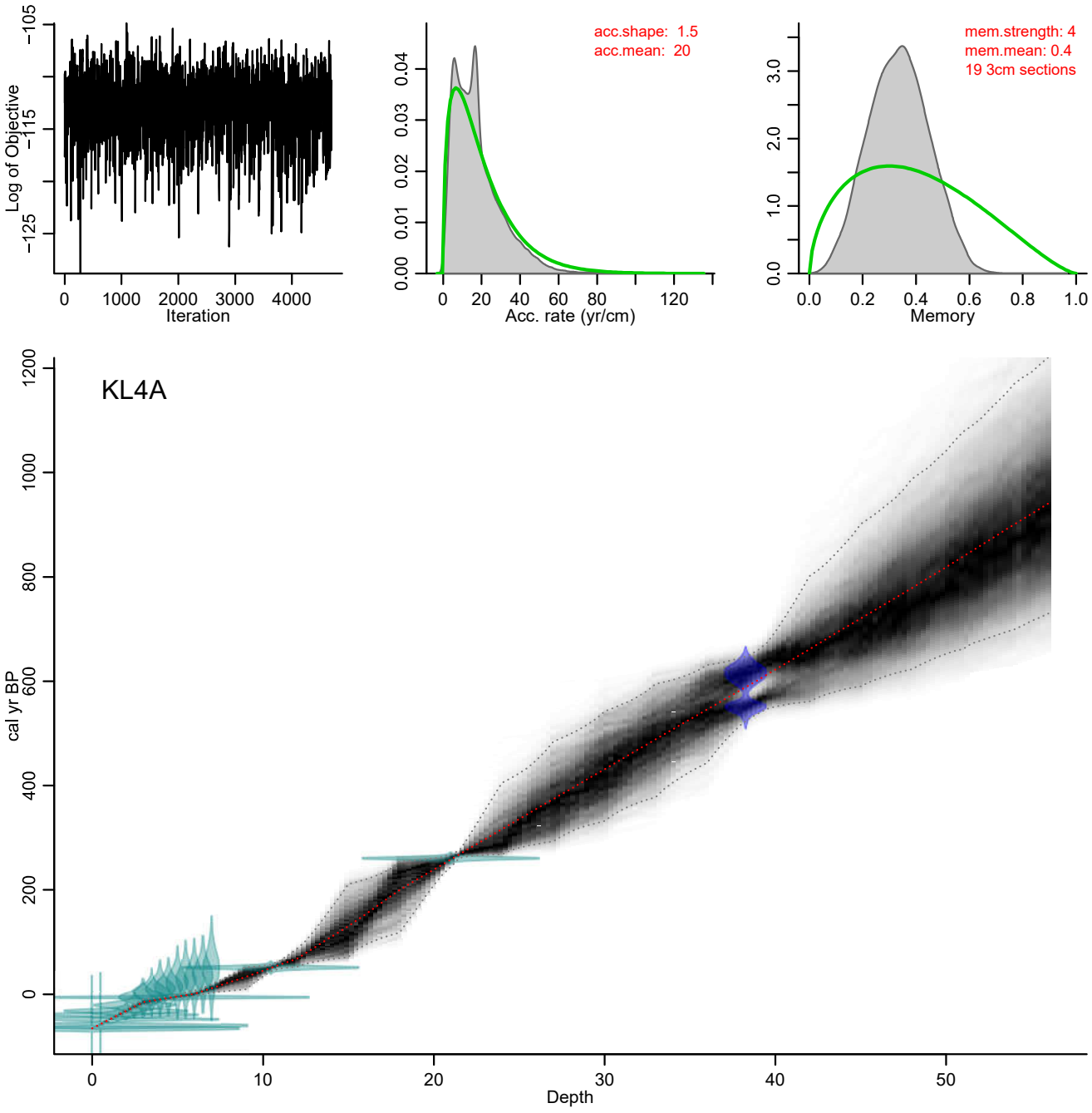
Log of Objective
−105
−115
−125
0
1000
2000
3000
4000
Iteration
acc.shape: 1.5
acc.mean: 20
0.00
0.01
0.02
0.03
0.04
0
20
40
60
80
120
Acc. rate (yr/cm)
mem.strength: 4
mem.mean: 0.4
19 3cm sections
0.0
1.0
2.0
3.0
0.0
0.2
0.4
0.6
0.8
1.0
Memory
KL4A
cal yr BP
0
200
400
600
800
1000
1200
0
10
20
30
40
50
Depth

Figure A.6. The Bayesian age-depth model for core 4A. The lower plot depicts the age-depth model: user-supplied data are shown as a distribution in teal, radiocarbon dates are shown as a blue distribution, the weighted mean age-depth relationship is shown with a red dotted line, the 95% confidence intervals are shown in grey dashed lines, and the MCMC iterations are shown as densities in black. The upper-left plot depicts the MCMC iterations. The upper-middle and upper-right plots depict the prior and posterior distributions for accumulation rate (middle) and memory (right). See Blaauw & Christen (2013) for further information.

Appendix B

Raw Data

Included in this appendix is the raw core data and associated information used for analysis.

Core Collection Locations

	Latitude	Longitude
Site 1	61.0341	-138.4242
Site 3	61.2176	-138.6225
Site 4	61.3831	-138.7119

Core 1A Raw Data

Section Top Depth (cm)	% Water (ww)	% Organic (dw)	% Carbonate (dw)	Dry Density (g cm^{-3})	Dry Mass Acc. Rate (g m^{-2} yr^{-1})	Magnetic Susceptibility	[THg] (ppm dw)	Hg Acc. Rate (µg m^{-2} yr^{-1})
0.0	36.25	3.83	20.62	1.05	5240.99	3.58	0.088	462.67
1.0	46.11	4.25	19.04	0.79	3966.17	2.31	0.100	397.82
2.0	45.51	4.70	19.91	0.76	6373.36	2.11	0.063	400.35
3.0	41.89	4.12	19.90	0.86	7854.77	2.67	0.050	393.18
4.0	42.73	4.79	21.91	0.90	7494.85	2.16	0.045	341.01
5.0	42.02	3.63	24.74	0.77	5934.00	2.20	0.042	251.45
6.0	42.23	4.98	23.56	0.77	5483.29	2.59	0.042	229.68
7.0	42.87	3.61	25.15	0.87	6190.92	2.09	0.038	234.61
8.0	40.97	4.24	22.92	0.83	6880.18	2.16	0.046	314.76
9.0	41.08	3.92	22.78	0.83	6894.01	2.61	0.049	338.98
10.0	39.77	2.61	24.30	0.85	7105.15	2.20	0.037	265.15
11.0	37.13	2.88	24.11	0.96	8038.02	2.88	0.041	326.72
12.0	42.08	3.67	23.63	0.85	7758.58	2.16	0.037	283.37
13.0	32.31	4.14	21.68	1.05	9541.11	3.36	0.038	365.67
14.0	39.18	3.46	23.32	0.86	8617.80	0.93	0.051	435.26
15.0	41.38	3.57	23.23	0.94	8569.72	1.88	0.042	359.55
16.0	35.88	2.89	22.59	0.81	8149.46	2.73	0.042	340.04
17.0	38.36	3.51	24.95	0.92	8407.33	2.46	0.042	354.81
18.0	37.59	3.44	25.16	0.93	9310.63	2.82	0.038	357.89
19.0	40.48	0.90	30.43	0.93	9305.22	2.35	0.044	407.34

20.0	40.46	3.32	23.61	0.81	8085.56	2.85	0.040	322.80
21.0	34.62	4.36	20.85	0.98	9754.49	2.55		
22.0	40.97	4.26	23.48	0.88	8770.76	1.73	0.037	326.07
23.0	39.45	2.95	25.32	0.86	8633.78	3.33		
24.0	36.44	2.20	25.50	0.96	9641.46	2.95	0.033	321.84
25.0	38.46	2.29	25.48	0.85	7713.36	1.77		
26.0	43.65	3.37	24.03	0.88	8768.94	2.49	0.036	316.60
27.0	42.07	4.97	21.16	0.80	8898.92	2.18		
28.0	41.93	4.17	19.43	0.91	8245.99	2.31	0.056	465.55
29.0	38.60	4.12	21.76	0.90	9972.17	2.47		
30.0	36.57	4.58	22.64	0.94	9352.54	2.86	0.033	305.15
31.0	37.34	3.48	23.76	0.94	9360.33	2.71		
32.0	45.13	2.65	25.13	0.82	8169.89	2.55	0.037	301.60
33.0	37.93	3.97	21.22	0.96	9559.22	1.99		
34.0	36.66	3.87	23.77	0.97	9744.22	2.56	0.038	369.20
35.0	36.21	3.37	24.40	0.95	9506.69	2.61		
36.0	34.26	3.49	21.90	1.02	9244.83	3.27	0.037	337.90
37.0	43.31	2.17	25.58	0.88	8805.63	1.72		
38.0	41.43	4.87	21.66	0.86	8627.39	2.16	0.039	332.52
39.0	34.92	3.28	23.98	1.01	10083.34	2.63		
40.0	37.01	3.40	24.11	0.97	8814.99	2.00	0.036	320.46
41.0	41.72	3.68	22.88	0.89	8874.14	3.69		
42.0	43.66	3.49	20.95	0.83	8263.93	2.55	0.044	362.30
43.0	43.53	3.26	23.33	0.87	8692.87	2.82		
44.0	44.50	3.02	23.22	0.81	8102.26	2.82	0.042	343.12
45.0	38.85	3.89	22.45	0.93	9303.90	2.70		
46.0	46.22	3.41	23.43	0.78	7128.14	1.42	0.041	289.36
47.0	40.96	3.33	23.68	0.82	8231.97	2.81		
48.0	40.44	3.11	22.98	0.94	9445.85	2.63	0.038	356.02
49.0	42.76	3.25	22.17	0.89	8944.31	2.86		
50.0	43.74	3.68	25.35	0.82	8177.45	1.83	0.041	331.66
51.0	39.69	3.91	21.46	0.95	9507.86	2.24		
52.0	39.11	3.32	23.80	0.94	9398.99	3.52	0.038	355.47
53.0	30.22	3.88	21.61	1.10	10964.53	2.64		
54.0	40.98	4.20	20.87	0.89	8884.88	2.71	0.039	342.21
55.0	39.09	3.63	22.58	0.89	8876.74	2.94		
56.0	42.12	2.33	22.77	0.89	8931.82	3.56	0.039	348.17
57.0	43.34	4.79	16.95	0.87	8711.20	2.82		

58.0	41.66	5.00	14.94	0.92	8320.27	2.41	0.106	880.68
59.0	39.26	4.42	19.95	0.90	9009.91	2.94		
60.0	38.16	3.82	20.72	0.96	9607.86	3.06	0.039	371.34
61.0	35.88	4.02	22.73	0.99	9899.72	3.15		
62.0	39.39	4.50	19.13	0.97	9667.63	4.32	0.063	613.74
63.0	35.01	4.39	18.77	0.98	8947.50	2.33		
64.0	37.45	5.39	17.26	1.00	9980.70	2.11	0.107	1068.86
65.0	38.97	4.55	18.13	0.90	9012.36	2.55		
66.0	33.69	6.26	16.79	0.97	9707.59	2.56	0.123	1195.27
67.0	37.95	4.91	19.49	1.04	10402.81	3.36		
68.0	36.77	5.48	20.53	0.85	8533.03	3.00	0.070	598.12
69.0	41.65	4.68	18.40	0.84	7664.53	3.42		
70.0	35.73	3.48	23.45	0.91	9123.41	2.22	0.041	372.22
71.0	39.02	3.86	21.71	0.91	9065.40	2.64		
72.0	39.17	3.69	21.83	0.90	8968.84	2.65	0.042	373.93
73.0	44.22	3.12	22.22	0.86	8563.29	2.60		
74.0	38.19	2.91	24.76	0.92	9180.87	1.59	0.046	419.72
75.0	40.57	3.22	23.36	0.84	8371.26	2.81		
76.0	34.04	2.96	25.36	0.97	8787.52	2.68	0.045	394.65
77.0	38.30	4.70	20.91	0.92	9207.96	2.14		
78.0	38.35	4.26	22.83	0.97	10771.02		0.052	559.67
79.0	35.59	3.65	21.84	1.09	10923.90	2.63		
80.0	38.82	3.61	20.18	0.96	9585.74	3.00	0.061	582.81
81.0	44.12	4.27	17.97	0.85	8492.75	2.54		
82.0	38.52	3.84	22.04	0.95	8610.01	2.49	0.050	426.54
83.0	36.54	4.78	18.01	0.96	9601.97	2.28		
84.0	38.68	3.65	22.35	0.90	9025.96	2.43	0.041	371.29
85.0	41.81	4.30	21.37	0.89	8062.60	2.76		
86.0	37.66	3.82	21.44	0.96		2.57	0.040	

Core 1B Raw Data

Section Top Depth (cm)	% Water (ww)	% Organic (dw)	% Carbonate (dw)
0.0	42.55	3.29	21.62
1.0	39.83	3.48	21.08
2.0	45.76	3.63	19.63
3.0	46.20	3.25	21.56

4.0	42.31	3.30	22.29
5.0	46.87	3.15	23.99
6.0	44.09	2.95	25.63
7.0	45.39	2.91	25.95
8.0	38.89	2.82	25.35
9.0	43.19	2.92	25.31
10.0	36.74	2.88	24.46
11.0	45.25	3.00	24.34
12.0	39.94	2.96	24.19
13.0	46.58	2.81	25.50
14.0	37.90	2.87	23.14
15.0	39.89	2.80	25.10
16.0	40.60	3.01	24.13
17.0	40.03	2.97	25.36
18.0	40.81	2.81	25.40
19.0	42.89	3.00	24.96
20.0	37.73	2.89	25.49

Core 3A Raw Data

Section Top Depth (cm)	% Water (ww)	% Organic (dw)	% Carbonate (dw)
0.0	57.76	4.59	7.74
0.5	51.41	4.62	7.49
1.0	52.56	5.60	5.69
1.5	61.27	4.45	6.98
2.0	53.66	4.56	5.66
2.5	49.25	4.10	6.63
3.0	47.77	4.56	7.16
3.5	52.40	4.60	7.54
4.0	49.35	4.26	7.54
4.5	43.68	4.57	6.19
5.0	44.02	5.44	5.97
5.5	42.59	4.73	6.31
6.0	52.52	4.86	5.94
6.5	61.64	5.12	4.58
7.0	49.09	3.70	6.71
7.5	54.13	4.77	4.36
8.0	57.84	3.60	5.95

8.5	52.23	4.48	5.13
9.0	55.30	3.95	5.40
9.5	51.33	3.49	5.66
10.0	48.78	4.62	3.86
10.5	54.80	3.74	6.23
11.0	52.23	3.78	5.61
11.5	48.42	4.75	4.86
12.0	43.22	5.15	5.43
12.5	45.37	4.61	5.85
13.0	32.16	3.69	5.38
13.5	43.65	5.60	5.43
14.0	48.59	5.83	8.29
14.5	55.49	4.23	6.62
15.0	51.16	4.46	6.43
15.5	51.57	5.49	5.25
16.0	53.42	4.16	6.27
16.5	57.63	3.66	5.78
17.0	54.86	4.90	4.55
17.5	51.14	4.51	4.55
18.0	59.88	3.77	5.63
18.5	49.12	4.50	3.88
19.0	46.46	5.03	4.54
19.5	45.66	4.38	5.48
20.0	52.18	4.50	4.85
20.5	47.47	5.02	4.23
21.0	44.33	4.94	4.47
21.5	48.25	5.74	5.04
22.0	47.37	3.97	5.60
22.5	52.09	5.05	4.11
23.0	54.82	4.03	4.73
23.5	51.27	4.76	4.09
24.0	47.84	4.09	5.17
24.5	50.88	4.92	4.60
25.0	48.36	4.96	5.10
25.5	53.56	4.01	5.17
26.0	51.75	4.54	4.15
26.5	51.20	4.05	5.72
27.0	48.12	4.10	4.61
27.5	45.81	4.02	5.32

28.0	51.14	3.72	6.19
28.5	55.39	4.84	5.24
29.0	56.07	5.64	4.37
29.5	57.57	4.39	4.89
30.0	63.70	4.48	5.36
30.5	53.81	4.79	5.33
31.0	56.04	4.15	6.24
31.5	53.11	4.92	4.95
32.0	57.24	4.44	5.16
32.5	59.74	5.25	4.91
33.0	57.43	4.69	6.15
33.5	53.77	3.24	6.07
34.0	49.63	4.37	6.62
34.5	52.95	4.69	5.26
35.0	55.80	4.83	3.14
35.5	59.49	4.57	5.22
36.0	55.68	3.59	6.05
36.5	54.59	4.93	6.11
37.0	49.27	4.82	5.14
37.5	60.11	3.85	5.54
38.0	53.99	3.64	5.72
38.5	54.86	4.13	5.84
39.0	53.17	3.82	5.90
39.5	48.73	4.01	6.42
40.0	50.91	4.25	5.92
40.5	54.39	4.90	4.58
41.0	56.36	4.53	4.33
41.5	51.77	4.62	5.07
42.0	53.26	4.80	4.53
42.5	53.13	3.64	5.75
43.0	53.74	3.92	5.55
43.5	48.73	4.14	5.46
44.0	52.62	5.05	4.55
44.5	52.47	4.35	5.20
45.0	58.16	4.90	4.80
45.5	51.09	4.28	5.07
46.0	55.47	4.48	5.33
46.5	53.23	5.02	4.49
47.0	57.45	5.12	4.37

47.5	49.33	4.33	5.62
48.0	56.00	4.90	5.18
48.5	49.28	4.93	4.32
49.0	49.10	4.91	4.67
49.5	48.23	3.88	6.76
50.0	49.91	4.00	5.87
50.5	54.76	4.40	6.02
51.0			
51.5	50.86	5.42	7.95
52.0	53.12	5.50	6.69
52.5	54.52	5.01	6.23
53.0	58.93	5.15	5.56
53.5	54.44	4.94	5.55
54.0	59.05	5.84	4.72
54.5	51.22	4.20	6.80
55.0	52.15	4.55	6.49
55.5	55.17	4.68	6.32
56.0	54.80	4.20	6.17
56.5	50.36	4.22	5.47
57.0	39.26	2.98	4.66
57.5	34.56	2.38	3.19
58.0	47.10	3.33	4.16
58.5	43.12	2.34	2.72
59.0	51.93	3.94	4.12
59.5	47.48	4.64	4.73
60.0	47.55	4.63	4.00
60.5	52.54	4.46	4.38
61.0	56.78	3.81	5.66
61.5			
62.0	50.22	4.60	5.51
62.5	54.00	4.23	4.94
63.0	51.08	4.60	5.35
63.5	53.61	4.82	4.59

Core 3B Raw Data

Section Top Depth (cm)	% Water (ww)	% Organic (dw)	% Carbonate (dw)	Dry Density (g cm^{-3})	Dry Mass Acc. Rate (g m^{-2} yr^{-1})	Magnetic Susceptibility	VRS-inferred Chl-*a* (µg g^{-1})	[THg] (ppm dw)	Hg Acc. Rate (µg m^{-2} yr^{-1})
0.0	68.18	4.62	6.40	0.45	223.32	6.05	0.66	0.084	18.83
0.5	60.71	4.83	5.94	0.43	214.10	5.53	0.20	0.088	18.83
1.0	60.66	3.83	6.97	0.48	236.80	7.16	0.07	0.093	21.94
1.5	55.53	4.30	7.02	0.53	262.52	5.86	-0.01	0.099	26.02
2.0	57.48	4.42	6.78	0.49	204.13	6.58	-0.26	0.118	24.08
2.5	57.77	4.67	6.55	0.53	216.95	8.23	-0.44	0.124	26.96
3.0	54.05	4.49	6.82	0.62	258.09	7.25	-0.86	0.131	33.70
3.5	52.72	4.48	6.12	0.65	266.91	7.94	-0.75	0.146	39.09
4.0	47.64	4.40	6.82	0.67	364.37	7.25	-0.73	0.131	47.91
4.5	43.55	4.47	6.65	0.77	415.40	8.90	-0.30	0.167	69.23
5.0	40.78	5.26	6.36	0.78	417.99		0.12	0.177	74.15
5.5	45.65	4.92	7.05	1.01	541.98	16.05	1.22	0.159	85.96
6.0	50.13	4.21	6.99	0.85	348.86	16.14	1.40	0.154	53.57
6.5	54.99	4.37	6.42	0.33	136.65	11.13		0.111	15.18
7.0	57.01	4.29	5.43	0.50	205.17	4.28		0.083	16.99
7.5	57.32	4.62	4.61	0.54	221.30	5.74		0.085	18.89
8.0	54.42	3.77	4.91	0.57	230.84	7.36	2.24	0.091	21.05
8.5	52.41	4.41	4.88	0.62	250.38	9.82		0.092	23.13
9.0	52.47	4.34	4.83	0.60	242.87	7.97		0.085	20.58
9.5	62.73	4.80	5.09	0.49	202.61	7.76		0.084	17.11
10.0	49.79	3.64	5.98	0.62	252.83	6.45	2.08	0.084	21.27
10.5	48.29	3.88	5.97	0.66	268.51	6.37			
11.0	49.89	3.61	5.15	0.62	254.44	6.16		0.103	26.18
11.5	48.91	4.01	6.02	0.68	279.34	8.16			
12.0	47.59	4.63	5.61	0.75	321.54	15.55	2.06	0.130	41.78
12.5	41.68	4.81	5.29	0.91	385.77	23.62			
13.0	39.46	4.72	5.93	0.91	371.58	24.04		0.128	47.64
13.5	42.14	4.72	5.21	1.14	469.95	26.24			
14.0	43.83	4.88	5.97	0.86	397.75	25.93	1.52	0.094	37.42
14.5	39.32	4.62	6.39	0.92	416.14	28.59			
15.0	39.62	4.12	7.27	0.88	421.05	30.83		0.102	42.85
15.5	49.29	3.92	7.34	0.65	311.24	17.58			
16.0	52.51	4.20	6.54	0.63	319.49	13.20	2.32	0.113	36.24

16.5	52.73	4.28	5.98	0.53	270.58	12.75			
17.0	54.22	4.75	4.56	0.62	317.05	6.23		0.094	29.66
17.5	52.85	3.62	5.46	0.60	315.03	5.54			
18.0	53.16	4.46	4.34	0.59	291.04	4.45	2.05	0.090	26.30
18.5	49.64	3.73	4.44	0.64	315.56	6.37			
19.0	51.16	3.69	5.20	0.65	324.24	7.85		0.096	31.26
19.5	47.81	4.50	4.23	0.68	345.41	10.10			
20.0	45.71	4.11	5.06	0.74	374.30	18.92	2.36	0.104	38.98
20.5	46.68	3.93	4.97	0.77	388.58	17.61			
21.0	44.98	4.45	4.86	0.72	371.98	10.99		0.161	59.94
21.5	44.73	3.70	4.89	0.77	402.30	10.63			
22.0	43.73	4.89	5.48	0.97	482.17	8.60	1.95	0.180	86.82
22.5	46.44	4.15	6.51	0.71	353.28	9.33			
23.0	54.90	4.37	4.11	0.57	281.86	8.69		0.151	42.68
23.5	48.74	4.69	3.47	0.62	306.69	8.22			
24.0	48.62	3.28	5.83	0.68	330.47	8.33	1.91	0.115	38.00
24.5	48.85	4.08	4.88	0.68	329.17	7.72			
25.0	49.81	3.44	5.11	0.69	338.95			0.130	44.03
25.5	44.18	3.56	5.75	0.68	326.21	9.94			
26.0	48.87	4.05	4.57	0.74	371.05	10.56	1.81	0.148	54.78
26.5	51.23	4.35	4.66	0.68	343.04	9.18			
27.0	50.40	4.00	5.09	0.65	327.02	8.88		0.113	36.82
27.5	48.92	3.80	5.12	0.68	337.75	8.88			
28.0	46.70	4.55	4.06	0.68	345.05	11.18	1.35	0.101	34.75
28.5	47.33	3.40	5.10	0.74	379.97	11.29			
29.0	48.77	3.97	4.75	0.70	365.14	10.15		0.095	34.53
29.5	50.38	4.20	4.77	0.68	352.44	9.61			
30.0	49.26	3.80	5.06	0.68	331.79	8.74	1.06	0.115	38.15
30.5	54.26	3.39	5.30	0.57	284.30	8.64			
31.0	52.51	3.90	5.31	0.59	290.35	9.15		0.109	31.59
31.5	54.75	4.77	3.70	0.54	267.06	8.63			
32.0	48.20	4.37	4.61	0.67	326.32	11.23	1.20	0.122	39.76
32.5	52.45	3.52	5.44	0.60	292.89	11.62			
33.0	54.91	4.17	4.26	0.60	292.30	10.61		0.094	27.47
33.5	50.83	4.56	3.42	0.61	302.41	9.35			
34.0	47.18	3.33	5.44	0.71	353.60	9.16	1.28	0.106	37.52
34.5	55.56	4.25	4.37	0.57	285.96	6.81			
35.0	51.18	4.28	4.71	0.65	326.21	10.02		0.125	40.73
35.5	49.45	4.54	3.99	0.64	319.48	8.77			

36.0	56.35	3.87	5.00	0.57	284.41	8.31	1.48	0.120	34.08
36.5	52.64	3.94	4.61	0.62	307.51	7.43			
37.0	53.36	4.05	5.23	0.60	295.44	8.45		0.110	32.56
37.5	58.51	3.31	6.91	0.50	249.25	8.45			
38.0	52.98	4.05	5.10	0.59	295.84	8.05	1.52	0.116	34.43
38.5	49.27	3.72	5.15	0.62	308.10	6.63			
39.0	50.20	3.98	5.03	0.64	321.57	8.46		0.113	36.22
39.5	56.96	4.01	4.70	0.56	272.54	7.38			
40.0	50.62	3.98	4.67	0.63	317.33	7.88	1.39	0.122	38.69
40.5	49.77	3.90	5.13	0.64	322.21	8.57			
41.0	48.15	4.20	4.16	0.73	360.29	8.09		0.110	39.79
41.5	47.96	4.18	4.17	0.67	336.70	9.84			
42.0	46.28	4.08	4.61	0.65	159.49	8.78	1.39	0.129	20.51
43.0	50.76	3.46	5.03	0.60	291.01	7.55		0.116	33.86
43.5	51.46	3.85	5.56	0.66	326.16	8.34			
44.0	44.53	4.12	5.30	0.72	367.58	11.10	1.48	0.145	53.14
44.5	48.54	3.52	6.25	0.67	344.30	9.96			
45.0	48.32	3.68	5.75	0.69	355.20	15.05		0.111	39.58
45.5	50.92	3.80	5.61	0.69	353.36	10.34			
46.0	49.53	3.88	5.55	0.61	294.21	3.91	1.00	0.103	30.32
46.5	49.00	3.68	6.19	0.67	326.61	9.72			
47.0	48.06	4.05	5.54	0.65	311.29	9.26		0.113	35.12
47.5	49.51	3.98	5.52	0.64	310.35	8.41			
48.0	48.90	3.61	6.26	0.70	348.07	9.16	1.12	0.091	31.62
48.5	47.91	4.13	5.97	0.71	353.04	9.94			
49.0	53.07	3.47	5.98	0.62	310.66	8.42		0.097	30.09
49.5	55.15	4.20	5.71	0.57	280.57	9.72			
50.0	47.28	4.11	5.72	0.69	352.48	6.64	1.26	0.129	45.52
50.5	52.99	4.12	6.24	0.64	314.39	7.25			
51.0	45.05	4.16	5.74	0.75	372.76	7.45		0.106	39.65
51.5	42.98	3.62	6.79	0.91	450.29	10.48			
52.0	50.58	3.89	7.74	0.61	312.97	10.76	1.36	0.083	25.97
52.5	46.66	4.16	7.31	0.64	329.09	9.57			
53.0	46.94	4.49	6.85	0.72	360.23	9.52		0.109	39.42
53.5	49.87	4.25	6.87	0.63	313.93	9.47			
54.0	51.70	4.30	7.08	0.71	328.08	12.50	0.92	0.081	26.42
54.5	49.38	3.86	8.07	0.62	286.49				
55.0	49.86	4.15	6.82	0.69	320.33	7.21		0.080	25.58
55.5	46.98	3.50	8.26	0.73	346.01	9.61			

56.0	54.85	3.92	6.17	0.59	284.28	10.19	0.80	0.075	21.35
56.5	49.14	3.85	5.79	0.64	308.27	9.85			
57.0	46.59	4.54	4.12	0.53	257.23	10.38		0.101	26.01
57.5	51.65	3.85	5.02	0.58	288.91	9.40			
58.0	49.97	4.14	5.11	0.58		7.02	1.42	0.131	

Core 4A Raw Data

Section Top Depth (cm)	% Water (ww)	% Organic (dw)	% Carbonate (dw)	Dry Density (g cm^{-3})	Dry Mass Acc. Rate (g m^{-2} yr^{-1})	Magnetic Susceptibility	VRS-inferred Chl-*a* (µg g^{-1})	[THg] (ppm dw)	Hg Acc. Rate (µg m^{-2} yr^{-1})
0.0	82.71	6.28	5.55	0.22	127.63			0.095	12.09
0.5	69.02	6.47	4.53	0.37	219.51		-0.78	0.099	21.75
1.0	67.52	5.46	5.46	0.32	191.63		-1.42	0.099	18.94
1.5	63.25	4.78	5.31	0.43	256.58		-1.47	0.094	24.15
2.0	61.01	5.05	4.67	0.44	260.05		-2.24	0.105	27.28
2.5	63.96	4.93	5.08	0.40	237.46		-3.06	0.100	23.63
3.0	55.91	4.65	5.57	0.59	1135.68	4.07	-3.32	0.099	112.27
3.5	57.98	5.27	3.84	0.62	1235.87	7.18	-1.13	0.088	108.90
4.0	59.60	4.39	4.03	0.47	902.40	7.72	-2.23	0.085	76.72
4.5	61.06	4.69	4.55	0.50	958.17	5.99	-1.11	0.086	82.13
5.0	54.17	3.73	4.68	0.57	1098.64	10.42			
5.5	59.06	4.26	4.95	0.47	906.32	8.23	-1.43	0.085	77.43
6.0	58.60	4.47	4.75	0.77	697.59	5.09			
6.5	59.92	4.21	3.93	0.38	355.62	4.71	1.68	0.077	27.35
7.0	61.52	4.19	4.10	0.52	473.44	6.52			
7.5	60.19	3.67	4.13	0.52	469.66	5.72	1.78	0.083	39.14
8.0	54.49	4.31	4.76	0.63	578.73	7.59	1.36	0.084	48.75
8.5	55.39	4.62	4.32	0.56	513.09	7.17	1.28	0.083	42.77
9.0	49.80	4.00	4.85	0.70	607.31	5.93	1.48	0.110	66.88
9.5	56.70	4.30	4.19	0.55	462.96	9.82	1.68	0.096	44.39
10.0	53.39	3.35	4.64	0.67	580.05	9.11	1.77	0.073	42.62
10.5	52.92	3.74	4.28	0.59	507.21	15.70		0.079	40.00
11.0	49.84	3.40	4.04	0.72	616.82	13.29	1.52	0.084	51.80
11.5	42.93	2.88	4.17	0.75	645.02	14.42		0.063	40.47
12.0	48.94	3.81	4.30	0.64	307.43	13.25	1.95	0.078	24.11
12.5	53.97	3.54	4.66	0.64	306.86	10.20		0.089	27.24
13.0	55.60	4.21	4.32	0.57	274.78	9.45	1.77	0.091	24.92

13.5	45.25	3.57	4.58	0.67	329.43	9.91		0.100	32.83
14.0	52.47	3.74	4.46	0.69	335.89	10.66	1.61	0.094	31.55
14.5	50.95	4.24	4.73	0.68	334.39	9.27		0.096	32.16
15.0	48.05	3.28	5.42	0.67	287.26	13.76	1.12	0.089	25.53
15.5	50.84	3.76	4.48	0.70	302.38	9.39		0.087	26.25
16.0	46.68	3.73	4.27	0.75	318.62	6.55	2.13	0.089	28.22
16.5	46.67	3.89	4.42	0.72	313.42	9.01		0.073	22.91
17.0	49.99	3.86	4.98	0.85	365.22	7.33	1.57	0.079	28.69
17.5	51.98	3.38	5.41	0.64	277.57	9.05		0.083	22.92
18.0	49.19	4.05	4.11	0.71	367.81	8.56	2.19	0.086	31.76
18.5	46.68	4.61	4.34	0.76	391.36	9.50		0.087	33.91
19.0	55.82	3.78	6.47	0.64	325.41	8.15	2.23	0.071	23.24
19.5	43.68	4.01	7.96	0.90	464.35	9.87		0.059	27.53
20.0	37.22	4.26	8.08	0.80	405.64	12.65	1.97	0.054	22.06
20.5	38.37	3.55	10.61	1.18	608.12	16.77		0.050	30.32
21.0	35.49	4.18	10.84	1.37	690.47	20.43		0.064	44.00
21.5	47.02	4.60	7.19	0.48	245.24	10.99		0.068	16.78
22.0	50.12	4.79	5.16	0.68	351.81	9.29	1.89	0.073	25.72
22.5	53.43	3.91	5.63	0.66	340.56	11.87		0.067	22.68
23.0	47.49	4.11	5.67	0.72	377.17	7.59		0.063	23.86
23.5	51.97	3.98	4.80	0.69	357.64	7.91		0.064	22.95
24.0	51.57	3.94	5.37	0.67	345.15	8.30	1.56	0.068	23.33
24.5	48.31	4.24	5.51	0.74	386.00	8.05		0.058	22.42
25.0	44.58	4.55	6.39	0.74	386.71	8.65		0.064	24.73
26.0	48.08	4.84	4.58	0.76	395.55	10.15	1.53	0.070	27.64
27.0	46.76	4.49	5.61	0.72	377.67	8.90			
28.0	49.22	4.69	5.05	0.75	391.14	7.99	1.61	0.064	24.89
29.0	46.94	3.86	5.93	0.76	397.40	8.89			
30.0	49.15	4.22	5.49	0.72	374.73	7.92	1.62	0.065	24.36
31.0	45.07	3.75	6.21	0.76	399.48	8.87			
32.0	51.45	4.18	5.69	0.69	357.36	8.23	1.92	0.062	22.33
33.0	48.42	3.70	6.04	0.72	380.55	7.51			
34.0	44.40	5.15	5.21	0.78	410.48	6.59	1.51	0.070	28.65
35.0	50.82	3.84	6.68	0.73	384.81	7.22			
36.0	49.06	4.43	6.26	0.72	382.87	6.57	1.66	0.087	33.33
37.0	51.74	4.77	4.52	0.70	368.45	6.10			
38.0	46.36	4.76	6.85	0.76	402.27	5.83	1.91	0.083	33.38
39.0	47.53	4.99	5.05	0.76	378.56	7.82			
40.0	50.49	4.31	5.72	0.69	357.12	8.24	1.96	0.070	24.92

41.0	49.61	4.40	5.64	0.70	363.77	6.69			
42.0	52.06	4.01	4.60	0.71	355.80	7.70	1.90	0.080	28.29
43.0	46.82	4.46	4.88	0.74	374.65	6.54			
44.0	47.50	3.75	6.22	0.69	361.67	7.78	1.95	0.070	25.19
45.0	46.95	4.27	7.07	0.80	409.48	7.81			
46.0	46.89	4.94	6.11	0.80	414.63	7.75	2.13	0.070	28.97
47.0	44.14	4.65	6.68	0.81	415.86	7.38			
48.0	45.26	4.49	5.54	0.76	376.72	7.89	1.89	0.070	26.42
49.0	45.61	5.29	4.97	0.76	379.76	7.62			
50.0	42.72	4.73	6.32	0.83	404.89	6.92	1.91	0.075	30.38
51.0	43.99	4.37	7.92	0.95	466.72	7.66			
52.0	45.03	4.12	7.64	0.82	396.77	8.95	2.09	0.064	25.46
53.0	43.40	3.96	7.70	0.86	413.59	7.19			
54.0	40.62	3.93	8.47	0.89	444.81	8.17	1.95	0.064	28.36
55.0	44.17	5.49	6.00	0.74		7.51			

Core 4B Raw Data

Section Top Depth (cm)	% Water (ww)	% Organic (dw)	% Carbonate (dw)
0.0	72.89	5.27	5.50
0.5	64.87	4.96	5.47
1.0	58.50	4.71	4.74
1.5	61.31	4.76	5.19
2.0	57.90	4.43	4.70
2.5	57.72	4.44	3.97
3.0	52.22	4.25	4.67
3.5	51.40	3.74	4.87
4.0	53.05	4.04	4.42
4.5	55.01	3.51	2.53
5.0	53.97	3.71	4.92
5.5	54.63	4.14	5.39
6.0	57.01	3.50	4.66
6.5	55.84	4.37	3.23
7.0	55.97	3.78	4.55
7.5	50.77	3.93	3.80
8.0	57.15	4.03	3.88
8.5	53.48	4.29	4.54
9.0	58.69	4.05	3.81

9.5	53.96	3.63	3.35
10.0	52.29	3.88	2.71
10.5	50.16	3.25	3.14
11.0	42.81	2.46	3.94
11.5	51.74	2.95	4.36
12.0	56.71	3.65	4.64
12.5	47.74	3.16	4.29
13.0	51.33	3.79	4.25
13.5	51.44	4.03	3.68
14.0	51.19	3.55	4.54
14.5	49.85	3.84	3.68
15.0	53.98	3.63	4.54
15.5	54.66	3.52	4.30
16.0	48.37	3.95	4.63
16.5	47.05	3.98	4.06
17.0	44.79	3.26	4.90
17.5	49.36	3.51	5.04
18.0	52.76	3.77	5.70
18.5	48.53	3.79	5.91
19.0	46.98	3.26	7.04
19.5	39.75	3.50	8.17
20.0	42.35	3.45	9.13
20.5	36.72	3.27	11.20
21.0	39.56	3.08	11.77
21.5	46.19	3.52	9.83
22.0	51.45	3.75	7.85
22.5	51.24	3.57	6.10
23.0	53.46	3.56	5.71
23.5	50.95	3.77	5.49
24.0	54.17	3.83	5.06
24.5	46.53	3.74	6.55
25.0	49.18	3.58	7.36
26.0	49.74	3.78	6.55
27.0	49.75	3.84	5.38
28.0	49.35	3.43	6.83
29.0	42.23	4.01	6.05
30.0	48.18	3.79	6.91
31.0	48.60	3.66	6.70
32.0	51.44	2.71	7.19

33.0	51.27	3.29	7.47
34.0	47.87	3.53	6.71
35.0	46.32	3.71	7.19
36.0	45.03	3.95	7.53
37.0	47.92	3.71	7.95
38.0	45.62	3.88	7.27
39.0	47.54	3.87	7.52
40.0	45.72	3.61	7.63
41.0	48.96	3.78	8.02
42.0	42.75	4.08	5.52
43.0	51.12	4.08	7.20
44.0	46.26	3.85	6.69
45.0	53.27	4.18	4.24
46.0	51.35	3.83	6.13
47.0	48.46	3.93	5.70
48.0	46.37	4.21	6.48
49.0	43.76	3.18	8.59
50.0	46.42	3.61	8.52
51.0	41.78	2.75	7.28
52.0	47.79	3.58	7.58
53.0	47.56	3.62	8.37
54.0	43.54	3.89	7.46